POLITECNICO DI MILANO

Scuola di Ingegneria Industriale e dell'Informazione

Corso di Laurea Magistrale in Ingegneria Biomedica

FINITE ELEMENT ANALYSIS OF SOCKET OPTIMIZATION IN ACCORDANCE WITH THE DEFORMATION OF EXTERNAL SURFACE OF THE STUMP

Relatore: **Prof. Carlo Albino FRIGO**

Correlatore: **Prof. Stefano MICCOLI**

Tesi di laurea di:

Hossein ANSARIPOUR

Matricola 879138

Sara CHEMELLO

Matricola 873383

Anno Accademico 2017-2018

INDEX OF CONTENTS

Index of figures

Index of tables

SOMMARIO

L’amputazione di arti inferiori può accadere per diverse motivazioni, tra cui diabete, eventi traumatici, tumori e deformazioni congenite. L’ablazione transtibiale è una delle più comuni tipologie di amputazione che avvengono sotto al ginocchio, nella quale la gamba viene rimossa al di sotto di questa articolazione. La cura e la riabilitazione dell’arto dopo l’amputazione è una grande sfida. Le conseguenze di una riabilitazione di successo con un arto artificiale si traduce in un maggiore comfort relazionato all’uso della protesi e una corretta distribuzione del carico nell’interfaccia tra l’arto residuo e la superficie interna della protesi.

Questo progetto analizza lo stato dell’arte dell’analisi agli elementi finiti per l’ottimizzazione del socket protesico basato sulle deformazioni del moncone. Per raggiungere questo obiettivo primario, abbiamo imposto delle pressioni distribuite sulla superficie esterna del moncone, principalmente costituito da tessuti molli, finché non si è ottenuta la reazione vincolare desiderata in percentuali di peso corporeo. Di conseguenza, i momenti angolari sono risultati comparabili con dati sperimentali ottenuti da gait analysis su pazienti reali, così escludendo possibili problematiche e ripercussioni a livello dei tessuti interni.

In questo caso, in quanto il modello è basato su un paziente reale, l’acquizione di immagini è stata ottenuta tramite risonanza magnetica, ottentendo come output dei file DICOM.

Di seguito, la segmentazione è stata svolta utilizzando il software Mimics Medical Image, estraendo così le superfici tridimensionali di ossa, muscoli, grasso, cartilagini e pelle per ulteriori simulazioni. Lo scopo è raggiungere un prototipo che possa migliorare la forma del socket.

In questo modo, le simulazioni sono state svolte considerando diversi scenari per quanto riguarda le proprietà dei materiali, nel tentativo di avvicinarsi ad un modello il più simile possibile al caso reale. Ciò si è tradotto, nei materiali iperelastici, a maggiori deformazioni che si sono riflettute in valori di picco più alti per quanto riguarda sforzi e deformazioni rispetto al caso elastico, dove tutte queste caratteristiche avvengono in un range fisiologico.

Perciò, questo modello può essere considerato come un paradigma per lo sviluppo del socket.

ABSTRACT

Lower limb amputation occurs due to several reasons including diabetes, trauma, malignancy and congenital abnormalities. Transtibial ablation is one of the common below knee amputations in which the leg is eliminated below the knee. The care and rehabilitation of the limb after amputation is substantially important challenge. The successful rehabilitation outcome with a prosthetic limb is contingent upon comfortable prosthesis and appropriate load transfer at the residual limb and prosthesis interface. This project investigates the state-of-the-art finite element analysis of socket optimization based on the deformations of the stump. To accomplish this primary ambition, we imposed pressure on the external surface of the soft tissue residuum until the desired reaction force which emerges from the percentage of body weight, was acquired. Consequently, the moments were commensurate with the data obtained from the gait analysis of human movement impeding the incidence of severe problems. In this case, since the model is based on a real patient, the image acquisition was obtained by the virtue of magnetic resonance imaging technique in the *DICOM* format file. After that, segmentations were performed by utilizing the *Mimics medical image* software and extracted the 3D surface of bones, muscles, fats, cartilages and skin for further simulations. The aim is to reach a prototype in order to improve the shape of the socket. Thus, the simulation was carried out by considering different scenarios of material properties for soft tissue in order to approach the real model. The turning point was that hyperelastic material underwent large deformations and resulted in higher peak values of stress and strain with respect to linear elastic assumption whereas all these discrepancies occur in the physiological condition. Hence, this model can be accounted as a paradigm for the development of the socket.

CHAPTER 1 : INTRODUCTION

1.1 Amputation Overview

1.1.1 Epidemiology

Currently, the patients with limb loss outnumber because of several factors. Therefore, an upward trend of requisite for rehabilitation intervention is inevitable. An aging population and an increment in number of patients who suffer from dysvascular diseases or osteomyelitis which leads to lose the limb, are factors that increase rehabilitation requirements. Studies foresee a twofold increase of elderly dysvascular amputation population by 2030 and a doubling of overall amputation population prevalence by 2050. The vast majority of people with lower limb amputations (Fig. 1-1) undergo amputation as a result of disease processes (82%), such as diabetes mellitus (DM) or peripheral vascular disease (PVD). Other causes include trauma (16%), malignancy (1%), or congenital abnormality (1%). DM expands the risk for amputation up to a greater extent than either smoking or hypertension. DM is reported to contribute to 67% of all amputations, and cigarette consumption is associated with a reamputation risk 25 times greater than that of non-smokers. Individuals with amputation at an earlier age require a longer continuum of care. The most frequent amputation level of lower extremity varies according to etiology. To some extent, the toe amputation is the most common level in both minor and major types. However, the transtibial amputation is the most prevalent level among the major type and transfemoral amputation can be placed in the second position[1].

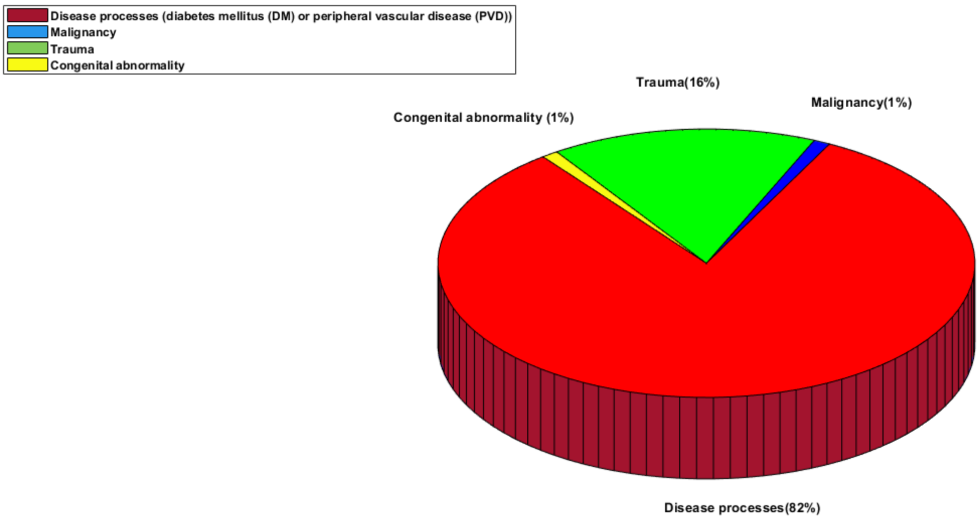

Figure 1-1 Indications for amputation

1.1.2 Amputation terminology

When it comes to amputation, it is literally related to the limb which is cut off due to trauma, medical maladies and during operations.

The lower limb amputation might be broadly categorized into two aspects: minor and major amputations. The amputations of digits can be generally accounted in minor type. The latter one commonly considers the above knee amputations (AKAs) and below knee amputation (BKAs).

According to ISO 8549-2:1989, there are a wide variety of amputations which can be taken into account as the major field. Thus, a list is drawn up here which briefly describes distinctive types of lower limb amputations (Fig. 1-2):

Partial foot amputation which illustrates the amputation of lower limb distal to the ankle joint.

Ankle disarticulation which indicates the removal of lower limb at the ankle joint.

Trans-tibial amputation that lower limb is taken away between the knee joint and the ankle joint. It is worthwhile to mention that this type widely refers to a below knee amputation (BKA).

Knee disarticulation which points out the lower limb eradication at the knee joint.

Trans-femoral amputation that lower limb is eliminated between the hip joint and the knee joint. This kind of elimination considers as an above knee amputation (AKA).

Hip disarticulation which depicts the amputation at the hip joint section.

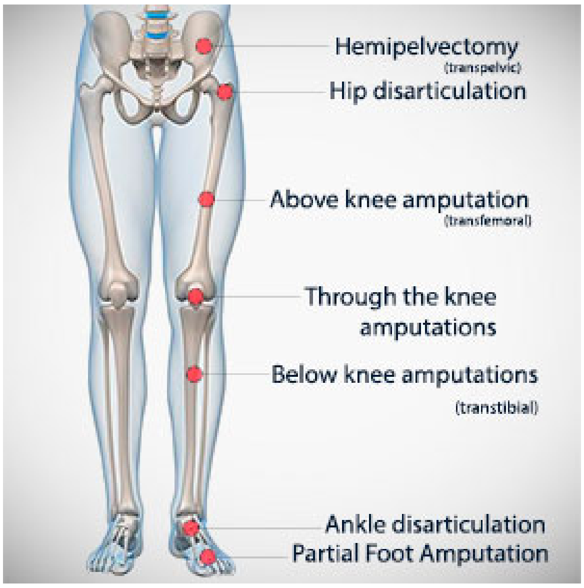

Figure 1-2 Different levels of lower limb amputations

Trans-pelvic disarticulation which represents the whole lower limb amputation with some part of the pelvis altogether. This is also known as a hemipelvectomy or hindquarter amputation.

1.1.3 Etiology

There exist a broad variety of reasons which lead to amputations including medical illnesses, accidental casualties, trauma and so forth.

Dysvascular amputation is a substantial consequence of diabetes. In some situations, diabetes might result in peripheral artery disease (PAD). Hence, the blood vessels are shrunk and subsequently, PAD diminishes the blood flow to legs and feet. It can also endanger nerves which is called peripheral neuropathy. Therefore, the patients could not feel pain in cases which they are in agony of wound and ulcer on their own feet. So, exerting continuous pressure on the damaged area causes the growth of affected zone and infection. On the other hand, the reduction of blood flow can slow down the healing process then, it makes body proceed ineffectively in order to overcome the infection. As a result, it is a no-brainer to expect the occurrence of tissue damages and death(gangrene) or propagation of infection to the bone. If the tissue damage is severe or the spread of infection cannot be halted, the amputation acts as a last remedy. The amputations of the toes, feet and lower legs are prevalent for those whom suffer from diabetes[2]. Furthermore, the coexistence of comorbidities including diabetes, peripheral artery disease and renal disease contribute to the development of gangrene, sepsis that eventually impose a requirement on limb amputation[3].

As herein stated, that, Diabetes coupled with neuropathy can spark off foot ulcerations. These acute injuries are quite prevalent in areas of increased pressure such as the first and fifth metatarsal heads and calcaneus, as well as areas predisposed to repetitive trauma including the tips of the toes[4] . Ischemic lower extremity alterations can convolute the recovery period. These situations can escalate the risk for osteomyelitis which is an infection of bone spreading through blood stream or surrounding tissues[5] . other issues which develop osteomyelitis are the usage of intravenous drug, removal of spleen and trauma to the area[6]. The diagnosis can be confirmed via bone biopsy, blood testing or imaging. albeit highly sensitive for osteomyelitis, bone scans convey very little specificity for osteomyelitis (Fig. 1-3).

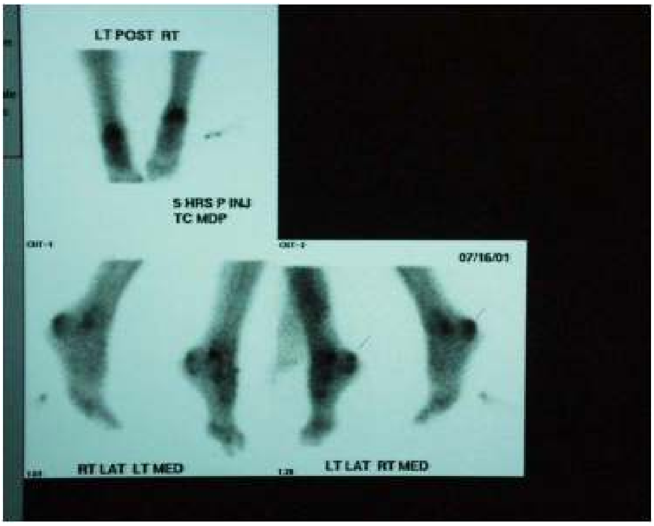

Figure 1-3 Positive bone scan of diabetic patient with bilateral calcaneal osteomyelitis

The treatment might be considered surgically in which the infected bone is excised following antibiotic prescription for several weeks or long-term antibiotic consumption without any operation. If there is poor blood flow, amputation eventuality is demanded[5] (Fig. 1-4).

Figure 1-4 Distinctive sorts of lower limb amputation caused by osteomyelitis

Frostbite is highly probable when the body's tissue exposed to extremely cold temperatures. Fingers, toes, ears and cheeks are the most parts of the body which are widely sensitive to this condition. Since the first body's priority is to maintain the temperature at the physiological condition in central part. So, there should be the blood flow transition from extremities towards the center. Afterwards, the patient feels numb at the peripheral part. There are two levels of frostbite:

1. Superficial frostbite which mostly affects the surface areas such as skin.
2. Deep frostbite which also poses a problem for underlying tissues.

When the body's tissue is frostbitten, then the ice crystal formation in cells are definite, leading to permanent changes in cell chemistry and finally cell death. Moreover, the lack of blood perfusion and oxygen to the peripheral parts can cause the death of tissues and irreparable injuries to extremities. Finally, the amputation is required as a last resort[7].

Bone and cartilage-forming tumors are the subset of malignant neoplasms which can be potentially harmful. The clinical features of bone tumors are often non-detected in early phases. Pain, swelling and general discomfort are the symptoms that can be taken into consideration. The sudden fractures can also be mentioned as a symptom due to the structural alterations of the tumor-bearing bone. Osteosarcomas, chondrosarcomas and Ewing's sarcomas are rife among malignant bones. These tumors are clinically aggressive which spread quickly in the bone. It means that a spur-of-the-moment treatment must be administered in order for the limb salvage. By contrast, the amputation is necessitated in some cases[8].

Traumatic amputation which depicts an unpredictable loss of the limb during the course of incidents for instance, motor vehicle collisions, railway accidents, building collapses, war casualties to name but a few[3]. Factors which foresee the indications of amputation are:

- Energy that causes the injury
- Limb ischemia
- Age
- Shock

Congenital limb deficiency can be triggered via genetic modifications, exposure to an environmental teratogen or to gene-environment interactions[9]. The effects can range from the loss of a finger or two to full bilateral limb loss[10] . Limb Deformities in childhood can be congenital, since in children pre- or postaxial hypoplasia for example, tibial deficiency, fibular deficiency, proximal focal femoral deficiency (PFFD) and ray defects of foot. The reasons why such these deformities occur are sepsis or trauma involving growth plates or tumors and sequel of the tumor resection[11] . Fig. 1-5 illustrates the classification of tibial deficiency in which type 1 is due to the absence of tibia and divided into two subsets. Type 1a depicts hypoplastic lower femoral epiphysis; type 1b portrays normal lower femoral epiphysis. Type 2 indicates the absence of distal tibia. The proximal tibia is disappeared in type 3 and finally type 4 represents diastasis of the distal tibiofibular joint[12].

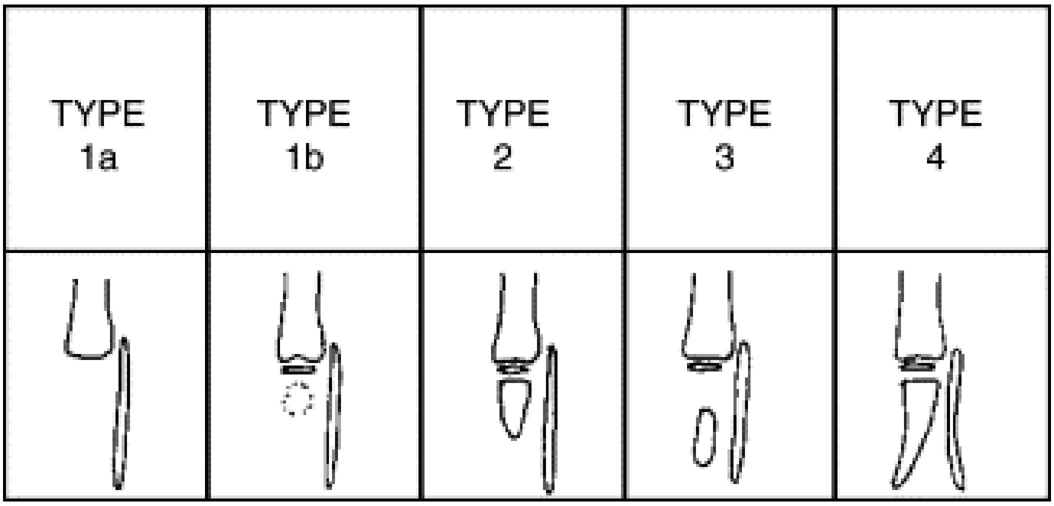

Figure 1-5 Classification of congenital tibial deficiency

The rate of any amputation is generally low, comprising about0.8 % of all amputations, consistently, over a 10-year period, and perhaps 26 per 100,000 live births, and multiple limb loss is incredibly rare Upper limb loss is slightly more common, making up about 58.5 % of known cases[10].

1.2 Surgical Treatment

Most surgeons reckon that amputation can be a surgical failure albeit a well-organized amputation may help to ease a painful, dysfunctional limb and allow rehabilitation with a prosthetic limb to a functional, painless state. A significant milestone of surgery is to eliminate diseased or damaged tissues to achieve a healing process. Without healing, the prosthetic training can not commence[1].

1.2.1 Amputation site preferences

Surgeons are prone to perform an operation at the most distal site compatible with wound healing to accomplish an optimum situation for ambulation and future prosthetic fitting outcomes[1][13].

There have been strong proofs which indicate that energy expenditure with prosthetic ambulation is noticeably increased in more proximal amputation. There exists a technique which can be recruited in order to measure the energy cost of walking impacted by the level of amputation. According to a study case, the patients walked around a route 60.5 meters in circumference while the exhaled air was accumulated in an adjusted Douglas bag for carbon dioxide and oxygen analysis. The mensuration of cadence, heart rate and respiratory rate was performed via transducers which were connected to the patients. All gas volumes were regulated with respect to standard pressure, temperature and humidity. They were supposed to walk approximately five minutes. The first three minutes walking considered as a warm-up then in the following two minutes the data were garnered when the respiratory and heart rates reached stability. Two tests were conducted: the first at unrestrained speed and the latter case at the fastest possible speed. Bear in mind the fact that oxygen uptake relies on walking speed. Thus, the oxygen consumption and hear rate derived from fast walk were exploited as the estimation of maximum aerobic capacity. The energy cost was evaluated in three ways:

1. Rate of energy expenditure which signifies the amount of oxygen consumed per minute.
2. Energy cost per meter which indicates the amount of oxygen is used per meter walked.
3. Relative energy cost which describes the ratio of oxygen uptake to the individual's maximum ability to perform aerobic exercise[14].

Amputation Level	Energy Above Baseline (%)	Speed (m/min)	O_2 Cost (mL/kg/m)
Long transtibial	10	70	0.17
Average transtibial	25	60	0.20
Short transtibial	40	50	0.20
Bilateral transtibial	41	50	0.20
Transfemoral	65	40	0.28
Wheelchair	0-8	70	0.16

Table 1-1 Energy cost, speed and oxygen consumption in accordance with distinctive degrees of amputations

Table 1-1 depicts the energy expenditure, speed and oxygen consumption for different levels of lower limb amputations. There is an upward trend in energy expenditure and oxygen consumption in conformity with short stumps[15].

Furthermore, the preservation of knee joint is also a noteworthy criterion especially when the rate of contralateral limb amputation is regarded. In this case, the ability of ambulation is more intricate than unilateral amputation[13].

The overwhelming methods have been developed to specify the most distal level at which the amputation is likely to be successful. The clinical parameters including the lowest palpable pulse, skin temperature and bleeding at surgery have been utilized in order to predict the healing at amputation [13].

The utilization of doppler ultrasonography to assess arterial blood pressure at the predicted amputation site has been recommended to roughly determine the amputation area. For instance, transtibial amputations in patients with popliteal systolic pressures of more than 70 mmHg, have healed. In addition, if the ratio of pressure at proposed amputation area to that brachial artery is greater than 0.35 is sufficient for non-diabetic healing, while the ratio of more than 0.45 is required for the diabetic one. Controversially, the doppler usage is in contradiction to prediction of proposed amputation site since a calcified, non-compressible artery will be inferred spurious values. On one hand, the pressure in deep artery may be irrelevant to skin healing[13].

The clearance of 133xe is a method for dermal vascularity determination. In this approach, cutaneous diastolic pressure is calculated by specifying imposed pressure which is crucial to halting clearance of 133xe administered intradermally. In accordance with some findings which have examined 60 transtibial amputees, it illustrated when the skin perfusion pressure was less than 20 mmHg, only 25% of these amputations healed; when the skin perfusion pressure was greater than 30mmHg, 90% of successful healing was reported. The 67% of modest recovery was achieved when the pressure was between 20 mmHg and 30 mmHg (Fig. 1-6)[13].

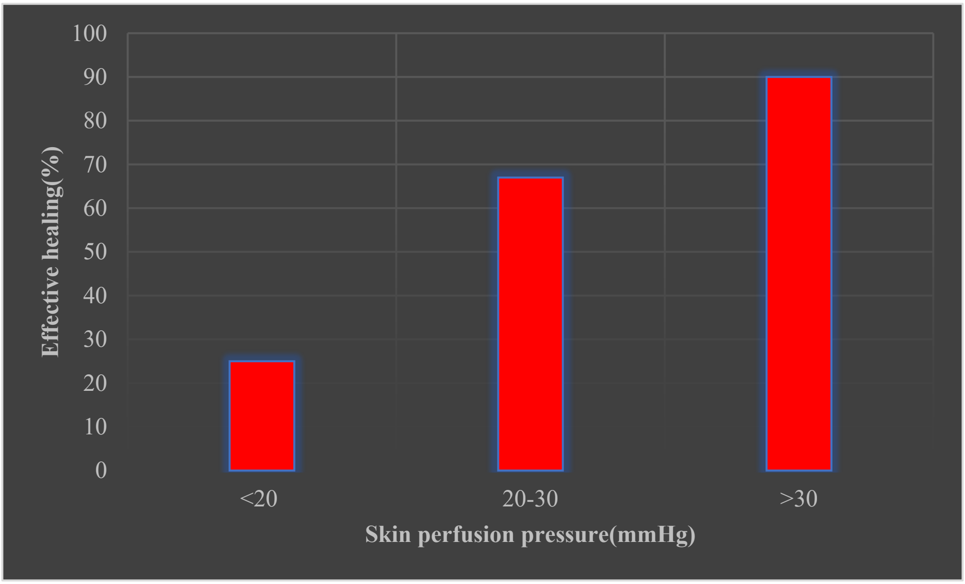

Figure 1-6 Obtained data from clearance of 133Xe for designation of amputation site

There are other practical methods for investigation of amputation site including fluorescein angiography, skin temperature measurements, pulse volume recording and laser doppler velocimetry (LDV)[13].

1.2.2 Meticulous approaches for operation

These days, amputation is no longer to be considered as a failure. notwithstanding losing the limb extremity, supreme efforts have been taken to restore ambulatory function[13]. Accomplishing this ultimate goal requires the presurgical planning including consultation with physiatrist and aids in discussion about the amputation level and future prosthetic fitting[1]. The demand to construct a dynamic and sensory motor-end organ can play a prominent role in surgeons mind achieving better outcomes[16] . General principles for ablation surgery entail appropriate management of skin, bone, nerves and vessels as follows:

- Maintaining of the skin length as much as possible for muscle coverage and a tension free closure.
- As a matter of muscle-stump stabilization, muscle is positioned over the cut end of bones through a myodesis (the attachment of sectioned muscles under suitable tension via drill holes into bone), a long posterior flap sutured anteriorly to anterolateral deep fascia and tibial periosteum with a reasonable provision of muscle fixation without risk of strangulation, or a well-organized myoplasty (antagonistic muscle and fascia groups sutured together). Myodesis adds operative handling of tissues and encircling of suture may lead to muscle constriction. Thus, muscle-to-bone suture is not apt for below knee ablation especially those induced from vascular disease. Hence, myodesis is reserved for non-ischemic patients.

- Nerves are transected under tension, proximal to the cut end of bones in a scar-and tension-free environment, diminishing the chances that neuromas will form and be a source of pain; placing the cut nerves in a more proximal scar-free environment assists in decreasing potential irritation and pain; ligation of large nerves can be performed when an associated vessel is present.
- The greater arteries and veins are cut up and ligated separately in order to avoid the development of arteriovenous fistula and aneurysms.
- Bony prominences around disarticulations are eliminated with a saw and filed smooth; diaphyseal transections can be covered with a local flexible osteoperiosteal graft; although maintaining the maximal extremity length possible is desirable, below-knee amputations are best performed 12.5-17.5 cm below the joint line for non-ischemic limbs.
- One application guide is to make a limb 2.5 cm long for every 30 cm of body height; for ischemic limbs, a higher level of 10-12.5 cm below the joint line is used because making limbs longer than this can interfere with prosthetic use and design[17][16].

If the amputation is the reason of injury, the surgeon will remove the crushed bone and file to prepare the remained part for artificial limb. In some cases, the temporary drain is employed to flow away the blood and other fluids which might be inserted. the surgeons take the advantage of some tact after removal of dead tissues. they may close the flaps which is called closed amputation or leave the site open which is opened amputation. In a closed amputation, the wound is supposed to be sutured. This method is practical especially when there is a risk of infection. In the latter one, the wound is open for several days to cleanse tissues that are on the verge of infection. After a while, the skin flaps are meant to be sutured together to shut the wound[18].

The transtibial amputation may also be classified as end weight-bearing amputations. The end weight-bearing amputations can also be categorized into osteomyoplasty(Ertl procedure) and singer procedure[13].

Amputation osteomyoplasty or bone bridging is a technique thrived to restore the residual limb to normal physiological condition. The turning point of this technique which is the bone bridging between fibula and tibia, indicates a greater and more stable end bearing structure with respect to conventional procedures. Furthermore, the vascularity of residual limb is enriched due to sealing the intramedullary canal. According to angiographic studies, it also reestablishes medullary pressure and increases blow flow to the residual limb. An amalgam of this method with myoplasty or myodesis recreats the normal length-tension of muscles and develops surface area stabilization which is crucial for prosthetic fitting. EMG testing is also warranted the normal working condition of muscles[19].

The singer procedure utilizes the heel pad and sole tissues as a flap to enhance the physiological weightbearing platform. This method is not very common and restricted particularly when there is the extensive diaphyseal bone loss preventing the skeletal reconstruction even though posterior tibial nerve and foot should be intact. The nerve is folded into the soft tissues of the residual limb, and a posterior tibial-popliteal arterial anastomosis is performed. The heel pad is then sutured over the end of the residual limb to provide end weight bearing after healing [20][13].

1.2.3 Instant postoperative care

There are a wide variety of postoperative dressings and treatments. Each one has its own pros and cons. Generally, there are four generic types of postoperative dressings, as follows:

1. Soft dressings which cannot take over the postoperative edema.
2. Soft dressings with pressure wrap which in this case the uniform pressure distribution is highly demanded, otherwise the limb strangulation occurs.
3. Semirigid dressings which are akin to rigid dressings with same advantages apart from the fact that immediate postoperative prosthesis cannot be utilized.
4. Rigid dressings which are abundantly available. It has the merit of feeling less pain, maturation of residual extremity, edematous decrease, early mobilization following with an immediate postoperative prosthesis and so forth. Controversially, poor access to the wound and intense pressure which leads to necrosis, are flaws that can be taken into account in these dressings.

Physical therapy and psychological support are also advocated for recovery of the patient physically and mentally[17].

1.2.4 Complications

Careful tackling of tissue and reconstruction of the limb to normal physiological condition are criteria considered during the duration of operation and before surgery. Nevertheless, there are prevalent inconveniences which may occur potentially as follows:

1. Pain
2. Swelling
3. Edema
4. Wound breakdown and skin problems
5. Joint contractures

Hence, daily skin care, residual limb shaping, and postoperative healing are key factors in handling of complications after amputation. The maintenance of appropriate limb shape can be fulfilled via the shrinkers or figure-of-8 wraps especially when the prosthesis is not donned [1].

Heterotopic ossification is the formation of mature lamellar bone due to osteoblast activity in non-osseous tissues. Heterotopic ossification is fairly mentioned the cause of pain in residual- limb pain in amputees (Fig. 1-7-A and 1-7-B)[21]. Consequently, it can lead to ambulation issues, the range of movement (ROM) problems, neurologic or vascular occlusion. The high contingency of heterotopic ossification can be diagnosed on the basis of increased alkaline phosphates and radiographs[1].

Figure 7-A

Figure 7-B

Figure 1-7 Anteroposterior (A) and lateral (B) radiographs of residual limbs with severe heterotopic ossification

1.2.5 Pain classifications after limb ablation

There are three main types of pains which frequently appear after amputation including:

1. Phantom limb pain (PLP) which illustrates a pain in areas which are no longer present.
2. Phantom limb sensation (PLS) that is rife immediately in the postoperative period. This pain can be eased by prosthetic use and desensitization strategies.
3. Residual limb pain (RLP) which is restricted to the influenced limb.

A wide variety of PLP descriptions can be indicated for instance cramping, dull, shooting, electric shock-like, squeezing, or sharp.

Medications for PLP include *N*-methyl-d-aspartate receptor antagonists, opioids, anticonvulsants, antidepressants, local anesthetics, and calcitonin. Mirror therapy and transcutaneous electrical nerve stimulation have also been used for PLP[1].

1.3 Prosthetic devices

1.3.1 Historical background

At the embryonic stage, the prosthetic limbs were made of fiber. And they were utilized as a sense of wholeness rather than function. The Egyptians were pioneers in this field.

An artificial leg dating to about 300 B.C. was unearthed at Capua, Italy, in 1858. It was made of bronze and iron, with a wooden core, apparently for a below-knee amputee.

In 424 B.C., Herodotus wrote of a Persian seer who was condemned to death but escaped by amputating his own foot and making a wooden filler to walk 30 miles to the next town. At the dark ages, the most prosthesis were supposed to hide deformities or injuries sustained in battle.At the renaissance period, the most of the prothesis were made of iron, steel, copper and wood.

French Army barber/surgeon Ambroise Paré is considered by many to be the father of modern amputation surgery and prosthetic design. He introduced modern amputation procedures (1529) to the medical community and made prostheses (1536) for upper- and lower-extremity amputees. He also invented an above-knee device that was a kneeling peg leg and foot prosthesis that had a fixed position, adjustable harness, knee lock control and other engineering features that are used in today's devices.

In 1800, a Londoner, James Potts, designed a prosthesis made of a wooden shank and socket, a steel knee joint and an articulated foot that was controlled by catgut tendons from the knee to the ankle. It would become known as the "Anglesey Leg" after the Marquess of Anglesey, who lost his leg in the Battle of Waterloo and wore the leg.

Douglas Bly invented and patented the Doctor Bly's anatomical leg in 1858, which he referred to as "the most complete and successful invention ever attained in artificial limbs." In 1863, Dubois Parmlee invented an advanced prosthesis with a suction socket, polycentric knee and multi-articulated foot (Fig. 1-8)[22].

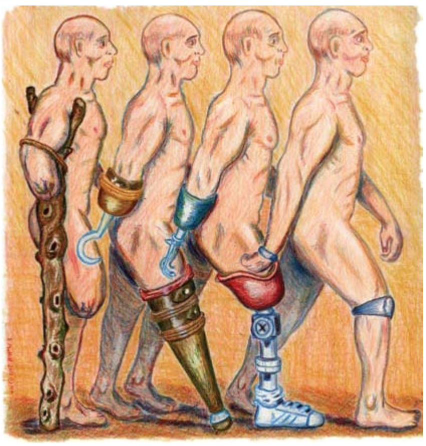

Figure 1-8 Illustration by Scott Mcnutt

1.3.2 Recent literature overview

After the second world war, the German company commenced to manufacture separate prosthesis including the prosthetic foot, the knee-shin component and sockets. The prosthesis was made of wood with the external surface of a normal limb. The structure of the prosthesis could buttress the load and the socket was designed as if it was able to host the stump smoothly. The joint was a single axis hinge and the foot was a rigid block. After a while, the knee was patterned more functional and flexible by virtue of four bar linkage. In this case, it helped patient stabilize equilibrium in both standing and walking positions by means of controlled flexion and extension. It is also worthwhile to mention that the excessive flexion during the swing phase was thwarted by elastic band usage. The paradigm of prosthetic foot was widely disseminated Solid Ankle Cushioned Heel (SACH) foot. The developed polymers like polyethylene, polypropylene and polyurethane were recruited to design sockets. A lot of effort has been put in order to model and manufacture socket corresponding to each patients' requirement. The cosmetic materials which are soft and deformable, give the prosthesis a visage of a normal limb [22]. Nowadays, microprocessors and Sensors are employed in some advanced lower limb prostheses to take over micro actuators which alter the mechanical characteristics of the joints in conformity with the different walking situations [22].

1.3.3 General concepts

In accordance with motor disabilities, the requirement for orthopedic devices is conspicuous in order to recover function and physical activity. For instances, in Lower limb amputees, the demand for artificial limb is vital to compensate the missing part and revive the physiological function to some extent. These devices are also called prosthetic devices. On the other hand, some Orthopedic devices are utilized to restore a part of function which is faded away due to the weakness or deficit in the neuromotor control system. These devices are called orthopedic orthoses. If the patient is obliged to use these devices, it is crucial to aggregate the cooperation of experts including physical therapists, orthotist and prosthetist, occupational therapist, and possibly a psychologist. Thus, this is a subtle task when the patient needs to be supplied with these devices. In other words, its performance must be sufficient for patient's demands[22]. Hence, there must be a trade-off between structure, function and cosmesis to obviate the discomfort.

When it comes to the terminology of orthopaedic prosthesis, a thorough definition illustrates: *"An orthopedic prosthesis is an internal or external device that replaces lost parts or functions of the neuroskeletomotor system"* (Lord & Turner-Smith, 2000).

Since there exists the interplay between prosthesis and stump, the stump is denoted the residual limb after amputation. Bear in mind the fact that the prosthesis recommended to a stump, cannot be useful and effective for the others (patient specific). A good stump has some characteristics followed by[23]:

- Suitable size and shape
- The skin and scar are free and healthy
- The strength of muscles is adequate
- The range of motion of the joint is impeccable and without any deformity
- No neuroma and no phantom sensation and pain

1.3.4 Prosthetic function

Prosthesis is modeled to be supplanted in the missing segment and perform the function of ablated part. The prosthetist assesses the biomechanical characteristic of the prosthesis for demanded task and the capability of residual limb must be investigated. It is worth mentioning that the energy consumption, kinematics and dynamic corresponding to the task ought to be evaluated.

Prosthesis should also be designed in a way that it can withstand an interval variety of loads during walking or daily activities. This issue would be satisfied if the mechanical interface between the prosthesis and the stump were fulfilled several factors which are drawn up:

- Characteristic of prosthetic component
- The socket
- The shape of the stump

Since the internal dimension of the stump is not thoroughly commensurate with the external surface of the residual limb, then some rectifications are considered in order to subside the pressure in regions which load tolerance is low. Furthermore, the soft material and liner are inserted between the socket and stump. Alignment is also another factor which is necessary especially in determination of forces and moments transmitted at the interface section between stump and socket during the supporting phase. Moreover, adjustability can also be sought out as a matter of functional optimization [22].

From the cosmetic point of view, the manufacturers are prone to produce the prosthesis like the shape of a normal limb (Fig. 1-9). One of the advantages of cosmetic cover is that it allows the patient to cleanse the prosthesis without any inconveniences or interferences in prosthetic function and structure.

Figure 1-9 Cosmetic prosthesis

1.3.5 Prosthetic structure

The prosthetic structure portrays the mechanical part which supports the component functionality. Generally, there are two kinds of prosthetic structures:

1. The Exoskeleton which is more traditional. This structure is also renowned for crustacean due to its shape and functional components inside.
2. The endoskeleton which is also known as the modular type. It is made of tubes linking the different components and enveloped by proper materials like polymeric foam. The endoskeletal prosthesis is easily adopted and adjusted to the individual patient.

At the structural level, the appropriate mechanical characteristics are crucial to bear the different levels of loads (dynamics or statics), shakes, fatigues and so forth. In addition to the aforementioned factors in the previous section, choosing the proper size of the component can regulate the functions of prosthesis up to an acceptable point. All these efforts have been made to warrant the safety and integrity of the patient.

There are also some complications by using prosthesis. In accordance with Saunders,

Inman, & Eberhart (1953) and Jacqueline Perry (1992) have called these features the '*determinants of gait*'. Among them are the plantarflexion of foot at early stance phase, the knee flexion-extension cycle at load acceptance, the smooth transfer of load to the contralateral side associated with pelvis rotation in the three planes, and the trunk compensation. Since the level of amputation varies patient by patient. In some cases, It is so complex to restore those saving energy mechanisms. Consequently, the walking can be appeared at irregular cadence level. [22]

1.3.6 Prosthesis in transtibial amputation

The 59 percent of lower limb amputation is transtibial amputation. If the length of the stump from tibial tubercle is 15 cm, it is accounted as ideal length. the minimum length is just below tibial tubercle. Generally, the type of prosthesis is recognized by the type of its socket [23].

The components which utilized in transtibial amputation (Fig. 1-10), are:

- Socket
- Suspension
- Shank or pylon
- Foot

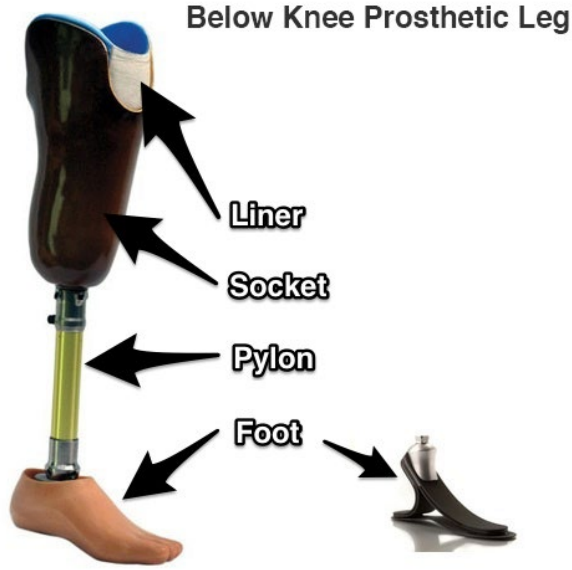

Figure 1-10 Below knee prosthetic components

1.3.6.1 Socket

The part of prosthesis which envelops the stump, is called socket. The socket creates a unified form between stump and artificial limbs. There are different types of sockets utilized including:

- Conventional below knee socket
- Patellar tendon bearing socket (PTB)
- Patellar tendon bearing supracondylar suprapatellar socket (PTB-SC-SP socket)
- Bent knee socket
- Slip socket

Conventional below knee socket was the initial socket which used before PTB. Elderly people with unstable knee and those with quadricep weakness utilized such this socket. The socket is designed in a way that there is not any pressure on the distal tibia, the head of fibula or tibial crest. The material is wood, and it requires the external knee joint with thigh corset for stability and suspension. Paradoxically, the skin irritation due to friction and chocking of the stump with edema over the distal end of stump from constriction are considerable disadvantages of this socket.

Patellar tendon bearing socket (Fig. 1-11) which is the most widely used socket in transtibial amputation. The socket consists of plastic over the mold of stump and it is maintained 5 to 10 of knee flexion. three-fifth of the weight is borne with patellar tendon and two-fifth of the weight is withstood by tibial flare. The anterior brim is at mid patellar level and lateral and medial brim and same level. The posterior rim is at popliteal crease.

patellar tendon, medial tibial flare lateral pretibial muscles, the popliteal fossa and gastrocnemius muscle are considered as pressure tolerant areas.

The head of fibula, distal tibia, tibial crest distal end of fibula and hamstring muscles are accounted as pressure sensitive areas.

This type of socket can be fitted with suction suspension and the shank can be both endoskeleton or exoskeleton[23].

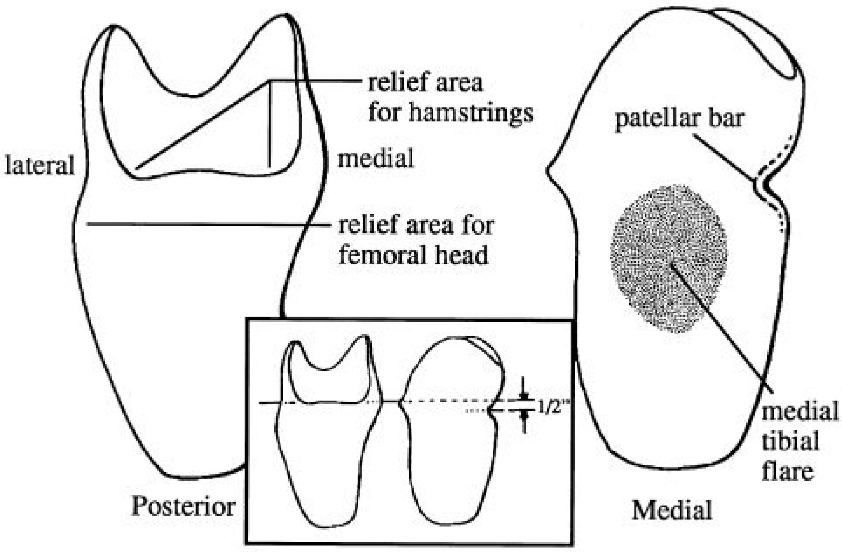

Figure 1-11 Patellar tendon bearing prosthesis

Patellar tendon bearing supracondylar suprapatellar is a type of socket in which the anterior trim line is supra patellar. Thus, the whole of patella is inside the socket. This socket is designed as if it provides the suspension autonomously. Hence, the addition of external suspension is not required. PTB-SC-SP socket is highly recommended for patients with short stump or those with genu recurvatum.

Slip socket consists of two layers. The external layer which is wooden or plastic and the internal layer which is fine leather and fits to the stump properly. It is joined to the thigh corset by elastic bands. This socket is appropriate for people who suffer from painful adherent scar and those with short stump [23].

1.3.6.2 Suspension

There are a wide variety of suspension all over this world for transtibial amputees. The suspension can be chosen well if the required function after amputation is vastly known. Thus, the prosthetist with enriched knowledge about suspension systems can have appropriate selection[24].

The suspension system and socket fitting are the prosthetic devices influence the mobility satisfaction and amputee’s comfort. The safe suspension diminishes the stump movement within the socket by means of a good attachment between socket and residual limb. In contradistinction to secure suspension, inappropriate suspension can aggravate the prosthetic fitting of the socket. Subsequently, the poor fitting leas to pain and skin ulcers. Hence, the patient cannot benefit from prosthesis till the pernicious effect of pain an ulcer is obviated[25].

Supracondylar cuff is a simple cuff that suspends the prosthesis to supracondylar area around lower thigh closed by Velcro or buckle closure[23].

External knee joint with thigh corset (Fig. 1-12) is useful for patients with unstable knee, obese or aged patients and even those with short stumps. Mediolateral stability is the result of utilizing this suspension accompanied by external knee joint with lock. In contrast, damages to cloth and discomfort in hot weather are cons of this product[23].

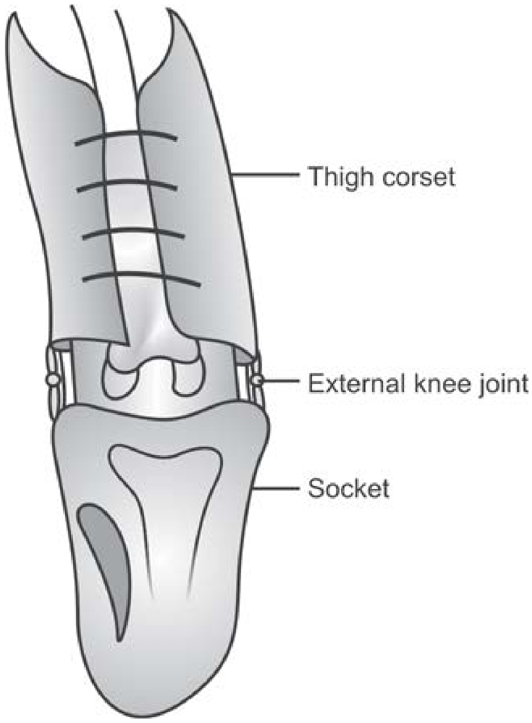

Figure 1-12 Thigh corset

Silicon suspension liner including distal locking pin, lanyard and suction suspension[25].

the suction socks which wrap the stump is attached to the socket with shuttle lock systems. The shuttle lock system is placed at the base of the socket. There is also a key at the lower end. The key in the prosthetic socks is pulled through the lower end of the socket and is locked[23].

The air pneumatic suspension system (APSS) which is a new model. The advent of this new pneumatic suspension overcomes the drawbacks of recent suspension models in donning and doffing, volume changes during quotidian activities, and pressure distribution at the stump-socket interface. The fitting problem at different levels of gait analysis is overcome up to a great extent. It also indicates more adaptability to the changes in stump volume. The volume changes are regulated with air pressure sensor. The APSS comprises a control board with microcontroller that includes a semiconductor pressure sensor (ADP41410/ Panasonic, USA), an air cuff attached inside the socket, air pumps, and pressure-regulating valves (Fig. 1-13)[26].

Figure 1-13 The components of APSS: a) Bladder. b) Control circuit board. c) Pump. d) Valve. e) Battery. f) Operation system. g) Assembled transtibial prosthesis

1.3.6.3 Foot

Familiarity with the characteristics of current prosthetic foot-ankle assemblies will enable physical therapists to participate more effectively in the management of individuals with lower limb amputation. All foot-ankle prosthetic components support the wearer, absorb shock, and simulate toe extension passively[26].

The foot-ankle prosthesis used in transtibial amputations are:

- Solid ankle cushion heel (SACH) foot
- Single axis foot
- Multiple axis foot
- Solid ankle flexible keel foot
- Energy storing foot

Solid ankle cushion heel (SACH) foot (Fig. 1-14) is the widespread utilized type of foot assembly. The components of this prosthesis are:

The solid heel comprised of wood or metal is directly connected to the ankle block and there does not exist any joint at ankle.

Cushion heel consists of rubber heel wedge or alternating layers of soft and hard rubber. The cushion heel compression relies on patient weight and mundane activity. The cushion heel compresses during heel strike simulating plantar flexion. The rubber heel wedge also absorbs shock at the heel strike

The cosmetic forefoot with/without individual toe consideration.

SACH can be modeled lighter than the other forms of foot assembly. This prosthesis is water proof and has high durability. Moreover, the price of this foot is not exorbitant. It is highly recommended for low activity and lighter weight users. Contrary to its merits, rigid cannot bend, and heel height is fixed. Therefore, it cannot be customized[23].

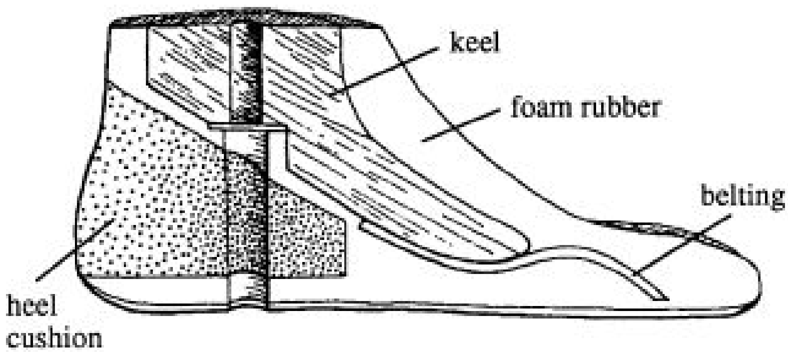

Figure 1-14 Solid Ankle Cushion Heel (SACH) foot

Single axis foot consists of hard rubber bumpers which allow the restricted plantar flexion and dorsiflexion. This type of foot is adequate for walking on the floor. The range of motion is less than anatomical situation [29].

Multiple axis assembly allows passive motion in frontal, sagittal and transverse planes. The multiple axis foot also has a flexible toe section. One of the new versions of multiple axis model is *the Mauch® hydraulic ankle (*Fig. *1-15).* There exists an oil-filled chamber enhancing the range of motion during the stance phase in sagittal plane. It allows 10 degrees of dorsiflexion and 20 degrees of plantar flexion, adapting automatically to the slope of the walking surface. The substantial creature of multiple axis assembly is that it absorbs stress in each plane [29].

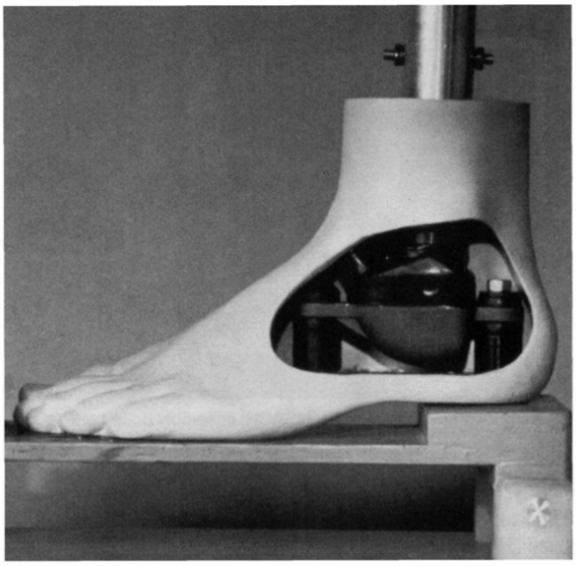

Figure 1-15 Mauch® hydraulic multiple axis assembly

Solid ankle flexible keel foot is analogous to SACH but with flexible keel. Thus, the performance of shock absorption is better than SACH model. This model brings a good result for obese amputee.

Energy storing foot (Fig. 1-16) or dynamic response foot developed for sports and active. It consists of a shock absorbing leaf spring or carbon graphite which grasps energy of heel contact and discharge it in terminal stance. In other words, it is propulsive. The patient can walk long time with energy foot than SACH foot. Light weight and efficiency at high speed are accounted as it's pros. But it is expensive[23].

Figure 1-16 Energy storing foot

1.3.7 Prosthetic Prescription Algorithms for Transtibial Amputation

The patient's aim for the use of prosthesis and demanded activity are remarkable criteria considered to opt for prosthetic components. Therefore, the centers for Medicare and Medicaid Services introduce some functional levels which depict the mobility scale.

FUNCTIONAL LEVEL ONE (K1):

Patients in this functional category can have an ambulation over level surfaces for the short household distances. The priority of this group is safety. The socket design should be a total contact style, with special considerations for comfort during sitting. The type of interface and suspension system utilized, should consider the patient's ability to don and doff the prosthesis and manage his or her hygiene independently. The shank or pylon is endoskeleton and may accompany with alignment ability in design. The foot-ankle assembly can be a SACH or single axis foot.

FUNCTIONAL LEVEL TWO (K2):

Population in this category can are able to ambulate restricted community distance and pass some environmental obstacles. The prescribed components in this module need to be aligned and the foot prosthesis should be multiple axis version. Suspension for this group can use a pin lock, sleeve or suction suspension with a sleeve, and one-way expulsion valve in the socket.

FUNCTIONAL LEVEL THREE (K3):

this group can have a mobility and different cadence levels and traverse the most environmental barriers. In accordance with this functionality, the foot part should be accounted as energy storing foot. The suspension system is an elevated vacuum technology. Furthermore, the pylon can be considered dynamic which permits greater accommodation over uneven terrain.

FUNCTIONAL LEVEL FOUR (K4):

Functional K4-level amputees are capable of ambulation which exceeds normal requirements. This may include sports or recreational activities that require high impact, high stress, or high energy levels, which are typical of the prosthetic demands of a child, high-activity adult, or athlete. At this level, specialty components are running feet, waterproof foot and ankle components, and components with heel height adjustability. Suspension is also a key for this group to avoid disastrous disruption of the prosthetic connection during activity. This may include use of a backup or secondary suspension method[1].

1.3.8 Prosthetic alignment

Prosthetic alignment influences the gait of the patients with transtibial amputation. It may impact energy efficiencies, gait symmetry and pressure distribution on the residual limb. The spatial relationship of the socket to the foot in transtibial amputation is called alignment. There are 3 phases for the alignment:

1. The bench alignment that is tuned on the work-bench before fitting
2. Static alignment that is tuned while the user stands up with the prosthesis
3. Dynamic alignment that is tuned during gait analysis

The adjustment occurs in three planes:

1. The sagittal plane which includes flexion, extension and socket translation
2. The coronal plane which includes adduction, abduction and socket translation
3. Transverse plane which includes the internal and external rotation of the prosthetic foot (toe-in and toe-out)

Alignment is commonly accomplished by inducing angle or translation displacements utilizing adaptors connecting the pylon to the foot and socket in the transtibial prosthesis. This alignment regulation process is generally conducted by prosthetists derived from their experience and visual inspection of gait in the clinical settings. Hence, it is subject to human errors and may not be thoroughly reliable.

It is worthwhile to mention that the alignment alteration can influence the kinetic parameters in a predictable manner, but their effects on temporal-spatial and kinematic parameters are generally unpredictable. The temporal-spatial and kinematic gait parameters can be estimated without using advanced tools which are required for the measurement of kinetic parameters. In most clinical settings where a prosthesis is fitted and adjusted, tools to measure and assess kinetic data, such as a 3D motion capture system with force plates, are not always available. To clarify this issue, techniques to guide the dynamic alignment process of transtibial prostheses based on kinetic data were developed. This technique demonstrated equivalent alignment outcomes when compared to conventional clinical alignment methods by prosthetists.

Socket reaction moments are external moments which are evaluated at the distal end of a prosthetic socket. Studies illustrated that the socket reaction moments in the sagittal and coronal planes are significantly impressed by sagittal and coronal alignment modifications, respectively, in individuals with transtibial amputation. Sagittal alignment changes were also suggested to affect socket reaction moments in the coronal plane. However, the effects of alignment changes in the transverse plane on the socket reaction moments are not known.

Traditionally, the rotation of the prosthetic foot is adjusted in such a way that it matches the contralateral limb during gait. However, it may also be important to consider the biomechanical effect of rotation on the amount and the direction of force exerted by the lever arm of the prosthetic foot. Extra toe-out compared to the contralateral side may not be symmetrical in appearance, but it may theoretically increase stability by widening the base of support. Therefore, there could be a trade-off relationship between symmetry and biomechanical considerations when adjusting the rotation of the foot [27].

1.4 Rehabilitation

Amputation is an extremely affecting condition, influencing patient’s wellbeing, mental and health status [28]due to functional loss, changes in mass distribution and alteration of coordination and proprioception[29].

Rehabilitation is a key factor and the most relevant process that allows the patient to overcome daily-life obstacles and tasks[28], [29]: it’s fundamental for it to be tailored according to patient’s needs[29]. The main purpose is making the patient independent again trying to resemble the pre-amputation quality of life. Functional gain must be the main focus as the restitution of ambulation and locomotive activity needs to be achieved by the use of a prosthesis[29].

For such a complex task a multidisciplinary team is needed, involving different professional figures and a strong collaboration with orthopedic technical services in order to understand patient’s desires[28], [29].

Rehabilitation outcomes are strongly related to amputee’s conditions, such as age, weight, and attitude. In particular, many studies tried to evaluate the obtained results as a function of age.

In 2013, Hershkovitz et al [30] tried to consider the rehabilitation outcomes for a set of elderly patients after one-year post discharge prognosis according to Functional Independence Measure (FIM), motor FIM (mFIM), rate of prosthesis fit and Length of Stay (LOS). It was observed that almost half of the patients were dead within the year and those with higher FIM and LOS were those with higher cognitive levels. Moreover, most of those that were eligible for a prosthesis underwent unilateral Trans-Tibial Amputation (TTA), showing higher LOS. In total, only 23% was considered suitable for prosthesis rehabilitation: the others could not manage to reach this phase due to comorbidities such as chronic renal failure, impaired cognitive function, low vascular supply, poor cardiovascular performance and high amputation level, thus leading to higher energy expenditure.

On the other hand, Chun et al [31] analyzed the prosthetic outcomes in TTA and Trans-Femoral Amputation (TFA) young patients after Sichuan earthquake. They noticed that in general adolescent have a higher potential to go back to pre-amputation quality of life, especially in TTA ones, reaching up to 90% of the total performance of a normal body. Decreased functionality was observed in those poorly involved into physical activity (mainly due to subsequent higher energy consumption) and due to ageing effect, both decreasing the overall quality of life.

Finally, also obesity effect was considered in [32]. Although a high Body Mass Index (BMI) has been proven to be a relevant parameter to consider mobility, that is lower for high-weight patients, and biomechanical reactions acting on lower limb joints, such condition doesn’t seem to have a high impact in general rehabilitation outcomes, meaning that it should not be considered as an obstacle.

The total rehabilitation process can be thought as subdivided in 5 main steps, that will be further deeply described[28], [29]:

1. Pre-amputation stage
2. Post-operative stage
3. Pre-prosthetic stage
4. Prosthetic stage
5. Follow-up stage

1.4.1 Pre-Amputation Stage

This phase is related to what happens before the surgical procedure. The patient in informed about his/her condition: different scenarios may show up, according to the amputation causes, as described in this chapter[29].

Kinesitherapy, involving bed exercises for healthy limbs and trunk, breathing exercises and aided ambulation, is already started in order to try to avoid further complications[29], [33].

From the psychological point of view, introducing the patient to successfully rehabilitated amputees might help[29].

Surgical planning, furtherly described in, is performed, requiring the stump to have:

- Adequate length
- Appropriate soft tissue distribution
- Fit shape for prosthetic equipment
- Enough leverage and stability

1.4.2 Post-Operative Stage

This phase starts soon after the surgical amputation is performed, until the wound is completely healed, lasting around 14 days [29]. It's common to have a tube in the stump to drain away all the excess fluid [33].

Special care is given to wound healing process, as the risk for thrombosis and embolism in this acute stage is still high [29]. Compression therapy and leg elevation are applied to speed it up [28], [29].

Churilov et al [34] tried to investigate and compare the role of providing the patient with a rigid or soft dressing for the stump, noticing that the former allows for earlier prosthetic fitting increasing wound healing process speed (almost doubling it) and reducing edema.

It is fundamental to prevent any knee contraction, reason why a proper bed position must be maintained and a wheelchair with a special board is provided. Knee must be kept in extended position [28], [29].

Kinesitherapy can also be started since the first day post-amputation, focusing on strengthening the healthy limbs and, in TTA case, knee extensors through isometric exercises, as they will be the key to success to maintain a correct joint mobility [28], [29].

First days training may include[33], [35], [36]:

- Stretching and ROM exercises
- Rolling on the bed, sitting and safe transfer to a chair
- Contractures prevention, to avoid tissue tightness that may limit knee's ROM

There are loads of exercises than can be performed. According to Northern Devon Healthcare, the main ones that can be performed while sitting or lying on bed in this phase are [35]:

- *Static quadriceps*: the patient keeps the leg straight while sitting pushing the knee's back toward the bed, holding this position (Fig. 1-17)
- *Straight leg raise*: leg is in front of the patient, he/she has to lift it, holding for some time and repeating the movement
- *Inner range quads*: sitting on bed, the patient place a soft object on the back of the knee, that due to gravity effect will be bent. He/she must straighten it for some seconds repeating the exercise for a certain amount of times (Fig. 1-18)
- *Hip adduction with resistance*: while sitting, he/she put a pillow between legs, trying to squeeze them together
- *Outer range quadriceps*: sitting on a chair, the patient keeps the hip still with his/her hands while trying to straighten the knee (Fig. 1-21)
- *Static gluteal contractions*: while lying, legs are straight, and buttock is squeezed.
- *Hip flexor stretch*: lying on the back, knee is flexed toward the chest holding with hands. The other leg is kept straight on the bed
- *Bridging*: while lying on back, pillows or towels are put behind the knee. By contracting abdominals, back is lifted up
- *Hip flexion and extension in side lying*: while lying on side, you first flex both knee and hip, then straighten it pushing It downward
- *Hip abduction in side lying*: patient lies on his/her side, bending the lower leg, then lifting the other leg with straight knee. (Fig. 1-20)
- *Knee flexion in prone lying*: while lying on stomach, knee is bent as much as possible, holding the position for some time (Fig. 1-19)

This phase is especially important, as after leg amputation a complex reorganization process takes place in the primary motor cortex of the patient.

A study in 2016 [37] compared bilateral corticomotor and intracortical excitability of primary motor cortex pre and post amputation by using transcranial magnetic stimulation. Patients prior amputation displayed a stronger short latency intracortical inhibition for the ipsilateral limb (the amputated one) and reduced long latency intracortical inhibition for the contralateral one whereas after amputation they had a reduced short latency on both sides and reduced long latency in the ipsilateral one.

Figure 1-17 Static quadriceps

Figure 1-18 Inner range quads

Figure 1-19 Knee flexion in prone lying

Figure 1-20 Hip abduction in side lying

Figure 1-21 Outer range quadriceps

Post-acute period therefore represents a critical window where brain may be eased up to adapt and organize, although at the moment it may not be fully exploited. Cortical environment is optimized, thus representing a key factor also in learning prosthesis mobility.

The whole system is consequently reorganized due to the altered biomechanics by influencing both hemispheres, even in unilateral amputation. Healthy limb misuse must be avoided to ensure a better gait ability, while preferring the use of the affected one. Wound healing process might be a limitation, but it was shown that early start of rehabilitation by using motor imagery and non-invasive brain stimulation could ease the task.

Verticalization is entitled as the main purpose, that's why already in the first few days the patient is also trained for balance, some assisted standing position, aiming at aided prosthetic ambulation with crutches around day 10 [29].

A total functional evaluation of the patient must be assessed, trying to follow a SMART (Specific, Measurable, Attainable, Relevant, Timely) paradigm for setting rehabilitation goals [28], [29].

1.4.3 Pre-Prosthetic Stage

After wound healing process is complete, the focus shifts toward preparing the patient to accept prosthesis [29]. It's fundamental for the wound to be totally healed and tissue swelling decreased. The patient also needs enough strength for healthy parts of his/her body [33].

Patient must be trained to bear stump strains with some strain conditioning exercises performed with kinesitherapy, progressively increasing them.

At the end of this phase, if no contraindications are present, the patient is provided with a prosthesis thus starting the related rehabilitation [29].

Early walking aid for gait re-education can be attempted using the so called PPAMAid, which basically is a sort of inflatable leg with a maximum inflation pressure of 400 mmHg [36], [38].

1.4.4 Prosthetic stage

The patient is finally provided with a tailored prosthesis. In this phase he/she must master prosthetic ambulation: the patient should be able to deal with applied strains on the stump and capable of managing the altered weight distribution with the contralateral limb.

Prosthesis bearing will soon be changed, as stump's shape is modified due to hypotrophy and edema reduction.

Muscles are furtherly reinforced, focusing on flexibility, cardiovascular training, transfer exercises, prosthesis verticalization and balance exercises.

They suggest a list of all possible exercises that can be performed [38]:

- Lateral weight shifting: the patient is put in between horizontal parallel bars. He/she must train the weight shifting from the healthy to the prosthetic limb. The effectiveness can be measured with scales under feet (Fig. 1-22)

- Forward/back weight shifting (Fig 1-23): this exercise is helpful for balance and orientation, by moving weight back and forward.
- High stepping: the amputee has to climb a stool with the non-prosthetic limb. This exercise builds up confidence and allows a better weight management.
- Throwing and catching: between parallel bars, a ball is thrown and caught by the patient, allowing him/her to manage balance. (Fig. 1-24)
- Obstacle stepping: the patient has to step over an obstacle, while standing between bars.
- Football: patient has to kick a ball with healthy limb, making the prosthetic leg as the weight-bearing one. (Fig. 1-25)
- Braiding: the amputee swings the leg backward and forward, in both sides. The higher the speed of the exercise, the more the balance compensation that needs to be achieved
- Single leg standing: it is performed on prosthetic side, enhancing balance

Some of the main activities that must be mastered are:

- Prosthesis donning and doffing
- Prosthesis-aided and prosthesis-transfer standing and sitting
- Ambulation
- Crossing barriers
- Climbing stairs and slopes (Fig. 1-26)
- Falling scenarios (Fig. 1-22)
- Getting in and out from a car
- Sport activities

[29], [38]

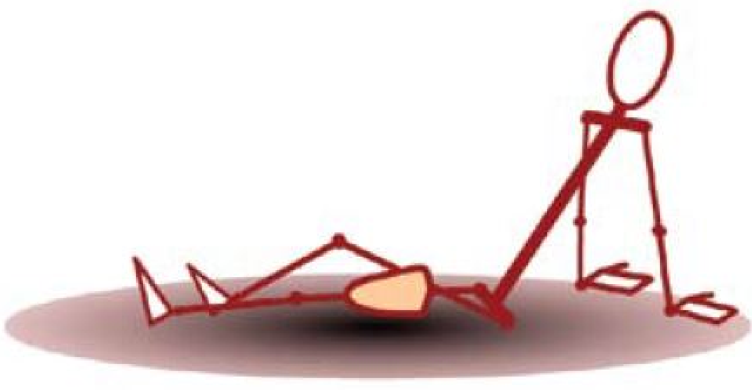

Figure 1-22 Falling scenario

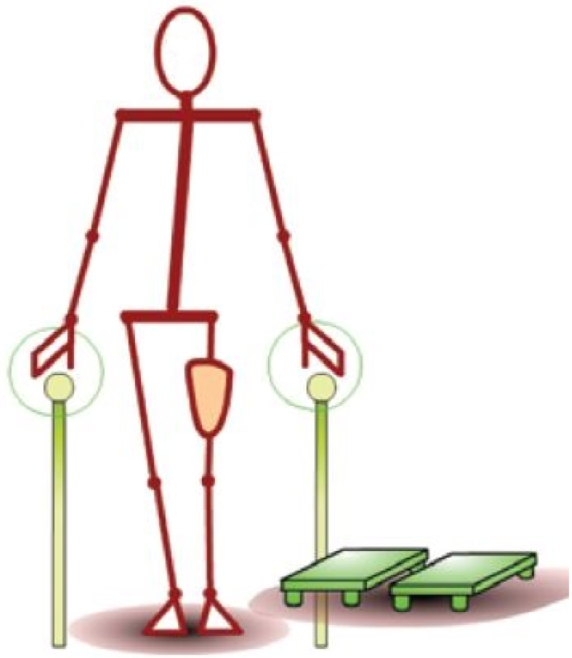

Figure 1-23 Weight shifting

Figure 1-24 Throwing and catching

As it was previously mentioned, plasticity is high in this phase, so it's advisable to act in this framework for better rehabilitation outcomes [39], [40]

In particular, obstacle crossing has been proved to be a good rehabilitation technique both for improvements and limb strengthening. It is shown that recent amputees are more receptive to adaptation by easily changing their obstacle-crossing strategy and leading limb [40].

Figure 1-25 Football

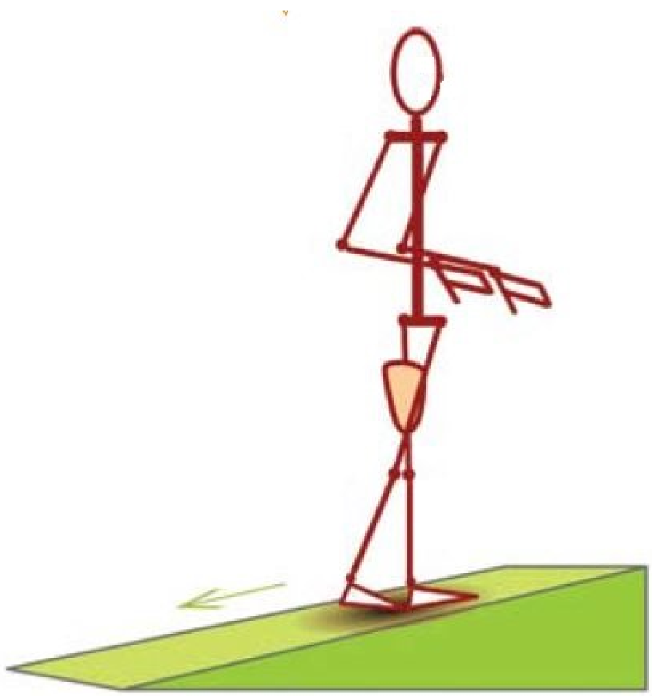

Figure 1-26 Climbing slopes

Therefore, TTA patients result in developing a greater flexibility, being less perturbated by walking pattern changes [39].

Some efficient testing tools in this phase can be the Six Minutes Walking Test and the FIM.

1.4.5 Follow-Up Stage

After successful prosthesis training the patient is finally released from rehabilitation, although such process may take months.

Independent gait, donning and doffing of the prosthesis must be mastered, and patient should aim at using the prosthesis in everyday activity.

The patient will be regularly monitored, keeping track on the follow-up and outcomes[29].

1.5 Biomechanics of human movement

As it was previously mentioned, amputation is a highly affecting condition for the patient. Therefore, walking patterns, applied loads and balances will be totally different once the patient will start walking again with his/her new prosthesis.

Gait cycle is commonly characterized by many phases:

- Initial contact (heel strike)
- Opposite toe-off
- Heel rise
- Opposite initial contact
- Toe-off
- Feet adjacent
- Tibia vertical

Of those 7 events, the first 4 are inside the so-called stance phase, the others represent the swing one [41].

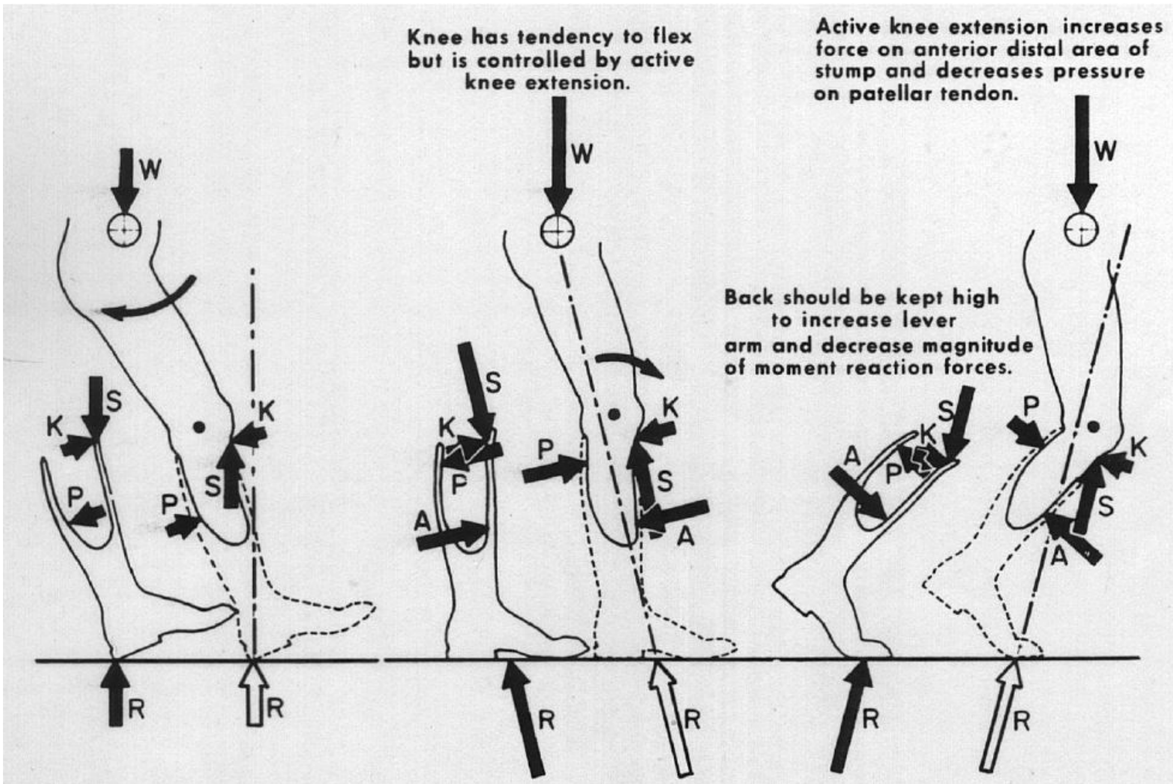

Figure 1-27 Reaction forces happening in the sagittal plane during gait cycle

We first consider what happens in the sagittal plane.

During heel strike phase, reaction force is partially discharged on patellar tendon. Ground force in this stage is headed in such a way that it would cause knee extension, due to its direction with respect to knee's center of rotation. To avoid bending, the patient needs to activate knee's flexors, causing a clockwise (Fig. 1-27) torque that is opposed by a reaction of the prosthesis. This will cause a higher-pressure concentration on the lower back part and in the upper frontal one of the legs, as shown in the left-most part of Fig. 1-27 [42].

Then, during stance phase, direction of reaction force will change, trying to flex the knee. At this point, the action of knee extensors is needed, causing a counterclockwise torque that is consequently translated into higher pressure distribution on the higher back part of the leg and on the lower frontal one.

The same situation is again repeated in the toe-off phase, where due to active knee extension pressure on patellar tendon is decreased.

We now consider the frontal plane.

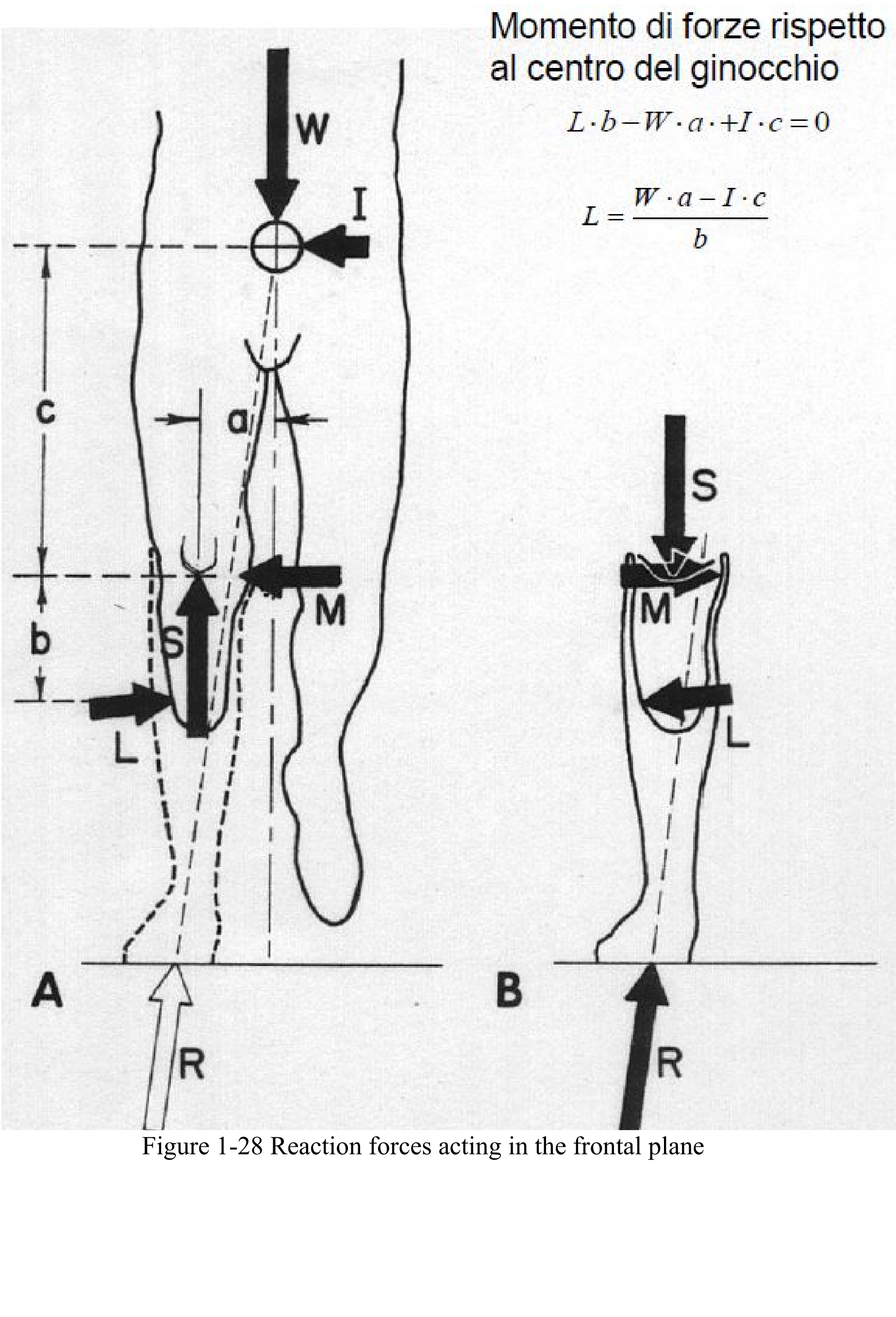

Figure 1-28 Reaction forces acting in the frontal plane

Due to inertial effects, reaction force is not perfectly aligned in the vertical direction but tilted. It is therefore balanced by bodyweight and an inertial component, both acting on the patient's center of mass as shown in Fig. 1-28 [42].

Considering the center of the knee as the rotation center, we evaluate the balance for the torque applied on the stump. Those forces require the socket to apply on the stump a lateral and a medial force component to equilibrate the whole system. The resulting equation is:

$$L*b-W*a+I*c=0$$

$$L= (W*a-I*c)/b$$

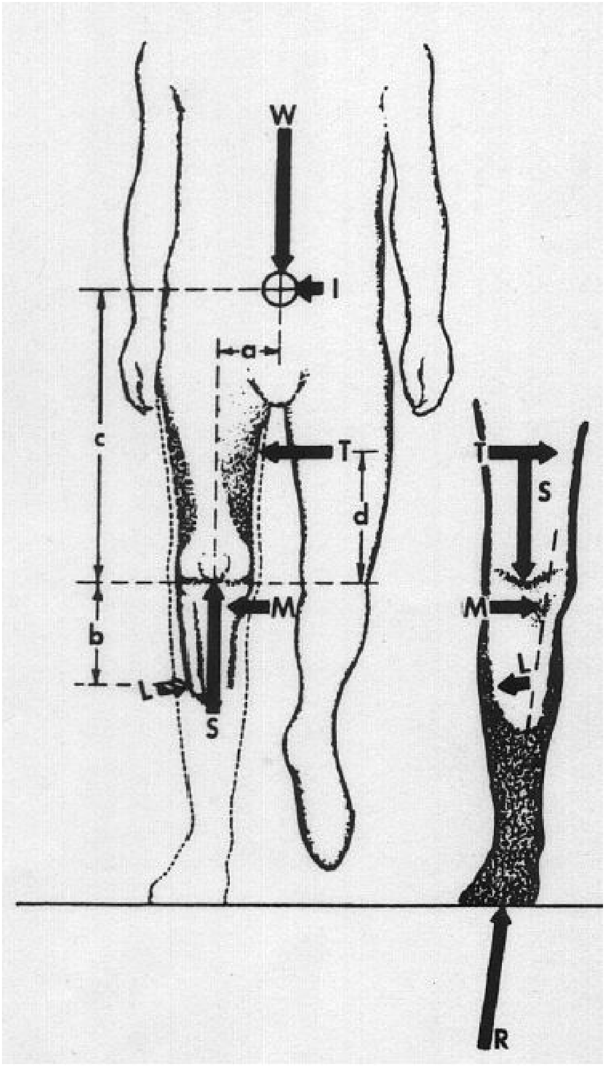

Figure 1-29 Effect of a femoral corset. A new force T is directly applied to the thigh, thus reducing the reactions on the knee

It is shown, from the computed equilibrium, that a short stump may cause higher reactions, thus representing a risk for patient's tissues.

In the worst-case condition, a femoral corset can be put on to reduce the forces, as a new force is going to be applied directly to the thigh as it can be seen from Fig. 1-29 [42].

1.6 Imaging techniques

In order to have a patient-specific model it is important to wisely choose the correct imaging technique, according to the purpose.

we will briefly deal with one of the main approaches in biomedical imaging, Magnetic Resonance Imaging.

1.6.1 Magnetic Resonance Imaging

Magnetic Resonance Imaging (MRI) (Fig. 1-30) is a non-ionizing imaging technique that allows to reconstruct 3D images providing a good contrast for soft tissues with high spatial resolution.

The whole process takes more time than CT, meaning that temporal resolution is lower. This may cause some artifacts due to movements of the patient.

It is relatively safe, although up to now there is no proof for possible biological effects. One of the main effects is actually heating of tissues: the scanner has to be set to not to overcome SAR (Specific Absorption Rate) safety values. Another common effect is Peripheral Nerve Stimulation (PNS), due to current in the tissue exceeding threshold values as a consequence of rapidly varying magnetic field.

The obtained signal comes from protons inside the body, that can be found in water (that may be present from 70% to 90% in most tissues) and lipids: each proton has a certain angular momentum, it can be ideally represented like a local magnet.

Given that, we can classify tissues in three main classes, according to their composition:

- Fluids
- Water-based tissues
- Fat-based tissues

The patient is put inside a magnet with a strong magnetic field (around 1.5 T), so protons may align in two ways with respect to it:

- Parallel
- Antiparallel

Protons will process around that direction, and their frequency, also called Larmor frequency or resonance frequency, is proportional to the strength of the applied static field.

The MR signal is obtained by using some specific pulse sequences, composed by RF pulses with Gs magnitude, arising the signal itself, and gradient pulses. Such RF pulse is also necessary to select the specific slice in use.

The spatial information is detected by taking advantage of magnetic field gradients. A linear variation is applied in all 3 directions, with the precise frequency being linearly dependent as well according to the location.

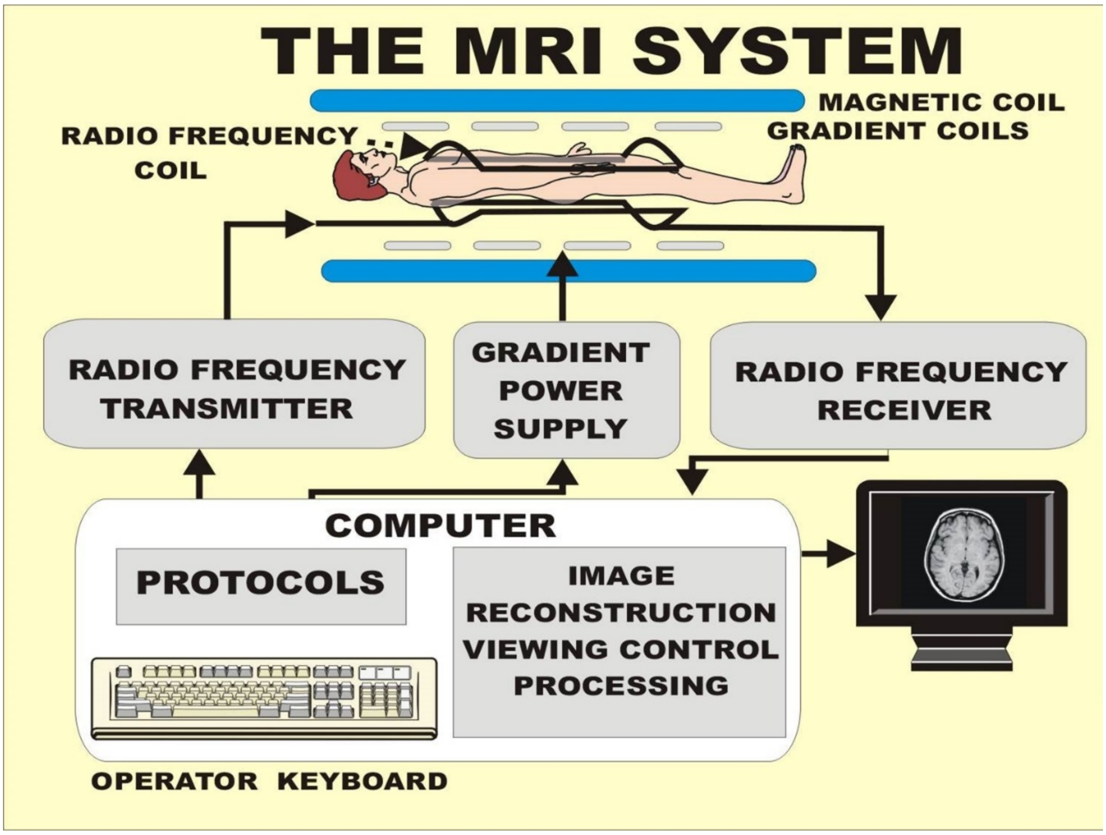

Figure 1-30 MRI system scheme

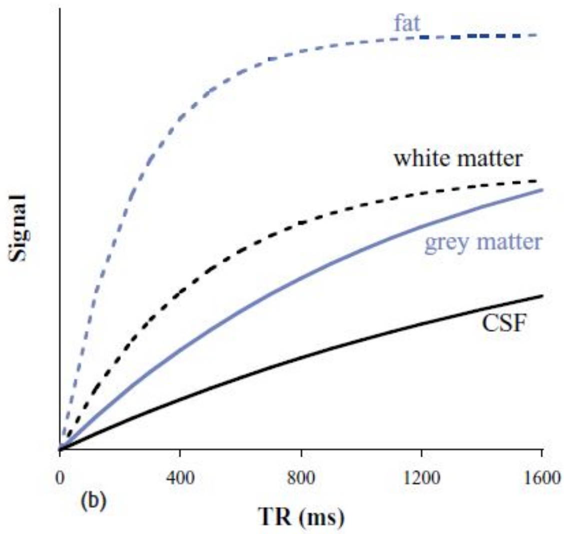

Figure 1-31 Signal intensity of some different tissues according to TR

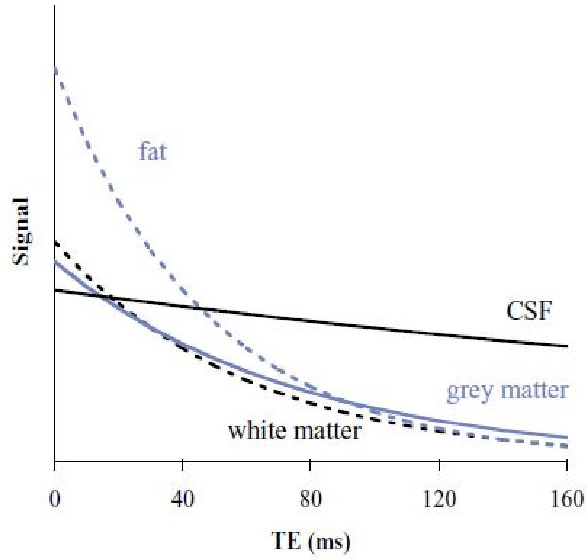

Figure 1-32 Signal intensity of some different tissues according to TE

Frequency and phase of protons are then measured with a RF coil and digitalized, finally applying 2D Fourier inverse transform to bring the signal back from frequency to spatial domain.

All kind of imaging sequences rely on the same parameters, that can be adjusted in order to set the contrast: TE and TR(Figs 1-31, 1-32) [43], [44].

1.6.1.1 Working principle of nuclear magnetism

Nuclear magnetism describes the interaction between protons and the applied magnetic field. In order to understand the leading working principle of MRI, we will first discuss about the quantum mechanics description, by successively passing to the classical description, to comprehend the origin of the signal.

Quantum mechanics description:

Spin is a property of all nuclei having an odd atomic weight or number. This property is particularly significant for MRI, considering the hydrogen. Basically, this property describes a proton spinning around an internal axis with an angular momentum P. As the proton is charged, this will produce a magnetic momentum μ that produces the magnetic field. Without any applied external field, they all have a random orientation.

The vector P is quantized, meaning that it can only assume some specific discrete values, according to the spin quantum number I (which depends on the total number of protons and neutrons in the nucleus):

$$|P| = \frac{h}{2\pi}\sqrt{[I(I+1)]} \quad (1)$$

And the magnetic momentum is related to is as following:

$$|\mu| = \gamma|P| \quad (2)$$

with γ representing the gyromagnetic ratio of the nucleus.

Classical description:

We now consider the interactions between protons and magnetic field. Let's consider applying a static B_0 field. The magnetic momentum will have a certain angle with respect to that, originating a torque T:

$$\vec{T} = \vec{\mu} x \overrightarrow{B_0} = \overrightarrow{\iota_n}|\mu||B_0|\sin\theta = \frac{d\vec{P}}{dt} \quad (3)$$

According to that it is possible to compute the precession frequency[43].

1.6.1.2 Magnetic resonance signal

In NMR the signal is given by the sum of the individual signals coming from each proton.

In order to have MRI signal you first need to induce a transition between protons at two energy levels: such energy is provided by an oscillating electromagnetic (EM) field with a defined energy gap ΔE considering the resonance frequency. You have to use a single pulse or Radiofrequency (RF) pulse to accomplish the objective.

There are two main types of pulse sequences:

- Spin echo (SE)
- Gradient echo (GE)

After the stimuli, each component of the magnetization components M= (Mx, My, Mz) should return to their thermal equilibrium value over time. This relaxation process depends in two main parts:

- Spin-lattice relaxation time (T1) for Mz: the proton is losing energy due to the surrounding lattice
- Spin-spin relaxation time (T2) for Mx and My: you have a decay of transverse magnetization, due to loss of phase coherence

Different kind of images are produced by considering relaxation times, the main ones are here described:

- T1-weighted images: they may derive both from SE and GE sequence. A short TR is adopted, in order to better differentiate the T1 parameter among tissues thus enhancing the contrast. Those images are called anatomy scans, as boundaries between tissues are better displayed.
- T2-weighted images: even in this case, the image may be produced both by SE or GE sequence, although the latter is affected by magnetic field inhomogeneity. A long TE and TR are required, thus increasing acquisition time. Fluids are here better displayed.

The RF pulse is applied with ωs frequency altogether with a magnetic gradient to localize the slice, with a certain bandwidth $\pm\Delta\omega s$, so all protons with resonant frequency falling within this range will be affected. The thickness of the slice is defined as:

$$T = 2\Delta\omega s/\gamma Gs \tag{4}$$

Paul Lauterbur in 1973 discovered that applying a short term magnetic spatial variation you would obtain a range of proton resonant frequencies depending on the position of the proton in the body. Gradient coils are needed to perform this task, one for each direction, with a controlled pulse sequence. This feature is the one causing loud noises, requiring ear protection as they may exceed safety values.

The B0 static field is directed in the head-to-foot direction of the patient, meaning the z axis. Then, by convention, x axis represents right-to-left and y axis is the spine-to-abdomen direction.

The z component is the only one that has to interact with the magnetic moment of protons, so Gz is the most relevant parameter, given that:

$$Gz=\partial Bz/\partial z \tag{5}$$

Considering the origin of the reference system, in which X= (0,0,0), there is no difference in the field with respect to the applied B0. Considering points along the z axis, the applied magnetic field will be:

$$B_z= B_0+zG_z \tag{6}$$

$$\omega_z= \gamma B_z \tag{7}$$

The same holds also in other directions.

According to the position, the phase of nuclei will be different:

$$\varphi= \gamma G_{slice}\ z\ \tau/2 \tag{8}$$

with τ representing the duration of the pulse.

To finally obtain the matrix representing the image in spatial domain, the signal needs to be phase encoded and frequency encoded [43], [44]. The whole process is depicted in Fig.1-33.

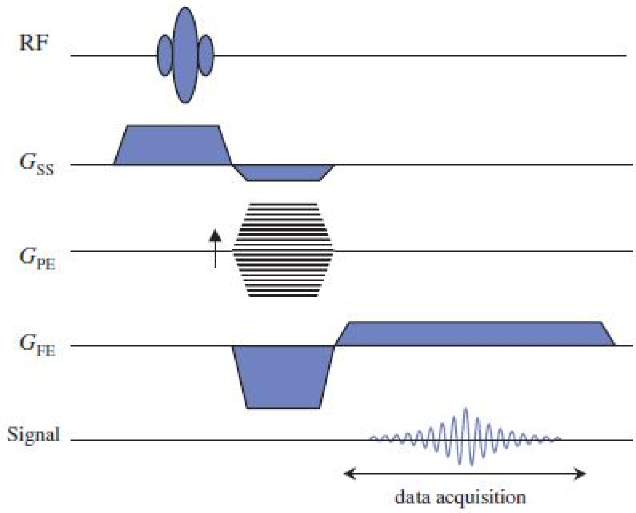

Figure 1-33 Standard GE acquisition pattern. Gss is the slice selective gradient, Gpe is the PE gradient, Gfe is the FE gradient

1.6.1.3 K-Space description

The image is basically represented by pixels and voxel (Fig 1-34). The data will be collected as a $N_r x N_p$ matrix. In order to describe it, k-space model is necessary.

N_r and N_p refers to frequency encoding (FE) axis and phase encoding (PE) axis.

Every time an acquisition is performed, a line in the FE direction is filled. This needs to be repeated line by line, along the PE direction, to fill the k-space: this means the PE gradient will be changed at each repetition, thus affecting the total acquisition time, as the higher the number of repetitions, the longer the acquisition will take. As each PE acquisition is performed in different time frames, along this direction some motion artifacts may be displayed.

Pixel dimension is determined by PE and FE values. The final voxel is obtained by also adding the pixel thickness, that is related to the slice thickness.

Let's consider the following coefficients:

$$k_x = \frac{\gamma}{2\pi} G_x t k_y = \frac{\gamma}{2\pi} G_y \tau_{PE} \qquad (9)$$

with Gx accepting only positive values, Gy going from the maximum negative to the maximum positive, x being the FE direction and y being the PE direction.

Our signal can be represented as equation 10:

$$S(ky, kx) \propto \int_{slice}\int_{slice} \rho(x, y)e^{-jk_y y}e^{-k_x x}dxdy$$

You can finally use the inverse Fourier transform to obtain ρ(x, y), to have the spatial distribution of proton density variation.

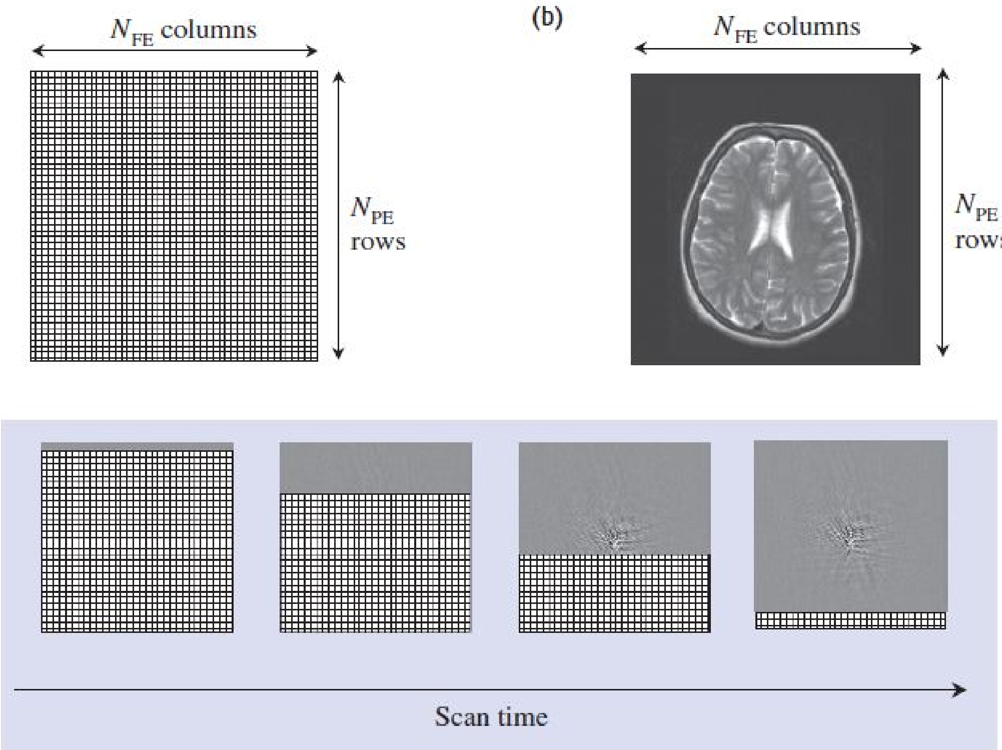

Figure 1-34 k-space representation

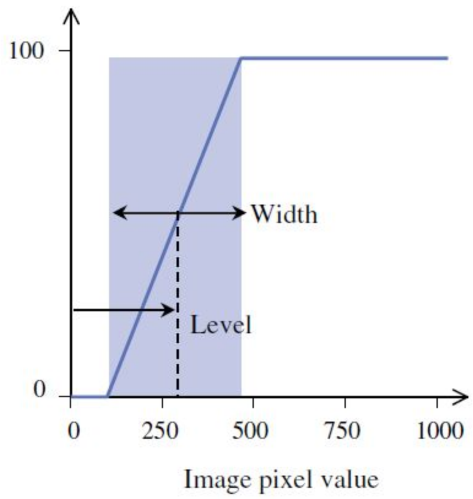

Figure 1-35 LUP characterized by a certain level and window width

Each pixel contains the MR signal intensity. As human eye is just able to distinguish a certain interval of grey levels, the range of values is compressed thanks to a Look Up Table (LUP) that allows to adjust the brightness. One of the most common LUP requires pixels above a certain threshold to have the highest brightness, pixels below noise level to have minimum brightness and in between a steep slope allows to expand the remaining levels within the whole range. This LUP(Fig. 1-35) can be adjusted according to window width (range of displayed pixels) and level (central value of window width)[43], [44].

1.6.1.4 Instrumentation

The MRI scanner is usually composed by three main components:

- Magnet: to polarize protons, producing a constant and strong magnetic field
- Three magnetic field gradient coils: they give the linear variation of frequency according to the position, allowing to localize the signal
- RF coil: it provides an oscillating magnetic field for phase coherence and it also acts as a receiver for the signal due to Faraday induction[43], [44].

1.6.1.5 Imaging sequences and image characteristics

The resulting image may display some noise, meaning that there might be some randomly different pixel values.

The grey intensity varies according to T_R and T_E: by tuning them you can try to maximize the contrast. Although you should consider that by reducing T_R the Signal-to-noise-ratio (SNR) is reduced, while total imaging time is given by $T_{TOTAL} = N_P T_R$ and increasing T_E contrast is enhanced but SNR is once again decreased. This means that a trade-off among all parameters must be found, to obtain the best image quality.

Image's features and grey levels are dependent on some specific tissue properties: in particular, signal depends on the mobility of molecules that can be more or less free to oscillate. This means that viscosity is the leading parameter allowing to distinguish one kind of tissue from the other.

So, what has to be found is a trade-off among:

- SNR
- Contrast-To-Noise-Ratio
- Spatial resolution

[43], [44]

1.6.1.6 Artifacts

The main causes can be divided into the following main topics:

- Motion artifacts, usually appearing along the phase encoding direction. Most of the time, movements are due to patient discomfort during the long scan time. Also, physiological motion plays a relevant role, for example in respiration, peristalsis, heart beating or blood flow. The image appears blurred.
- Fat excess, as fat is usually shown with high brightness
- Cross talking, as due to human complexity each voxel will physically contain more than one kind of tissue.
- Inhomogeneity artifacts, causing changes in signal intensity and distortion
- Digital imaging artifacts, that may show themselves with many faces [43], [44]

1.6.1.7 Clinical applications

The main clinical applications for such this technique are:

- Brain imaging
- Liver imaging
- Muscoloskeletal system (Fig. 1-36)
- Cardiac system [43]

Figure 1-36 Knee MRI

1.7 Anatomy of the lower limb

This chapter is also meant to describe the most relevant and important anatomical features that were considered during MRI segmentation. The main bones and involved muscles are briefly depicted, to furtherly understand their functions and role in the lower limb.

The main function of lower limbs is supporting the weight of the body with minimal expenditure of energy. This purpose is fulfilled also thanks to the knee joint, able to lock itself while standing. Moreover, locomotion is another fundamental property, that allows the body to move through space. In Fig. 1-37 the normal gait cycle is depicted. Hip joint movements are flexion, extension, adduction, abduction, rotation and circumduction, while knee and ankle joints can be summarized as hinge joints, although knee shows a sort of translation, with ankle being able of dorsiflexion and plantarflexion and knee capable of flexion and extension. Even in this case, minimal energy expenditure is the main goal, obtained by reducing the total fluctuation of center of gravity to 5 cm[45].

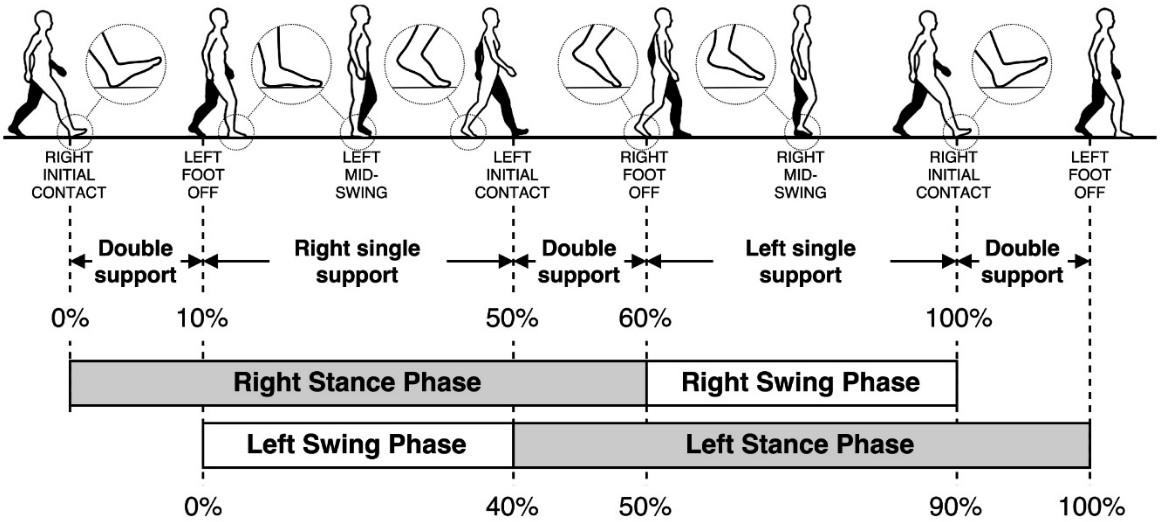

Figure 1-37 Gait cycle

1.7.1 Bones

The bones that were considered are four in total: femur, tibia, fibula and patella.

Femur

Femur is the longest and strongest bone in the skeleton [46]and it's the bone of the thigh [45]. It is composed by a body and two extremities [46]and the middle part of the shaft has triangular cross-section [45]. The distal extremity (Fig 1-38) is larger than the proximal one,

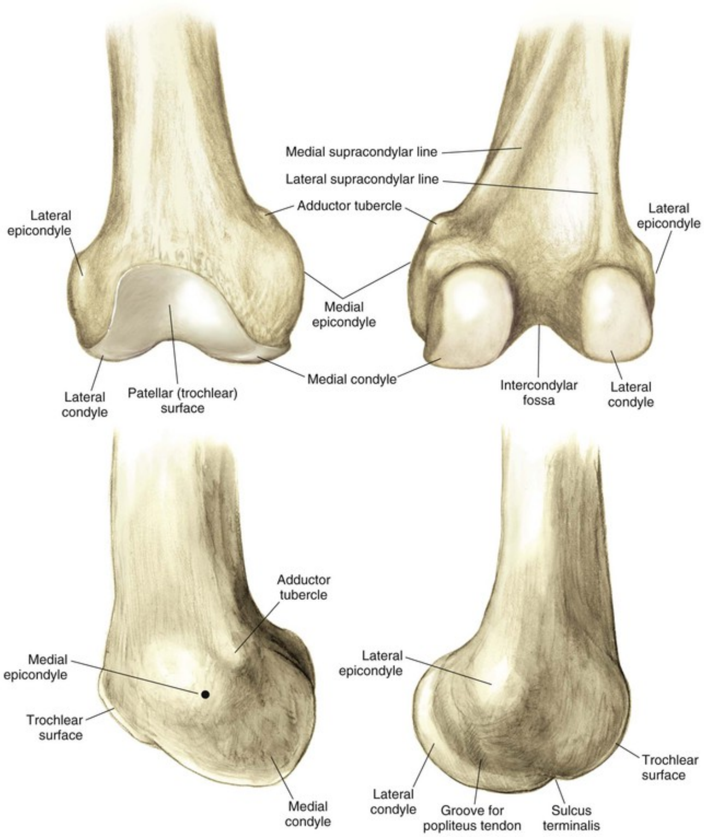

Figure 1-38 Distal end of femur

and it shows two prominences called condyles. On the anterior part, condyles are separated by a smooth articular surface, the patellar surface, while posteriorly there is a deep notch called intercondyloid fossa. Lateral condyle is broader, while medial is longer. Articular surface is also present in lower and posterior parts of condyles, called tibial surfaces. The complex structure of knee joint is stabilized by ligaments: the proximal part of posterior cruciate ligament attaches to the lateral surface of medial condyle, while the anterior cruciate ligament is attached to the medial surface of lateral condyle. That is the most weightbearing articulation [45]. (Fig. 1-39)

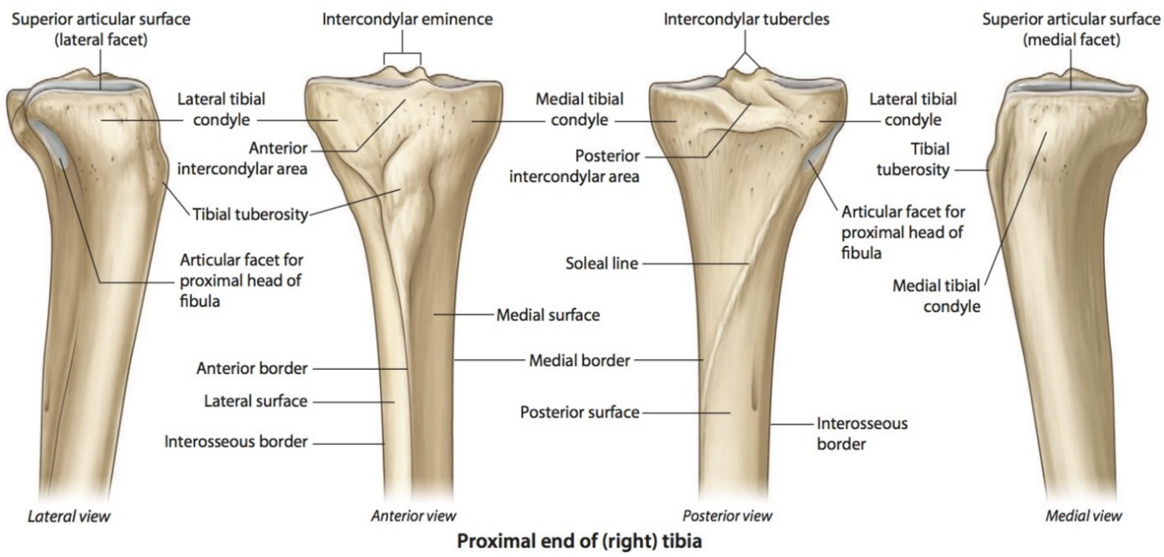

Figure 1-39 Proximal end of tibia

Tibia

Tibia is located on the medial side of leg, it is a bone with prismoid form. It is vertical for men while a bit more oblique for women to compensate the obliquity of femur. It has body with two extremities, distal and proximal. Upper one is large and expanded in two condyles, medial and lateral. Here there are two smooth and concave articular surfaces, whose central portion articulates with condyles of femur. Interarticular discs are present, called menisci, made of fibrocartilage. They are separated by and intercondylar region where cruciate ligaments are attached [45], [46].

Slightly below, there is a sort of elevation called tibial tuberosity, where the patellar ligament is attached.

The lateral border, also called interossus crest, is thin and originates the interossus membrane, where you can find the attachment between tibia and fibula. In the upper part of the posterior surface a ridge can be found, that represents the popliteal line.

Tibia represents the weightbearing bone [45], [46]. (Fig. 1-39)

Fibula

Fibula is positioned on the lateral side of tibia, connected both above and below, and smaller than the latter. Upper part is below knee level, so it doesn't interact with this joint. Upper extremity, the head of fibula, is irregular and quadrate, with a pointed apex on the lateral side. A superomedial facet articulates with the inferior aspect of lateral condyle of tibia [45], [46]. (Fig. 1-40)

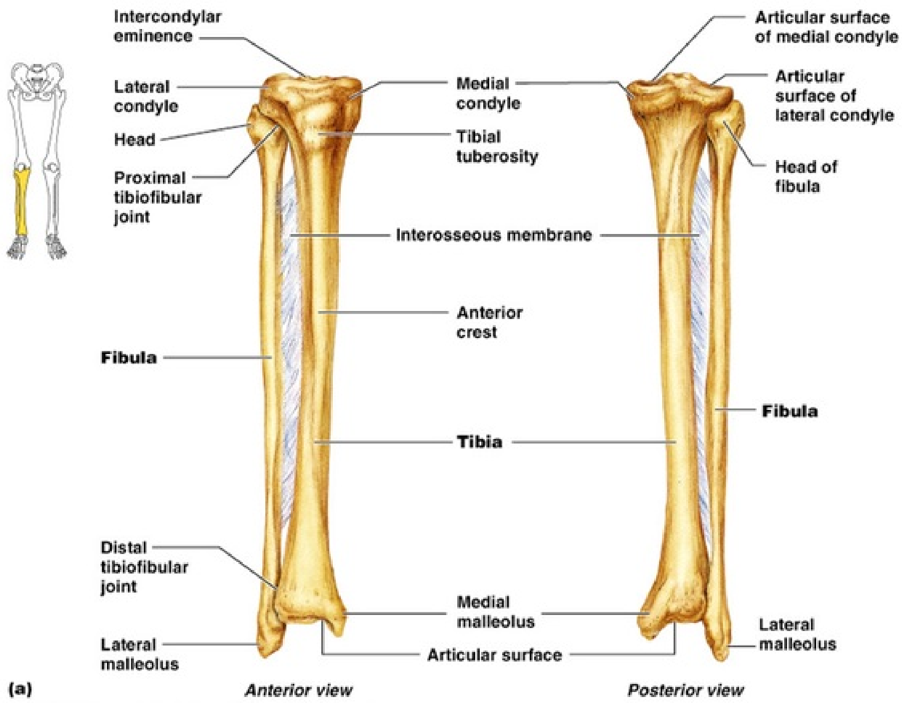

Figure 1-40 Fibula and tibia together

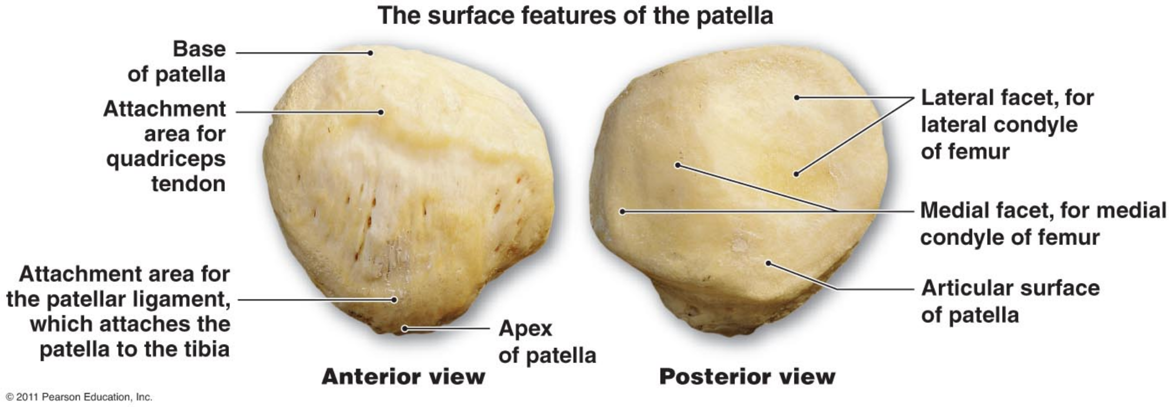

Figure 1-41 Patella

Patella

Patella is a triangular sesamoid bone (meaning that it develops from a tendon, in this case the Quadriceps one) located on the front of knee joint. Anterior surface is convex, and it is covered by the extension of tendon, that continues below from pointed apex with patellar ligament. Posterior surface is oval and articulates with femur. The base is broad, to allow the attachment of quadriceps tendon [45], [46]. (Fig. 1-41)

1.7.2 Muscles

The muscles of the lower limb can be divided according to their locations. Specific compartments in every location are specialized for specific functions:

- Thigh[45]:
  - Anterior compartment: mainly extensor of leg at knee joint
  - Posterior compartment: mainly extensor of hip joint and flexor of knee joint
  - Medial compartment: mainly adductors at hip joint
- Leg:
  - Posterior: mainly flexor of leg
  - Anterior: they mainly dorsiflex the foot, extends toes and inverts the foot

Sartorius

Sartorius is the longest muscle in the body and it is the most superficial one on the anterior compartment of thigh. It originates from anterior superior iliac spine. It crosses anterior part of thigh, then passing behind medial condyle of femur, finally ending in a tendon that inserts altogether with Gracilis and Semitendinosus in the upper part of medial surface of the shaft of tibia in the so-called pes anserinus. It flexes leg on thigh and thigh on pelvis. It also abducts and rotates thigh outward. It assists Semitendinosus, Semimembranosus and Popliteus in rotating tibia inwards[45]–[47]. (Fig. 1-42)

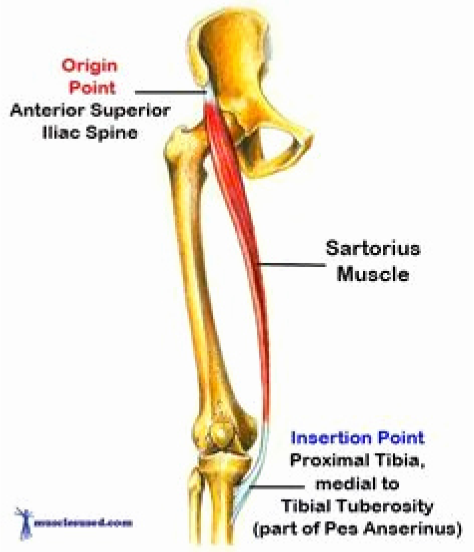

Figure 1-42 Sartorius

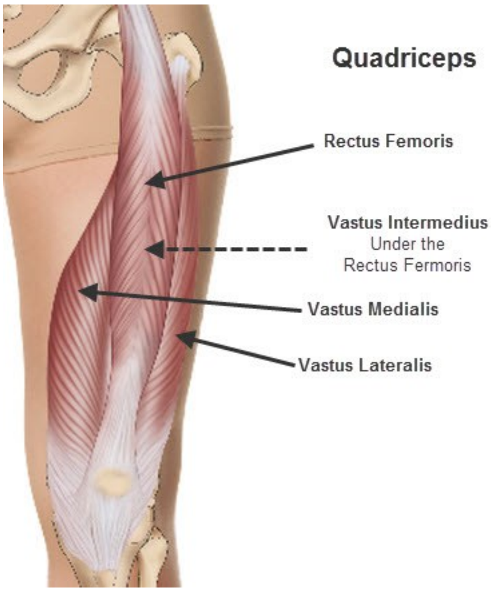

Figure 1-43 Quadriceps muscle

Quadriceps Femoris

Quadriceps Femoris is formed by four muscles, positioned in the frontal part of the thigh. It’s the main extensor of the leg, covering most of the anterior part of femur. As they all insert on margins of patella, they allow stabilization of its position[45]–[47]. The distinct muscles are:

- Rectus femoris: It is in the middle of thigh, with fusiform shape and bipenniform fibers. It originates from 2 tendons, one from the anterior inferior iliac spine, the other from a groove above the acetabulum[45]–[47]. The end of the muscle becomes a flattened tendon that inserts on the base of patella. It is a biarticular muscle, assisting flexion of thigh on pelvis[45], [46].
- Vastus lateralis: It represents the largest part of Quadriceps, attached to the upper part of intertrochanteric line and gluteal tuberosity. Its tendon is then inserted on the lateral side of patella[45], [46].
- Vastus medialis: It is originated from lower half of intertrochanteric line, medial part of linea aspera and proximal part of supracondylar line [47] and it is then inserted on the medial side of patella
- Vastus intermedius: it originates from upper 2/3 of anterior and lateral surfaces of femur, finally attaching to lateral margin of patella.[45], [47]

The tendons are then converged altogether forming a single strong tendon, the quadriceps tendon, that is inserted in the base of patella further blending with ligamentum patellae (going from patella apex to the tuberosity of the tibia)[45]–[47]. (Fig. 1-43)

Gracilis

Gracilis is the most superficial muscle on the medial side of thigh. It is originated from the ischiopubic ramus of pelvic bone. It is thin, broad and flat above, narrow below, descending along medial side of thigh. It furtherly flattens, inserting on the upper part of medial surface of tibia, with its tendon above the Semitendinosus and overlapped by Sartorius. It assists Sartorius in flexing leg and for inward rotation. It is also adductor of thigh[45]–[47]. (Fig. 1-44)

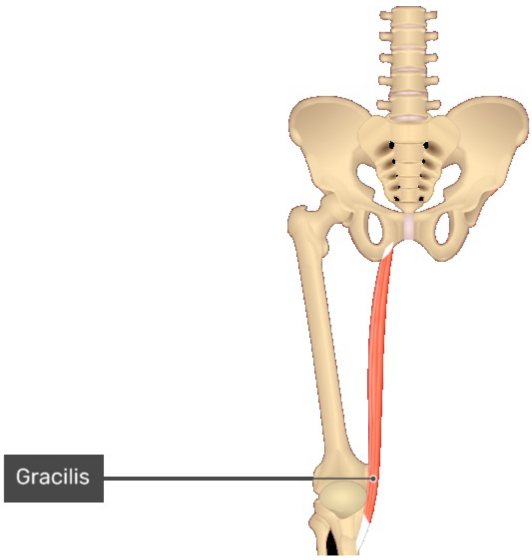

Figure 1-44 Gracilis

Biceps femoris

Biceps Femoris is situated in the posterior lateral side of thigh. It has two heads, long and short one. The long head is originated on the distal part of sacrotuberus ligaments and from the posterior part of tuberosity of ischium, while the short head starts from the lateral part of linea aspera and proximal 2/3 of supracondylar line. It consists in a fusiform muscle belly, gradually contracting in a tendon that is inserted in the lateral side of the head of fibula and by a small extent in the lateral condyle of tibia. With flexed knee it contributes to outward knee rotation. The long head also allows lateral rotation of hip. Altogether with Semitendinosus and Semimembranosus it forms the so-called Hamstrings, mainly responsible for leg flexion[45]–[47]. (Fig. 1-45)

Semitendinosus

Semitendinosus is situated in the posterior medial side of thigh. It is originated from the tuberosity of ischium, altogether with Biceps Femoris. It's a fusiform muscle, ending in a long round tendon lying along medial side of popliteal fossa. Its insertion is below Sartorius and Gracilis ones. It contributes to knee flexion and inward leg rotation. It also extends thigh at hip joint[45]–[47]. (Fig. 1-46)

Semimembranosus

The name is due to the membranous tendon of origin, located at back and medial side of thigh: it is originated from the superolateral impression of ischial tuberosity. Finally, it is inserted in the posterior medial side of medial and posterior condyle of tibia. It contributes

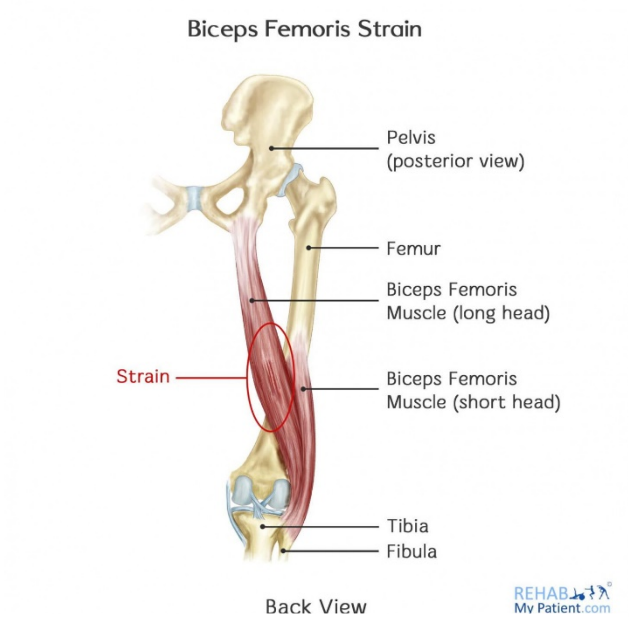

Figure 1-45 Biceps Femoris

to knee flexion and inward leg rotation. It also extends thigh at hip joint[45]–[47]. (Fig.1-47)

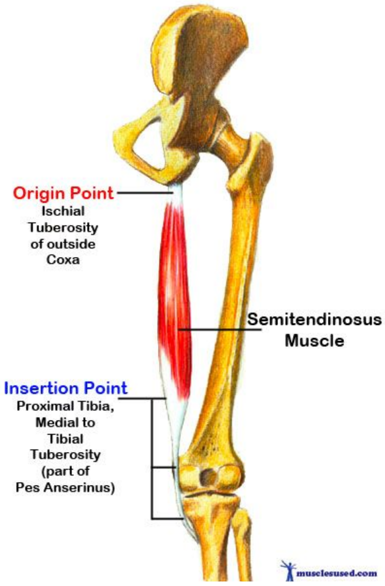

Figure 1-46 Semitendinosus

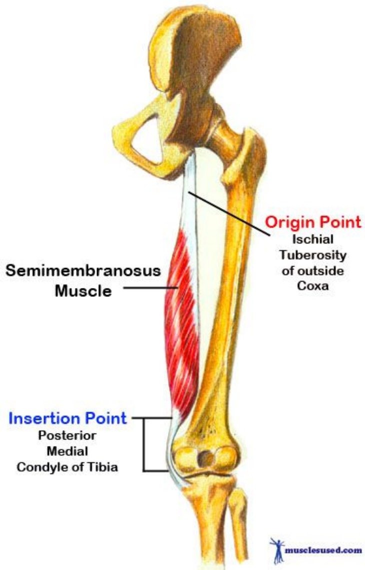

Figure 1-47 Semimembranosus

Tibialis Anterior

Tibialis Anterior is the most anterior and medial muscle located in the anterior compartment of the leg. It is positioned on the lateral side of the tibia, thicker above and tendinous below. It is originated from the upper 2/3 of lateral surface of tibia's shaft and the adjacent interossus membrane. The tendon is inserted in the medial surface of first cuneiform bone and base of the first metatarsal bone. It's flexor of foot and ankle joint (dorsiflexion)[45]–[47]. (Fig.1-48)

Extensor Digitorum Longus

Extensor Digitorum Longus is the most posterior and lateral muscle in the anterior compartment of the leg. It is a penniform muscle located in the lateral part of the leg. It is originated from the upper half of the medial surface of fibula, lateral condyle of tibia and adjacent intermuscular membrane. The tendon runs under transverse and cruciate crural ligaments. It is finally divided into four tendons, attached in distal phalanges of lateral toes. It extends phalanges, also flexing foot on the leg[45]–[47] (Fig.1-49)

Figure 1-48 Tibialis Anterior

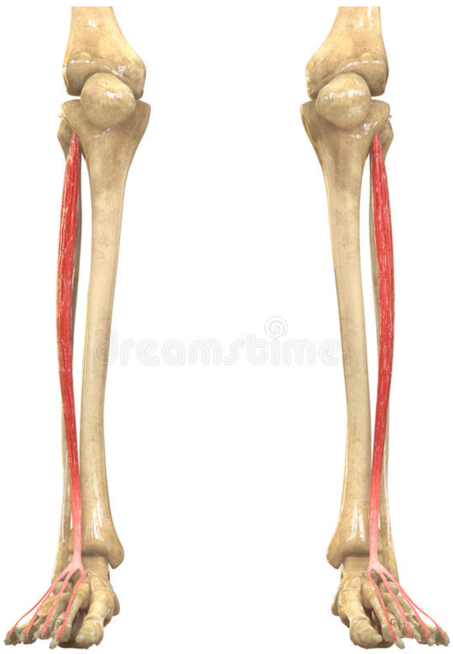

Figure 1-49 Extensor Digitorum Longus

Gastrocnemius

Gastrocnemius is a superficial muscle forming bigger part of calf. It originates by two heads, the medial one that is larger and the lateral one, connected to corresponding condyles of femur. Descending the heads unite, forming the so-called calf, furtherly expanding in aponeurosis, then contracting forming the tendo calcaneus with the Soleus. Gastrocnemius, altogether with Soleus, forms the so-called Triceps surae. It's extensor of foot at ankle joint and it's flexor of leg on tibia [45]–[47]. (Fig. 1-50)

Figure 1-50 Gastrocnemius

Soleus

Soleus is a broad and flat muscle in front of the Gastrocnemius. It originates from the back head of fibula and tibia and from soleal line. It gradually contracts into tendon, thus converging to the tendo calcaneus with the Gastrocnemius. It is extensor of foot at ankle joint and it is also important in steading the leg on foot preventing body to fall forward [45]–[47]. (Fig.1-51)

Popliteus

Popliteus is a thin, flat and triangular muscle, situated in lower part of popliteal fossa. It is the smaller of deep muscles in the posterior compartment. It is originated by the femoral groove on lateral condyle, it then descends medially passing behind lateral meniscus, then reaching the lower part of the knee. It is inserted on the posterior surface of the body of tibia, in an area proximal to soleal line. It assists flexion of leg upon thigh and inward leg rotation when tibia is flexed. It also unlocks the extended knee at the beginning of flexion, stabilizing it [45]–[47]. (Fig.1-52)

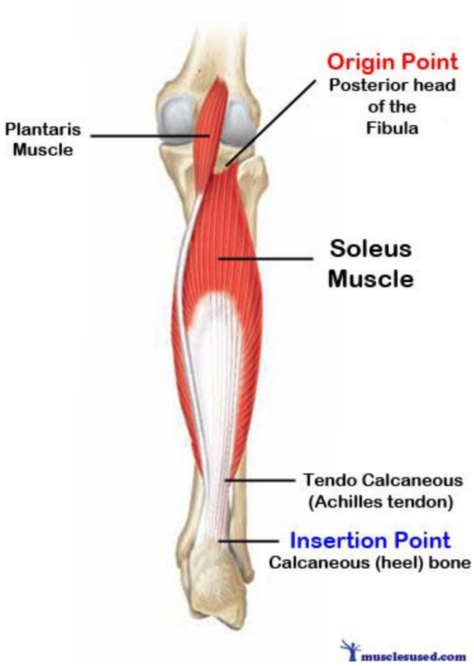

Figure 1-51 Soleus

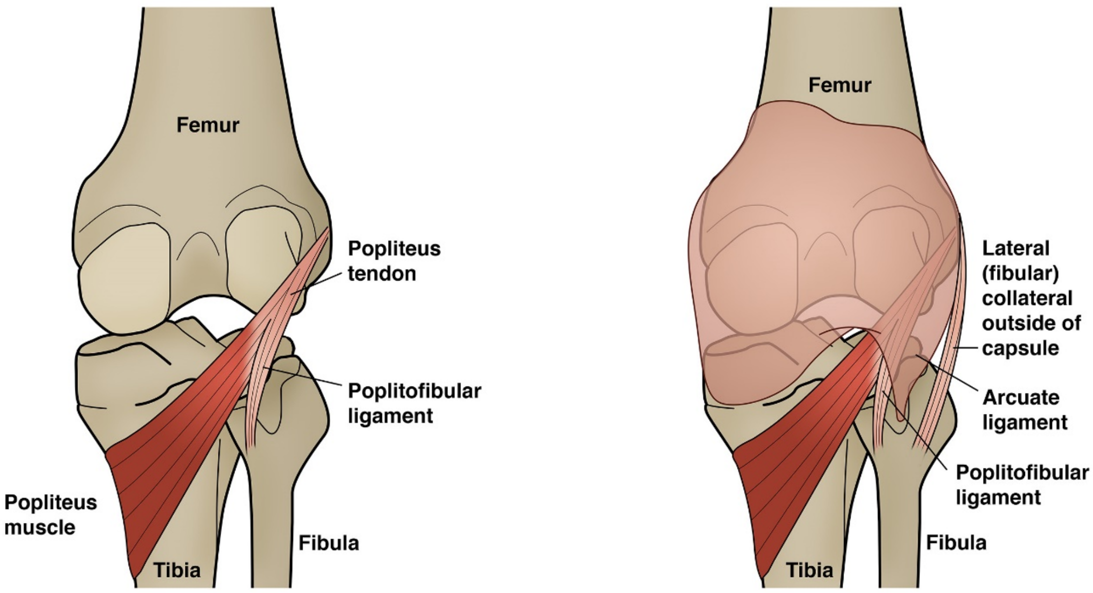

Figure 1-52 Popliteus

Flexor Hallucis Longus

Flexor Hallucis Longus is a long muscle located on the lateral and fibular side of leg. It originates from the inferior posterior surface of distal 2/3 body of fibula. The tendon inserts into the phalanx of the great toe. It is flexor of hallucis, also assisting in extending the foot (plantarflexion). It is crucial in the toe-off phase [45]–[47]. (Fig.1-53)

Tibialis Posterior

Tibialis Posterior is located between Flexor hallucis longus and Flexor digitorum longus, in the deeper part of leg. It is originated from posterior surface of interossus membrane and posterior surfaces of tibia and fibula. The tendon is then inserted in the tuberosity of navicular bone. It is an extensor of foot and ankle joint and it inverts the foot, also supporting the medial arch of the foot while walking [45]–[47]. (Fig.1-54)

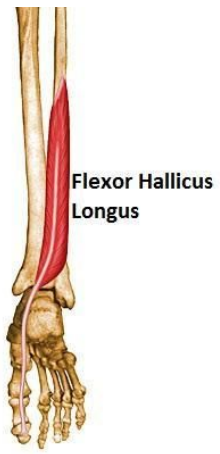

Figure 1-53 Flexor Hallucis Longus

Peroneus Longus

Peroneus Longus is located in the upper part of lateral leg. It is the most superficial muscle. It is originated from the lateral condyle of tibia, head and proximal lateral surface of fibula. The tendon ends behind lateral malleolus, in common with Peroneus Brevis, inserting on the lateral side of base of first metatarsal bone and medial cuneiform bone. It extends the foot on leg also everting the sole of foot [46], [47]. (Fig.1-55)

Figure 1-54 Tibialis Posterior

Figure 1-55 Peroneus Longus

1.8 State of the art in finite element analysis of lower limb amputation

The finite element investigation of residual limb is always conducted to further investigation of socket optimization, load transfer analysis, comparison of stresses with threshold values allows to diagnose deep tissue injuries (DTI) like ischemia or pressure ulcer in a patient. In fact, finite element analysis is numerical modeling which applied to the residual limb and provides profound information of socket design for prosthetists. It also accelerates rehabilitation procedure with less discomfort and treatment expenses. The state-of-the-art residual limb in finite element analysis which is assessed in literature can be categorized into[48]:

1. Residual limb- prosthesis interface mechanics
2. Mechanical properties of internal tissue of residuum
3. Finite element modelling of donning process
4. Identification of residual tissue characteristics
5. Analysis of the influence of prosthetic componentry concepts to improve load transfer to the residuum, such as the monolimb and structural socket compliance

These analyses are carefully evaluated to improve future modelling studies in terms of material, geometry, boundary conditions, interaction and so forth. Finally, the practical implementation of these issues is discussed. Fig. 1-56 illustrates [48]the numbers of articles have been published since 2000. They mainly assessed transtibial amputation, conventional transfemoral amputation and trans femora amputation treated with an osseointegrated prosthesis.

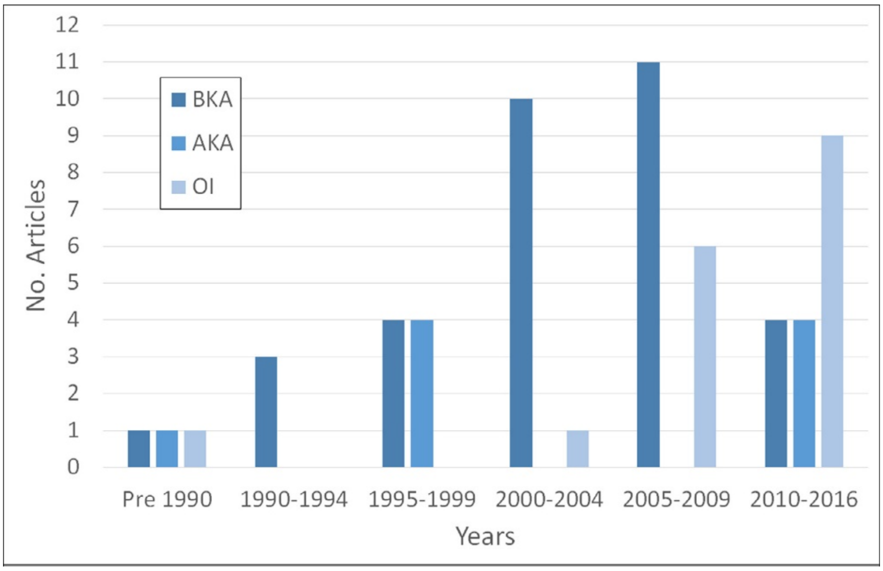

Figure 1-56 Articles and publication years related to the assessment of BKA (below knee amputation), AKA (above knee amputation) and OI (osseointegrated prosthesis).

The Cutting-edge in transtibial amputation research area copes with the progress in mesh and geometry optimization, different load scenarios, interactions, constraints and material properties and finally, monitoring and validation of the results with respect to the aim of the simulations. In this chapter we describe the most relevant development in these modules which delineated in literature.

Case 1 - Mechanical characteristics of prosthesis-residual limb interface

Zhang et la 2000 worked on the comparison of finite element modelling and experimental pressures and shear stresses, validated with triaxial force sensor. The model was below knee amputation (BKA) and the patellar tendon bearing socket was utilized for this assessment. The geometry of soft tissue was obtained via biplanar x rays. The static load of 800 N was applied to the model. The material properties of bone, soft tissue and liner were isotropic linear elastic with Young's moduli (G) of 15 GPa,260 KPa, 380 KPa and Poisson's ratios (v) of 0.3 ,0.49, 0.3 respectively. The socket was assumed a rigid body and the friction coefficient of μ=0.5 was considered at the interface of prosthesis and residual limb. The denouement of this work was the maximum 90 KPA of pressure at the patellar tendon and the maximum shear stress of 50 KPA at lateral tibia. Fig. 1-57 indicates the mesh structure of this model. The simulation was evaluated by employing the *ABAQUS* software[49].

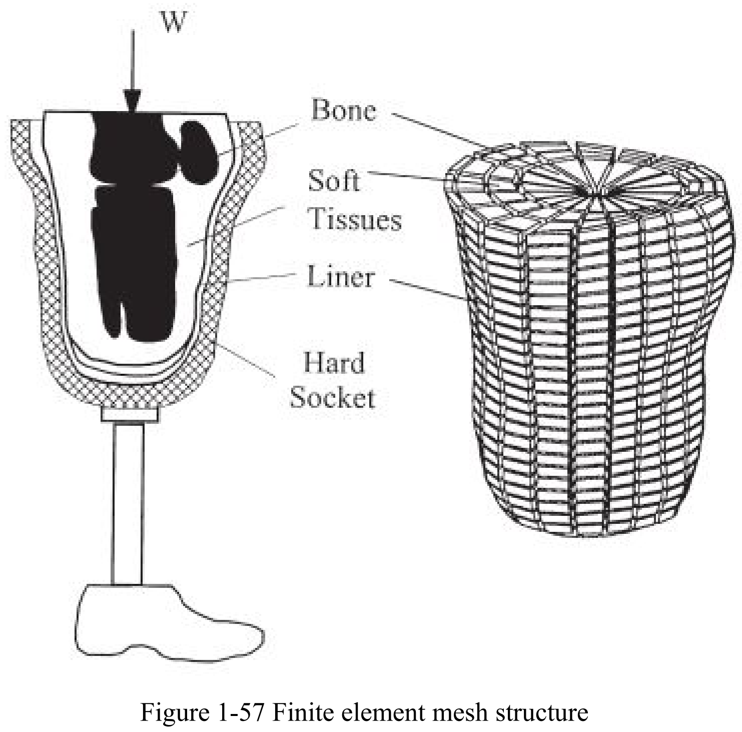

Figure 1-57 Finite element mesh structure

Wu et al 2003 carried out a research for socket design employing FEA, interface pressure and pain-pressure tolerance. The verification was followed by force sensing resistance sensors, the model was BKA and 3D surface acquisition was achieved by CT in a supine position. The static loads of 235N axially with scenario of two leg stance and 470 N axially with the assumption of single leg stance were imposed. The material properties of isotropic linear elastic were also considered in this model and the rigid body was accounted for the socket. They focused on two kinds of Kondylen-Bettung-Münster (KBM) and Total-Surface-Bearing (TSB) sockets. The model was meshed (Fig. 1-58) with brick elements (8 node hexahedral elements). The surface-to-surface contact elements were recruited at the interface between stump and socket. This type of contact element has better performance

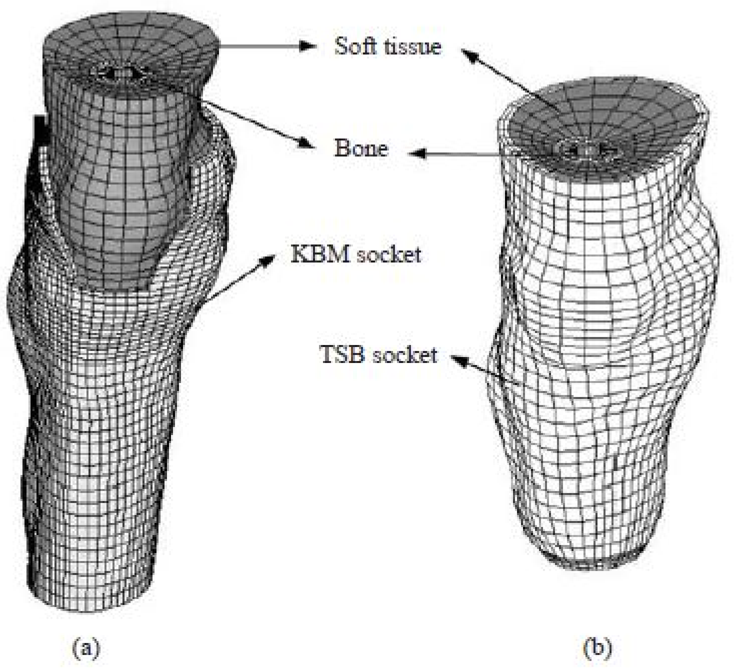

Figure 1-58 FE mesh structure of a) KBM socket and b) TSB socket

than the traditional point-to-point contact pairs in simulating sliding behavior within the stump-socket interface[50].

Lacroix and Fernandez Patino 2011 conducted the investigation of explicit (time dependent) model of prestress from socket fitting process. In this case, the model was above knee amputation (AKA). The 3D surface of the socket was accomplished from scan of the rectified cast. The image acquisition method for obtaining the surface body of bone and soft tissue was Computed tomography imaging. They worked on 5 patients. The load scenario was considered in a way that the donning procedure or displacement of socket was done at the velocity of 6-9 mm/s axially along the residual limb. The material property of the bone was isotropic linear elastic with G=15 GPa and $v = 0.3$. the soft tissue was supposed to be 3-parameter hyperplastic (Mooney-Rivlin) with coefficients of C_{10}=4.25 KPa, C_{11}=0 KPa, D_1=2.36 MPa^{-1}. Socket was considered isotropic linear elastic with G=1.5 GPa and $v = 0.3$. The friction coefficient between socket and residuum was assumed 0.425. what they obtained was the circumferential and longitudinal shear stresses and contact pressure. The interaction between socket and stump was surface to surface ABAQUS V6.10-2 contact condition, which avoid the penetration of stump node (slave surface) into the socket (master surface) when the displacement procedure was simulated. Due to the complexity of the geometry (Fig 1-59), the all model was meshed with tetrahedral elements[51].

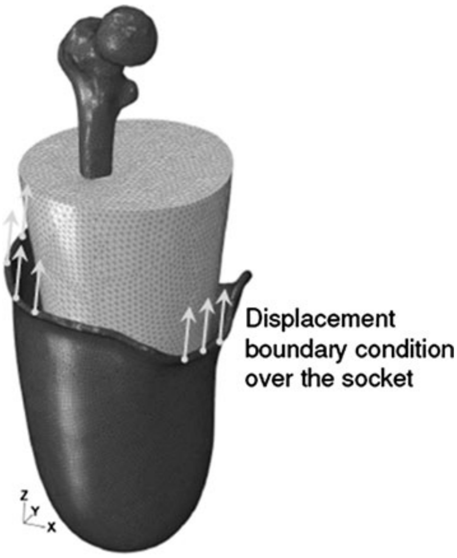

Figure 1-59 Relative position at the beginning of the simulation

Case 2 - Mechanical characteristics of residual soft tissue

Portnoy et al 2008 initially focused on the BKA. They extracted the 3D surface of the bones and soft tissue with open magnetic resonance. They considered the unrectified cast as socket. They characterized the mechanics of muscle flap after socket fitting process and with load bearing. The verification of the stress at the interface section was carried out by two thin film pressure sensors. The goal was to identify the risk for deep tissue injury (DTI) and improvement of donning procedure. The finite element modelling was followed in order to reach internal soft tissue stresses and strains in a female with transtibial ablation and during a static load-bearing condition. Movement of the truncated fibula and tibia during loadbearing was assessed by virtue of MRI and utilized as displacement boundary conditions for the FE model. consequently, the calculation of the internal strains, strain energy density (SED) and stresses in the muscle flap under the truncated bones were investigated. The bones were considered a rigid body in this "model and they were meshed with quadrilateral element(“SFM3D4”) in *ABAQUS* software. The socket was homogenous, isotropic linear elastic with G=1 GPa and $\nu = 0.3$. The skin was accounted as 2-parameter hyperelastic with coefficients of C_{10}=9.4 KPa and C_{11}=82 KPa. The constitutive behavior of muscle tissue was also depicted utilizing an energy function, but viscoelastic stress relaxation, which is considered important in static load-bearing, was incorporated. The instantaneous stress response of muscle was portrayed utilizing a neo-Hookean strain energy function:

$$W_{\mathrm{Muscle}} = G^{\mathrm{ins}}(I_1 - 3) \quad (1)$$

Where G^{ins}= 8.5 kPa is the short-term transverse shear modulus of nonpreconditioned muscle tissue. Viscoelasticity was then posited by virtue of a Prony series expansion:

$$S(t) = (1-\delta)\frac{\partial W_{Muscle}}{\partial E} + \int_0^t \delta \frac{\partial W_{Muscle}}{\partial E} e^{-(t-\xi)/\tau} d\xi \quad (2)$$

Where S is the second Piola–Kirchhoff stress, E is the Green–Lagrange strain, τ is the relaxation time constant and $\delta = 50\%$ is the percentage difference between tissue moduli at the instant of deformation and at the asymptotic response. Since they only account for tissue stress distributions at long terms (supposing that MRI scans took some minutes in order to acquire but most stress relaxation in transversally loaded skeletal muscle tissue already occurs within ~20 seconds; muscle stresses can be predicted as:

$$S \cong (1-\delta)\frac{\partial W}{\partial E} \quad (3)$$

Muscle tissue was meshed with second order 10-node modified quadratic tetrahedral elements(‘‘C3D10M’’). there is not any sip condition between muscle and bone. The skin is also meshed with 6-node triangular elements(“M3D6”). The cast was also meshed with “C3D10M” element type (Fig. 1-60) [52].

Ramirez and Velez work is related to finite element analysis of mechanical properties of residual limb by imposing boundary condition between muscle and bones (2012). They investigated this issue for transfemoral amputees. They considered two cases of boundary conditions between soft tissue and bone. At first attempt, they put tie contact between them and in the latter one they consider some friction with coefficient of μ=0.415 between bone

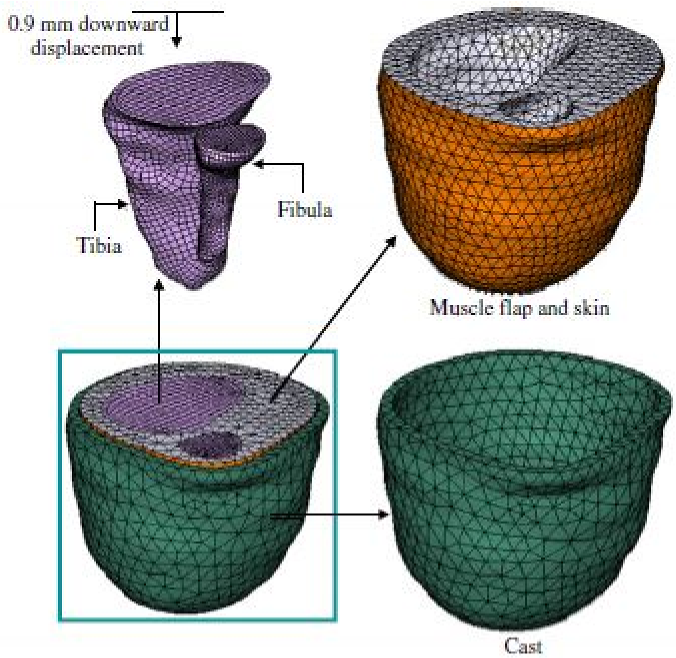

Figure 1-60 The finite element meshes of the tibia, skin, muscle, fibula and cast

and soft tissue. The 3D surface of socket and soft tissue were acquired through laser scans. And bone segmentation was achieved via CT scan technique. The load scenario was supposed to be socket preloading and quasi-static two leg stance (the 50% of body weight). The material properties of all bodies were presumed homogenous, isotropic, linear elastic. The Young's moduli of bone, soft tissue and socket were 15 GPa, 200 KPa and 1.5 GPa respectively. The Poisson's ratios were also 0.3, 0.475, 0.3 respectively. The result illustrated that the von Mises stress and strain in condition which friction existed was higher than the other case. Furthermore, the distribution pattern of strain and stress is different due to the variation of boundary conditions from tied to frictional contact. Due to the complexity of the model, the bodies were meshed with linear tetrahedral elements (Fig. 1-61) with four nodes(C3D4). It is also worthwhile to mention that the simulation was done by explicit module of *ABAQUS* software due to its better performance with respect to static and quasi static algorithms when there are kinematic nonlinearities caused by large deformations and the loading time has influence over the results[53].

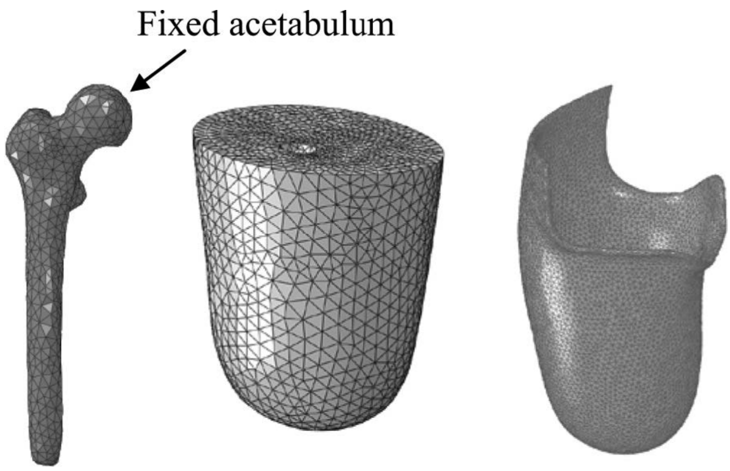

Figure 1-61 Finite element meshes of bone, socket and soft tissue

Case 3 - Analysis of osseointegrated prosthesis concepts

The concept of osseointegrated prosthetics has captured remarkable attention since 2000. This case can be accounted as a final main use of finite element analysis of lower limb amputation. Direct anchoring of the prosthetic limb to the residual bone in transfemoral amputation is provided by osseointegration. Two-step procedure is essential for this surgery. At first, First, an implant is located in the residual femoral canal, the amputation site is closed, and biological fixation is allowed to establish prior to a second procedure. Approximately 6 months later the distal bone tip is exposed again, and a skin-penetrating abutment or coupler is attached [54], [55]. Compared to socket suspension, OI prosthesis suspension is argued to improve function, gait motion and quality of life[56], to reduce the number of return visits to prosthetists and potentially the post-surgical rehabilitation cost [57]. Observed complications of OI prosthesis suspension has included early loosening, superficial infection, and occasional deep infection.

Stenlund et al 2016 hypothesized that the loads applied to the bone-anchored implant system of amputees would lead to locations of high strain and stress transfer to the bone tissue and hence contribute to complications including unfavorable bone remodeling, high inflammatory response or compromised sealing function at the tissue-abutment interface. In the study, site-specific loading measurements were made on amputees and used as input data in finite element analyses to predict the stress and strain distribution in the bone tissue[58].

CHAPTER 2 : PREPROCESSING

2.1 Segmentation

These days, researchers utilize the computer-based simulation and segmentation in order to assess pathologies, treatment in different scenarios. For instance, they investigate the deformation of bones and muscles in gait analysis. The simulation is meant to reach a good result if it is imposed on the best matched anatomical configuration of the patient. This performance can be achieved by virtue of segmentation and simulation set-ups.

The process of partitioning a digital image into multiple regions (set of pixels) is referred to the segmentation[59]. Each pixel includes the same property and characteristic. Thus, a set of regions which cover the whole image is the outcome of image segmentation. The aim of this procedure is to facilitate delineation of anatomical structure and other regions of interest[60].

In this project, bones, muscles and skin segmentations of five patients have been conducted. The *Mimics Medical 20.0* software has been employed to extrapolate the mentioned features in a 3D object for further simulations. It is worth mentioning that all patients suffer from transtibial amputation. The performances have been delivered by means of MRI imaging technique.

There are three main format of image files that are utilized including *DICOM*, *VTK* and *MHD*. The *DICOM* format was used in this investigation. *DICOM* stands for Digital Image Communication in Medicine. This version is very valuable for image exchanges in the medical field. This file format is developed by American association of radiologist and by national electrical manufacturers association. Fig. 2-1 illustrates the structure of *DICOM* file. The header can be existed or not. Data element is present and encodes the image [61].

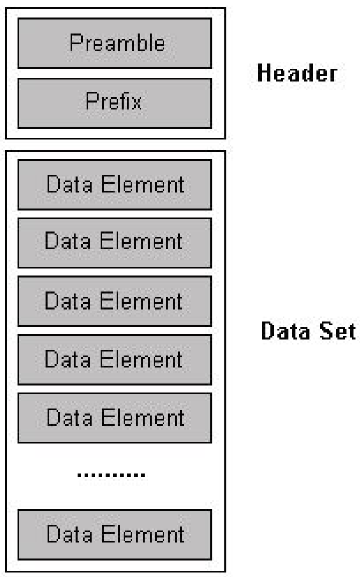

Figure 2-1 DICOM File Format

Materialise's Interactive Medical Image Control Systems (*MIMICS*), is a user-friendly 3D medical image processing and editing software. The extraction of full 3D cad models, finite element meshes from scanner images and surgical procedure simulations are processes that can be taken via this software. *MIMICS* can import the *DICOM* format file that are compressed with the *JEPEG* algorithm[62]. *JPEG* stands for Joint Photographic Experts Group, which was a group of image processing experts that devised a standard for compressing images (ISO)[63].

The *MIMICS* divide the screen into four views[62] (Fig. 2-2):

1. The original axial view
2. The coronal view
3. The sagittal view
4. The 3D view

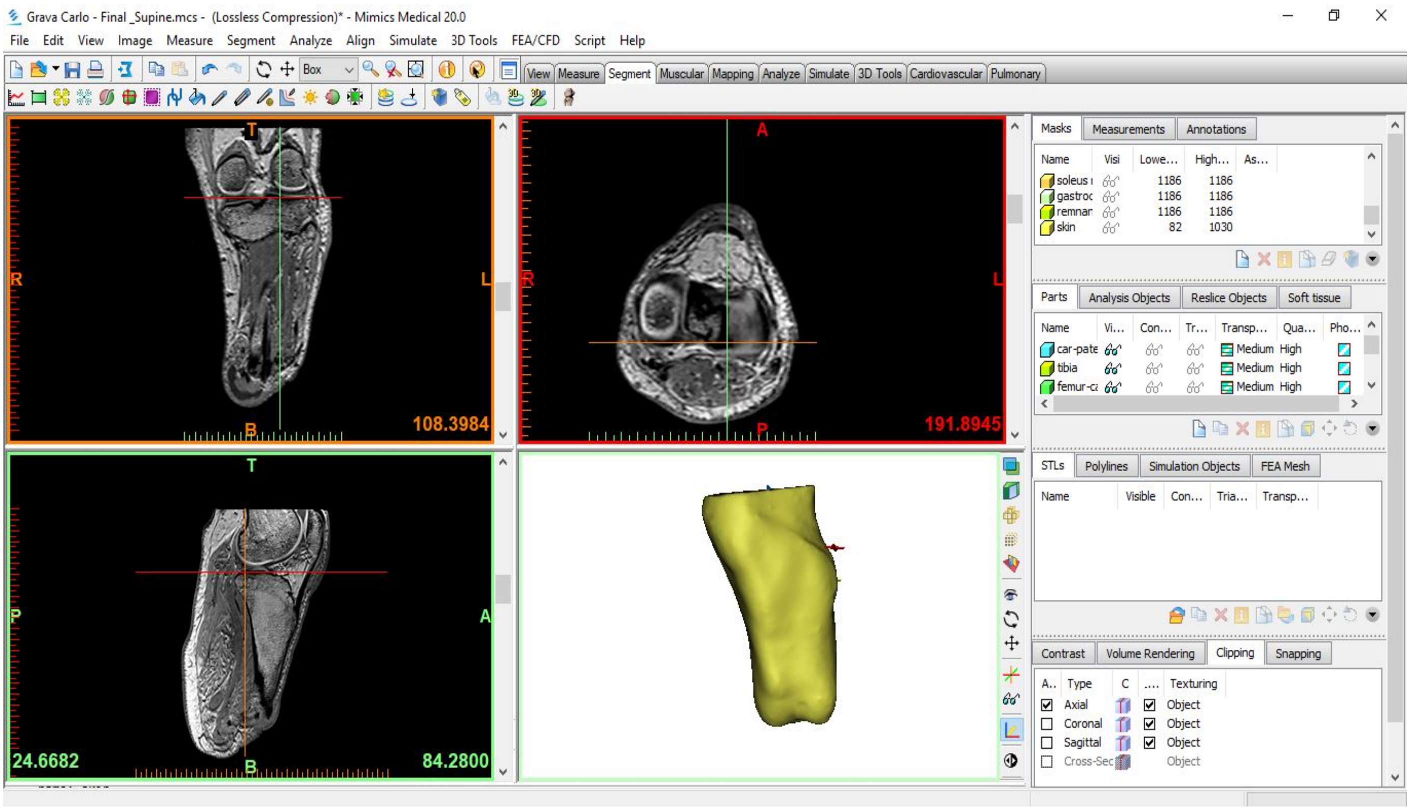

Figure 2-2 Various views of MRI images are loaded and registered in MIMICS. Top left (axial view), top right (Coronal view), bottom left (sagittal view), bottom right (3D view)

Some steps are taken into account in order to extrapolate the region of interest (ROI) which can be bones, muscles or skin. At the embryonic stage, it is necessary to create a mask with an appropriate name which is related to the part that is required to be extracted for instance, tibia, fibula, gastrocnemius muscle and so forth. Mask helps to highlight the tissue which is under assessment. After that, thresholding is the action which is proceeded to complete mask creation. The threshold adjustment should follow in a way that can cover the entire tissue which is the region of interest. Fig. 2-3 depicts the effort which is taken to put a threshold for tibia, patella and femur as a mask [62].

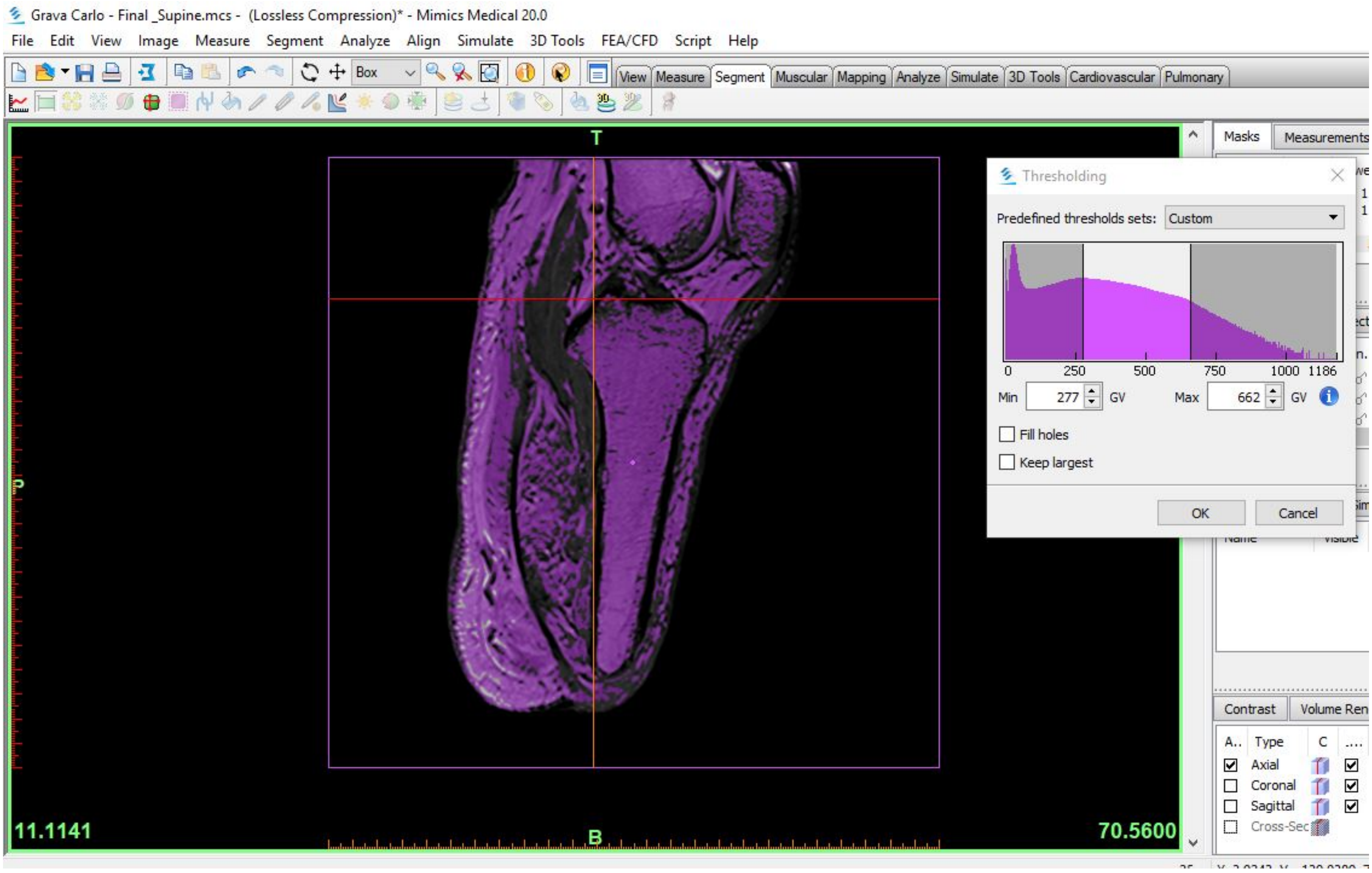

Figure 2-3 Thresholding attempt for lower limb bones

To achieve the accurate contour, some manipulations are required to restrict the highlight to ROI. Moreover, region growing tool is crucial to use in order to expunge noise and separate the structures which are not connected. In this example, femur, tibia and patella are bones that are not connected. Thus, region growing ought to be used and then create individual masks for each specific bone. From manual manipulation point of view, an editing tool which is called Multiple Slice Edit, is utilized to draw, erase or restore part of images with a local threshold value. Furthermore, the changes can be made on one slice to other slices in the multiple slice edit tool. This tool greatly reduces the amount of manual work needed to eliminate artifacts and separate structures due to the auto interpolation technique which is considered in this tool (Fig. 2-4)[62].

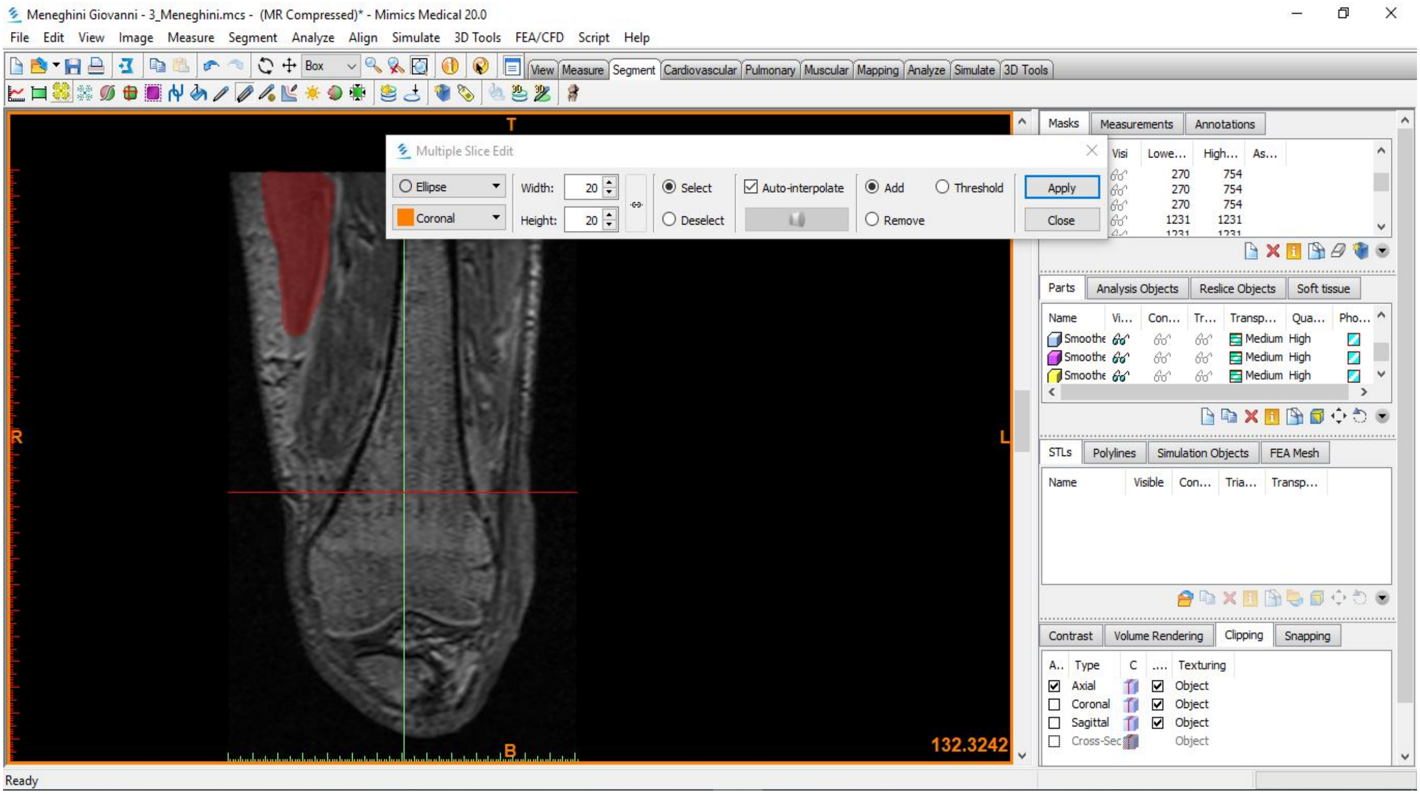

Figure 2-4 Multiple Slice Edit

When the desired part thoroughly highlighted by the virtue of aforementioned tools, then the calculate part tool is employed in the segment menu bar. This calculation can occur with a wide variety of qualities including low, medium, high or optimum. At this moment, the 3D part is created. But this is not the last step. Since the novel model is with discontinuities and rough surfaces (Fig. 2-5). Two last approaches are taken consecutively. Both tools are the subset of 3D tools menu bar. The first one is wrapping which helps to reduce noises, discontinuities and voids. Finally, smoothing tool which smooth the surfaces appropriately. Fig. 2-6 depicts the wrapped and smoothed part which is shown in Fig 2-5.

Figure 2-5 The novel 3D femur

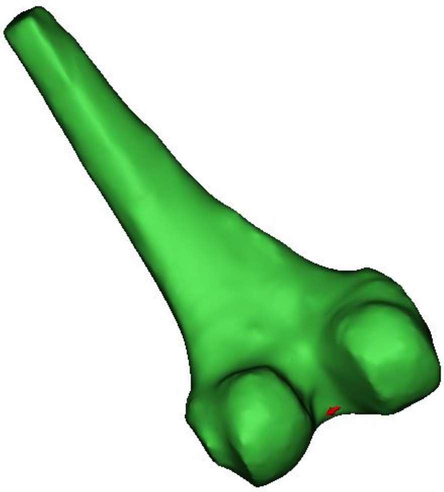

Figure 2-6 Wrapped and smoothed femur

Some features are obvious and can be highlighted just by knowing a bit anatomical knowledge like femur, tibia, patella, skin and fibula. For bone segmentation, we found sagittal plane more convenient than other planes. In contrast, for skin and muscles, coronal plane is more helpful compared to other planes. The aim of this part was also to extract and distinguish the individual muscles of the lower limb such as gastrocnemius, soleus, semitendinosus, semimembranosus, to name but a few. Thus, the profound knowledge of anatomical features is highly demanded to designate the location of each muscles in each slice and following slices. Since our models are not physiological condition and some surgical interferences are present and some muscles are also atrophied, we consulted with doctor to reach a consensus. In addition, an auxiliary reference (Fig. 2-7,2-8,2-9,2-10) is also used to help us get a rough idea of the location, insertion of each muscle[64].

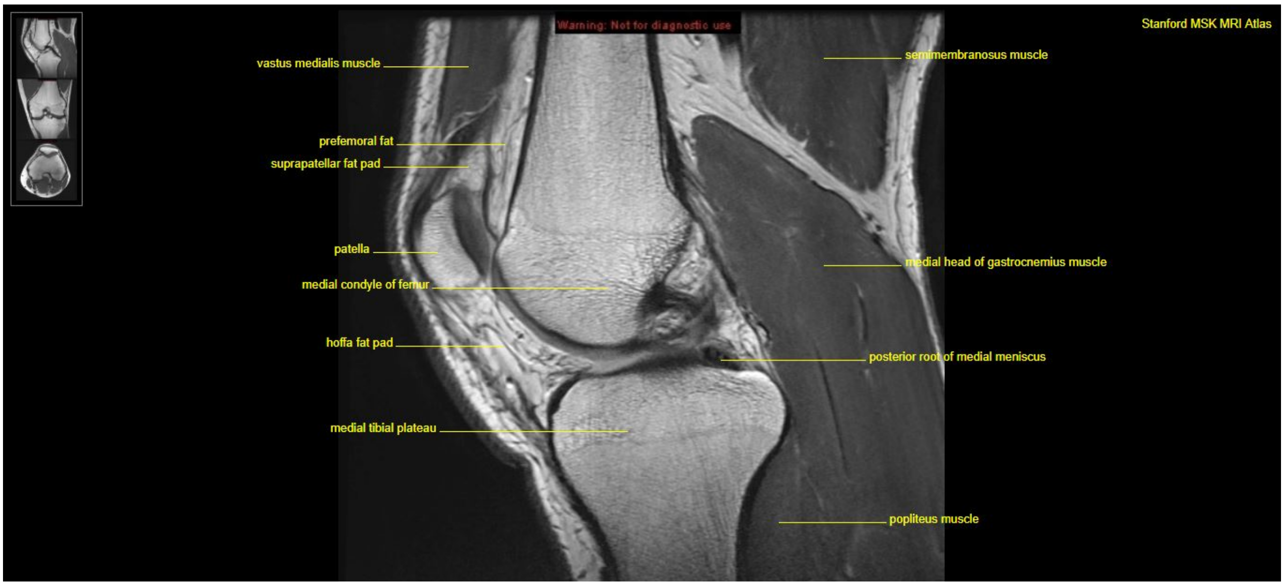

Figure 2-7 Anatomical features of lower leg

Figure 2-8 Anatomical features of lower leg

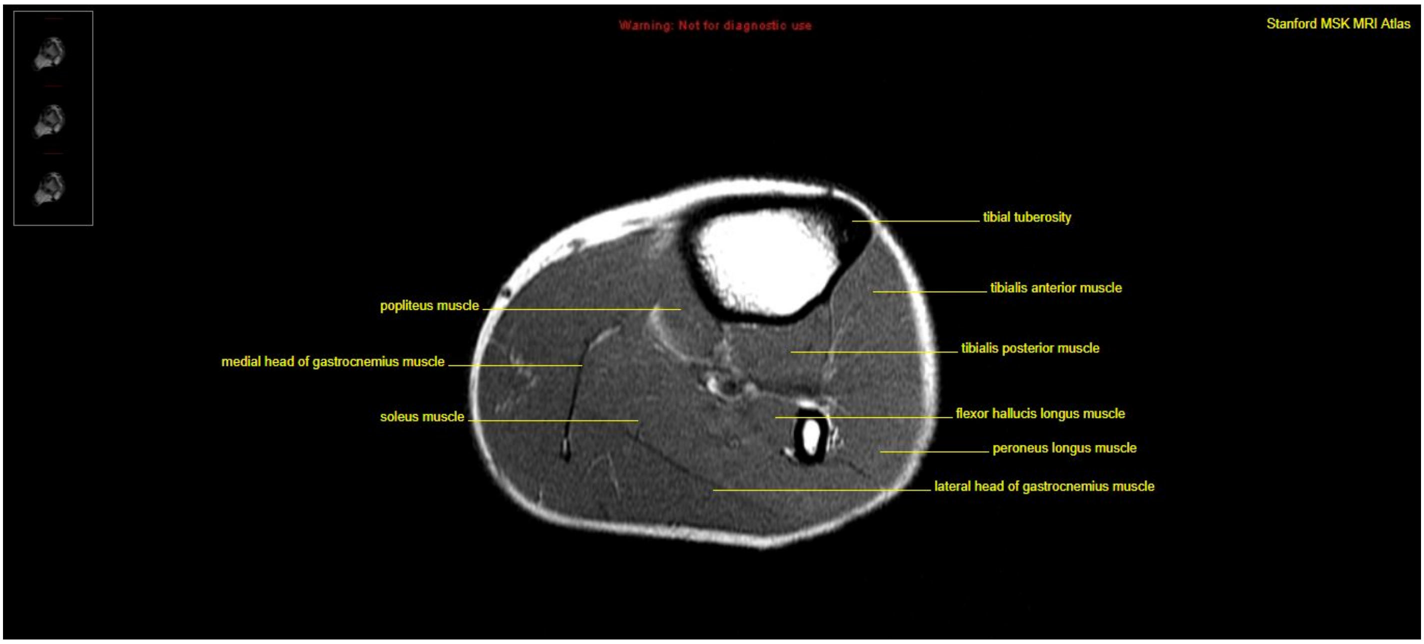

Figure 2-9 Anatomical features of lower leg

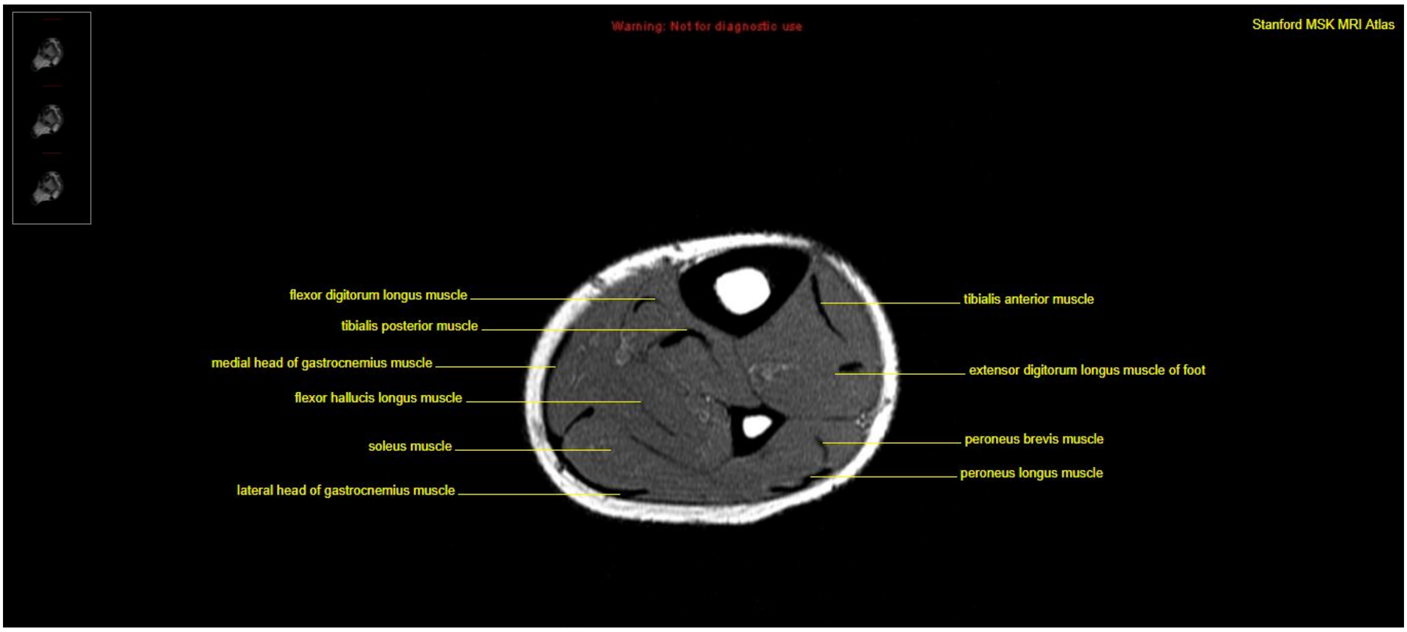

Figure 2-10 Anatomical featues of lower leg

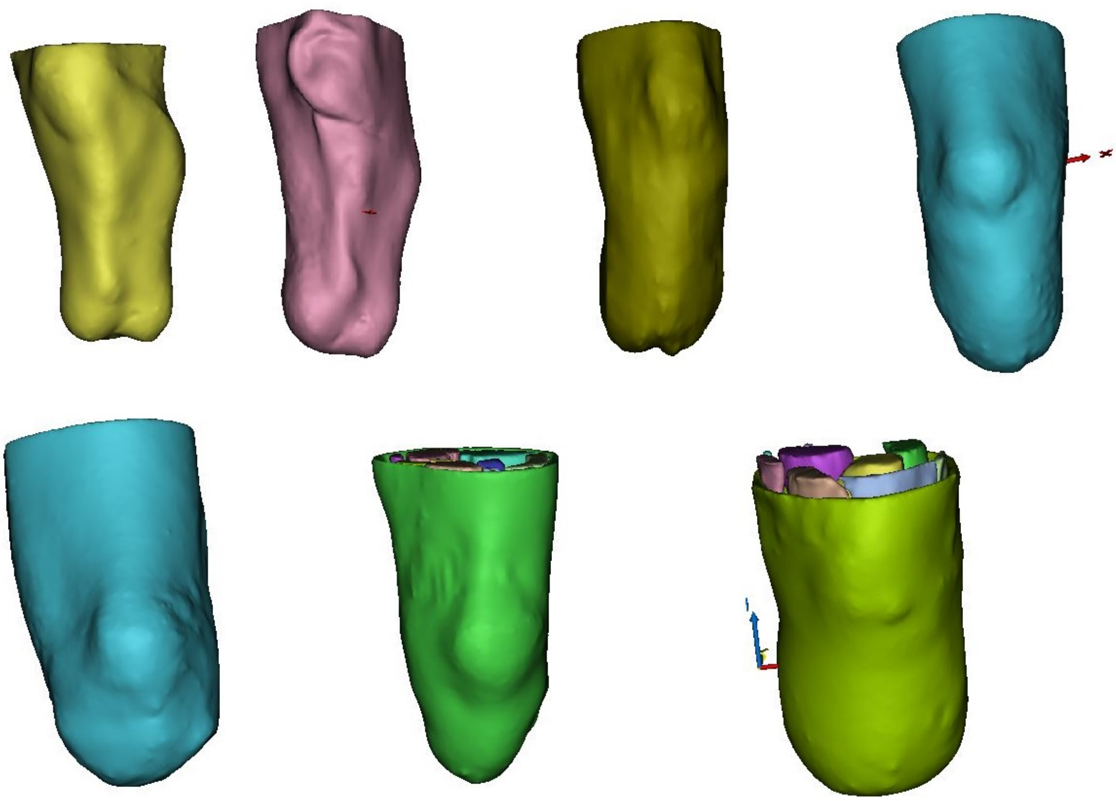

Figure 2-11 Skin segmentation of five patients from left top to right bottom: supine position of first patient, prone position of first patient, left leg of second patient, right leg of second patient, third patient, fourth patient and fifth patient. Apart from first model, all image acquisition has been carried out only in supine position.

The segmentation of lower limbs of 5 patients are accomplished by following the all approaches mentioned in this chapter. In order to get the better understanding of the segmentation, images are characterized in 3 different categories. The first module represents the skins (Fig. 2-11). To achieve the skin part. A subtle technique is utilized. At first, the mask is created by putting the all tissues in coronal plane in threshold. Then by Boolean operation, the other masks are subtracted from the skin mask. At the end, the border of the image in the coronal plane which is the skin representation of the skin, is highlighted by manual editing and several times refinement. It is worthwhile to mention that the image acquisition of the first patient was performed in both supine and prone position and the second patient was suffering from bilateral transtibial amputations. The other image acquisitions just took in supine position.

The second segmentation is related to bone acquisitions (Fig. 2-12).

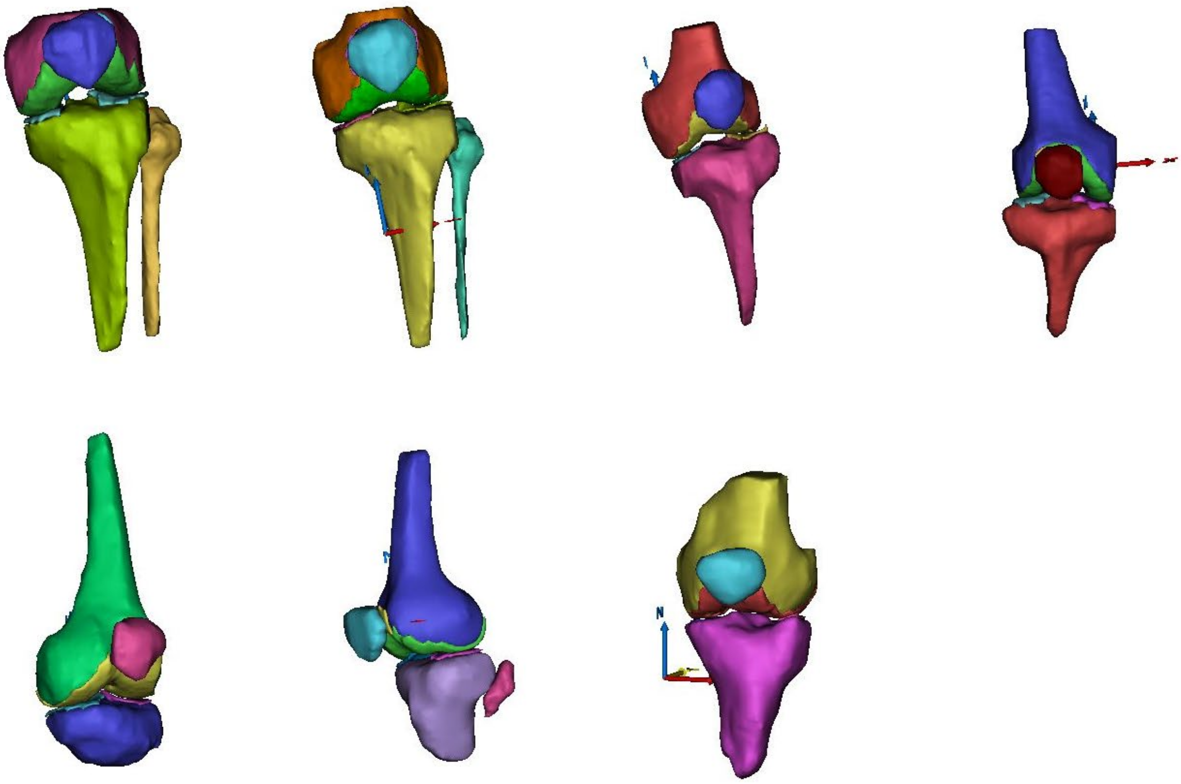

Figure 2-12 Bone segmentation of five patients from left top to right bottom: supine position of first patient, prone position of first patient, left leg of second patient, right leg of second patient, third patient, fourth patient and fifth patient. Apart from first model, all image acquisition has been carried out only in supine position.

The third investigation which was the most convoluted part, is muscle segmentations. In some cases, the differences between some muscles could not be distinguished. Hence, we took those muscles all together with this approximation that the material properties and their functions are similar (Fig. 2-13).

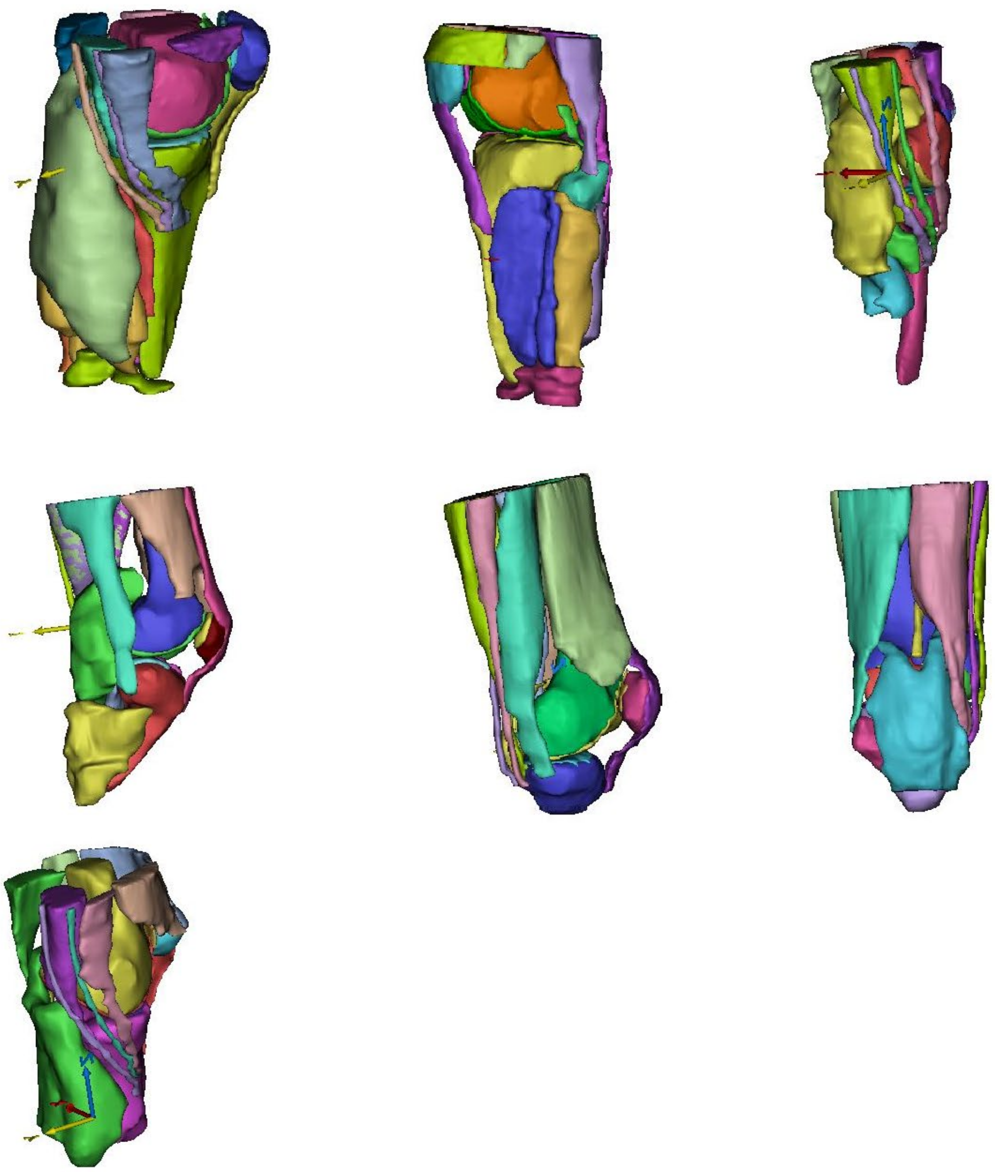

Figure 2-13 - Muscle segmentation of five patients from left top to right bottom: supine position of first patient, prone position of first patient, left leg of second patient, right leg of second patient, third patient, fourth patient and fifth patient. Apart from first model, all image acquisition has been carried out only in supine position.

At this moment, the models can be exported in *STL* format file.an *STL* format collects the information about a 3D model and it is the abbreviation of stereolithography. This file format is compatible with other software. 3D printing, computer-aided manufacturing and rapid prototyping are examples of the usage of *STL* format file[65]. The models in *STL* file format just represents the surface geometry of 3D object without any color or texture. Hence, in this situation, the simulation cannot be accomplished properly.

2.2 Geomagic Design X

The *Geomagic Design X64* is a user-friendly software that is utilized to convert a *STL* file format into a solid model. The *Geomagic Design X* helps to create parametric *CAD* models easier by means of design process and user interface that are familiar to *CAD* users. This software is very useful for a wide variety of applications including Medical field, civil engineering and quality inspection[66].

Some steps are followed in this software in order to export the *STL* format into *STEP* or *IGES* format. *STEP* file is a *CAD* file format, usually used to share 3D models between users with different *CAD* systems[67]. The *STEP* stands for Standard for the Exchange of Product model data. The Initial Graphics Exchange Specification (*IGES*) is a neutral file format that allows the digital exchange of information among computer-aided design (*CAD*) systems[68].

At the rudimentary stage, we decided to choose one of the patients to investigate simulation. The first model was opted since the muscles was more obvious compared to the other models due to the fact that the patient worked martial art. Thus, the muscles were not atrophied. Furthermore, this was only the model that fibula was not eliminated. Hence, it was a golden opportunity to be seized for analysis of more internal tissues behavior under simulation. In accordance with our work with *MIMICS*, the muscles were segmented individually but for simulation, it would not be a good idea to get all muscles separated because the computational cost would be heavy by considering more interactions and boundary conditions between more different parts. As a result, we unified all muscles together by Boolean operation tool. The outcome in this case is also reasonable albeit there is a discrepancy between this hypothesis and physiological features. The robust idea with buttress our claim is that the mechanical properties of the muscles at the sump is roughly alike[66].

The next step was to modify models converting them into solid versions. Fig. 2-14 shows the screen of working condition in *Geomagic Design X* software. There are a vast majority of tools embedded in this software, but we just focus on the description of the tools which were employed to create a solid surface.

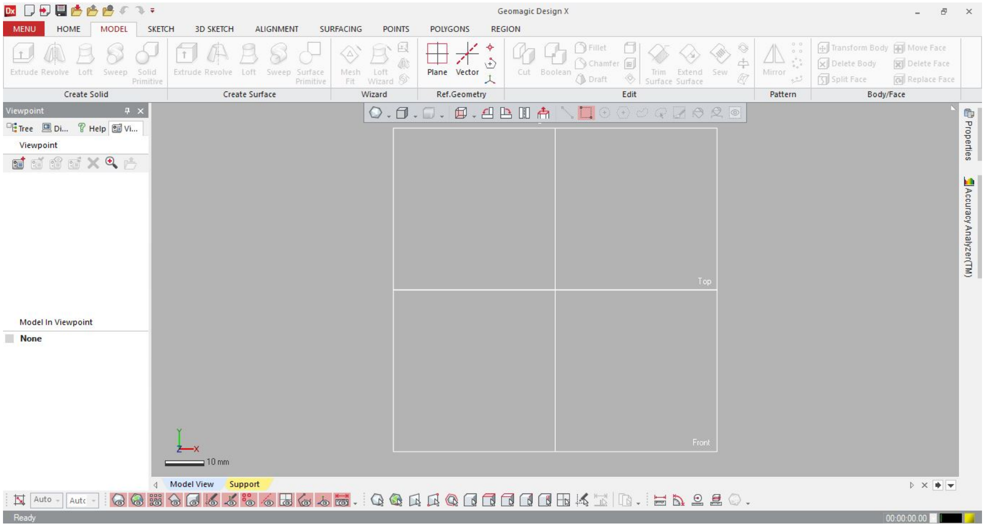

Figure 2-14 *Geomagic Design X 64*

As an example, Tibia was imported in a *STL* file format into this software. At first, the *polygons* was clicked in the menu bar. In this module, the *mesh build-up wizard* was chosen. This tool is practical for mesh creation from multiple raw 3D scan data. The command consists of up to 5 stages that enable speedy creation of merged mesh[66] (Fig. 2-15).

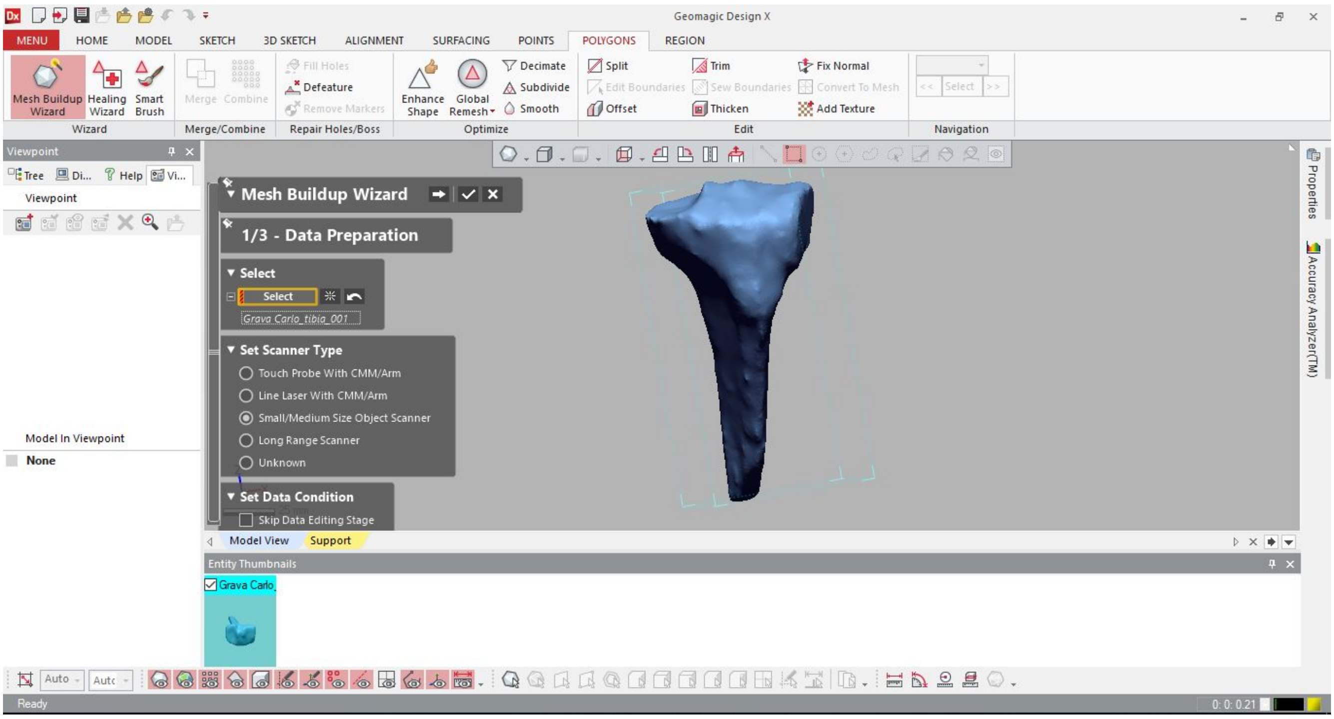

Figure 2-15 Mesh build-up wizard used for tibia

After this process, some holes are created in the model due to modification. Therefore, manual control of hole fill curvature is offered as well as advanced commands to modify or remove feature shapes from boundaries (Fig. 2-16). Then, healing wizard tool is utilized to reduce noise and defects in model and facilitate auto surfacing at the last stage (Fig. 2-17). Working with this tool is plain and proceeds automatically[66].

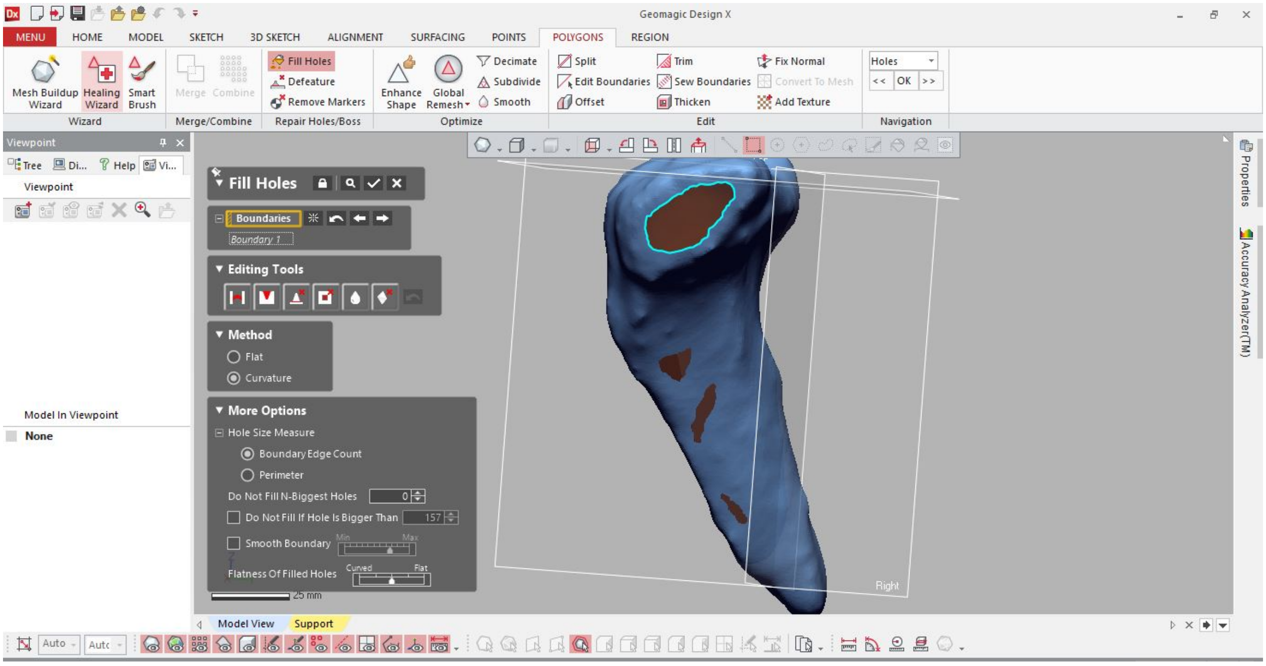

Figure 2-16 Fill holes Tool

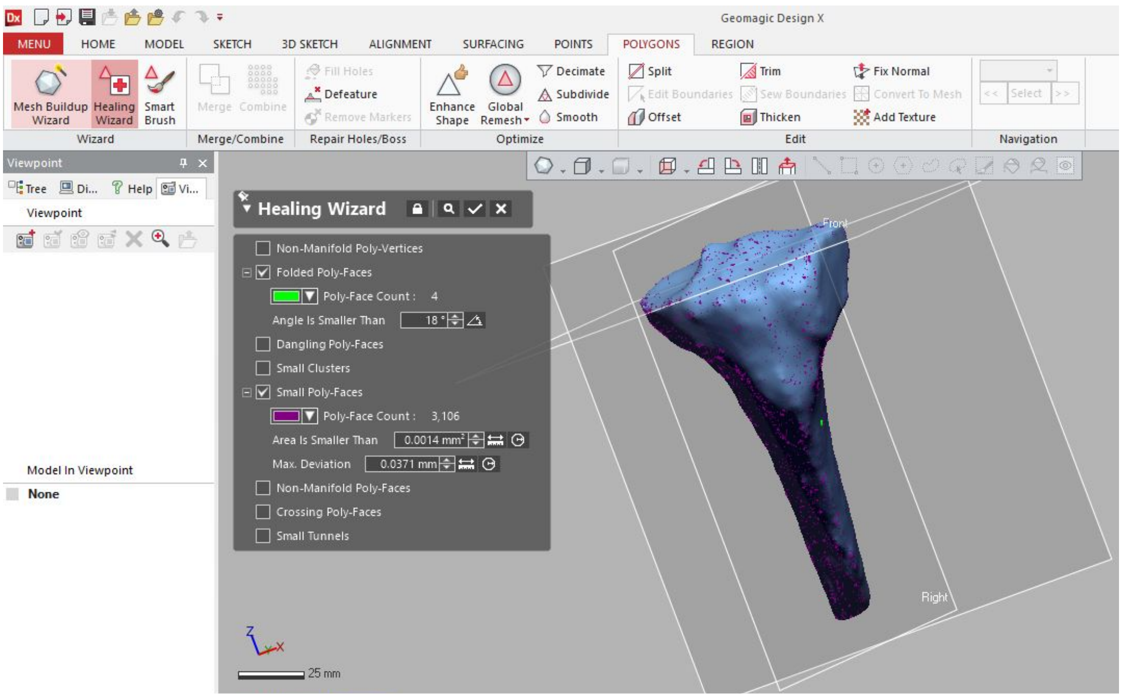

Figure 2-17 Healing wizard

The next step is to follow *Region menu bar* and take the advantage of *Auto Segment* tool. This tool allows to classify the mesh into different colored geometric regions based on the curvature and features of the scan data. The sensitivity and mesh roughness can be controlled manually by this method. The reason behind using this tool is to achieve the better fitting of surface with respect to the scan model and reduce artifacts (Fig. 2-18)[66].

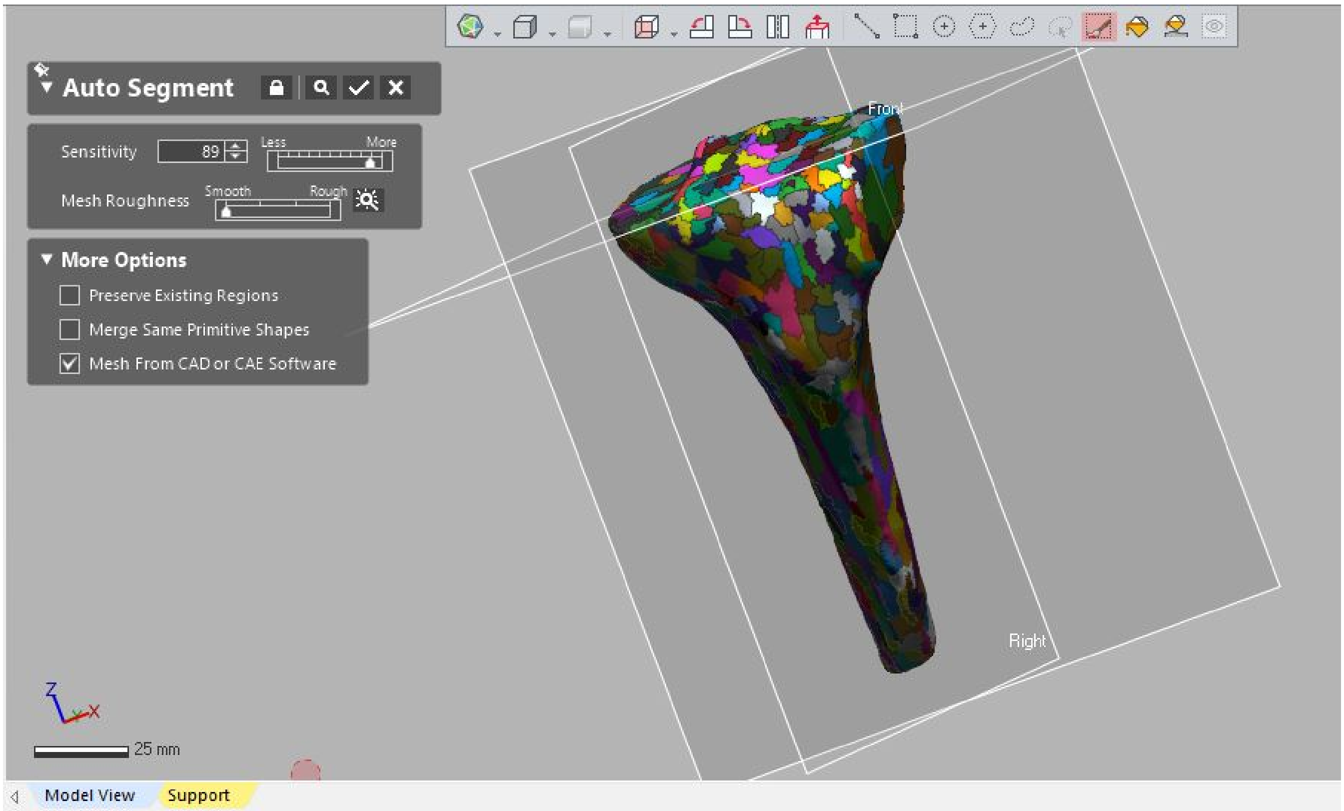

Figure 2-18 Auto Segment Tool

Finally, *Surfacing* in menu bar is clicked. In this module, *Auto Surface* tool develops curve networks on the mesh and fits surface patches to the network which maintain accuracy to the underlying mesh. The geometry capture accuracy can be manipulated to accomplish a good result (Fig. 2-19). When all procedures are conducted sequentially, the model is ready to be exported in *STEP* or *IGES* file format which is compatible with *CAD* users. It is also worthwhile to mention that after last step, you should investigate the model carefully to be certain that all mesh regions are followed by surfaces. Otherwise, it is obliged to go back to previous steps especially *Polygons* bar and use the *Enhance Shape* tool improving the quality of mesh by sharpening corners and smoothing flat or rounded areas[66].

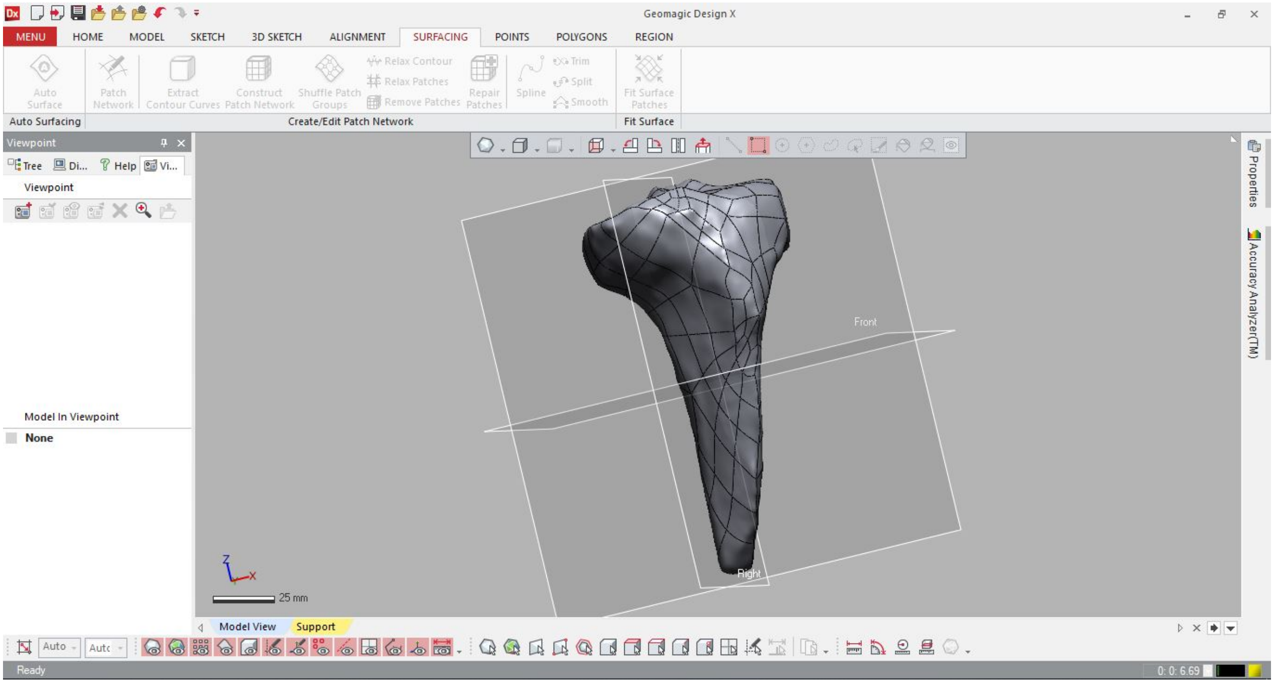

Figure 2-19 *STEP* format file for Tibia

The other parts including Femur, Fibula, Patella, Muscles, Skin and Socket in *STL* file format need to pursue the same strategy. The results are converted in *STEP* or *IGES* format file which represented in Fig. 2-20.

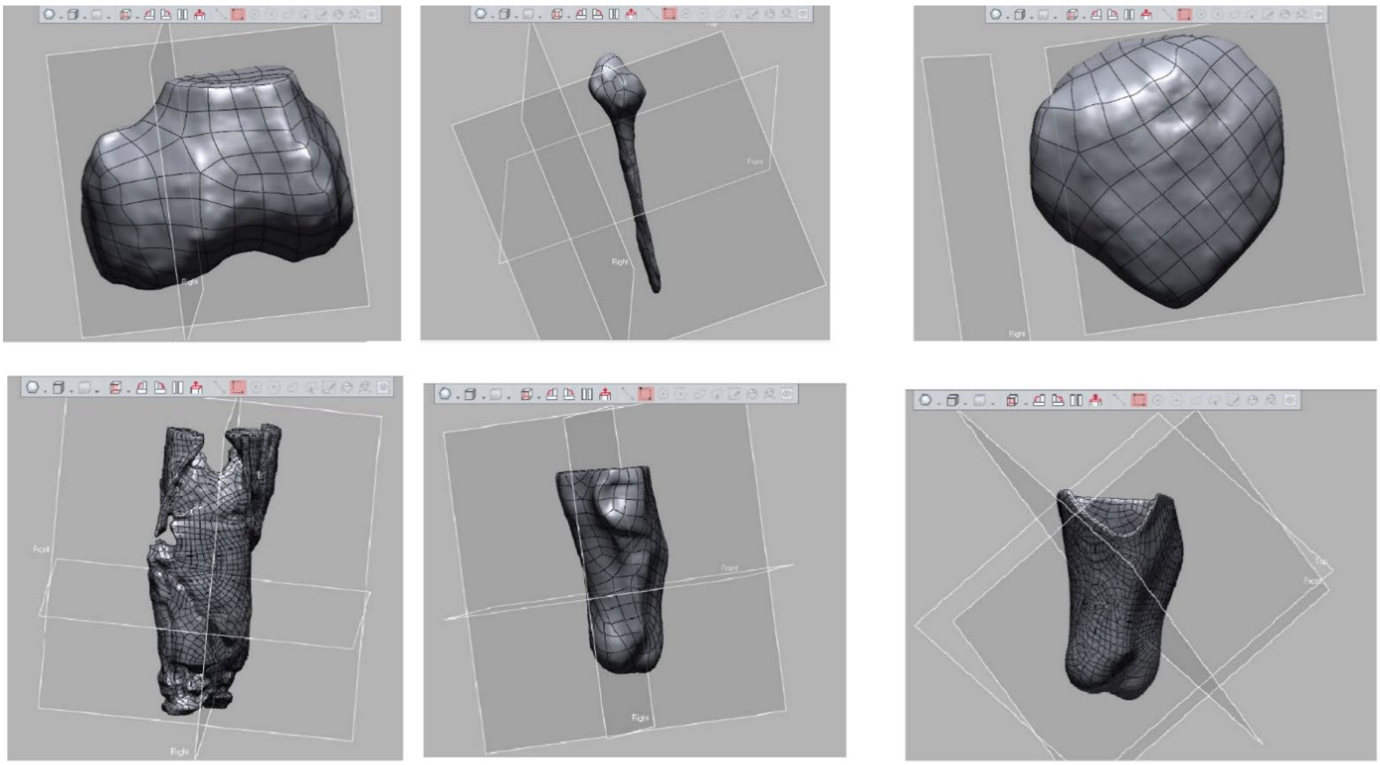

Figure 2-20 *STEP* format file of femur, fibula, patella, muscle, skin and socket from left top to right bottom respectively

2.3 Validation of the 3D model

Following the MRI acquisition, the 4th patient's stump was scanned through laser scan technology obtaining the external real shape.

The goals for this acquisition was validating the accuracy of the MRI segmentation relative to the external surface of the skin, to understand whether this approach is reliable or not

2.3.1 Blender software

The laser scan model, provided as an *STL* file, also shows the above-knee portion of the leg, that is perceived as a cloud of points due to coarser acquisition for that region, as it was not relevant for the purpose.

Moreover, that part is not represented in the MRI segmentation, as the volume of acquisition was kept as small as possible to preserve accuracy, thus making that portion source of outliers and unrelated to our purposes.

Therefore, the *STL* file first needs to be processed to cut away the not relevant region above the knee, leaving just the shape of the stump.

We consequently took advantage of the *Blender* software, that is particularly flexible and useful for the manipulation of 3D shapes. (Fig. 2-21)

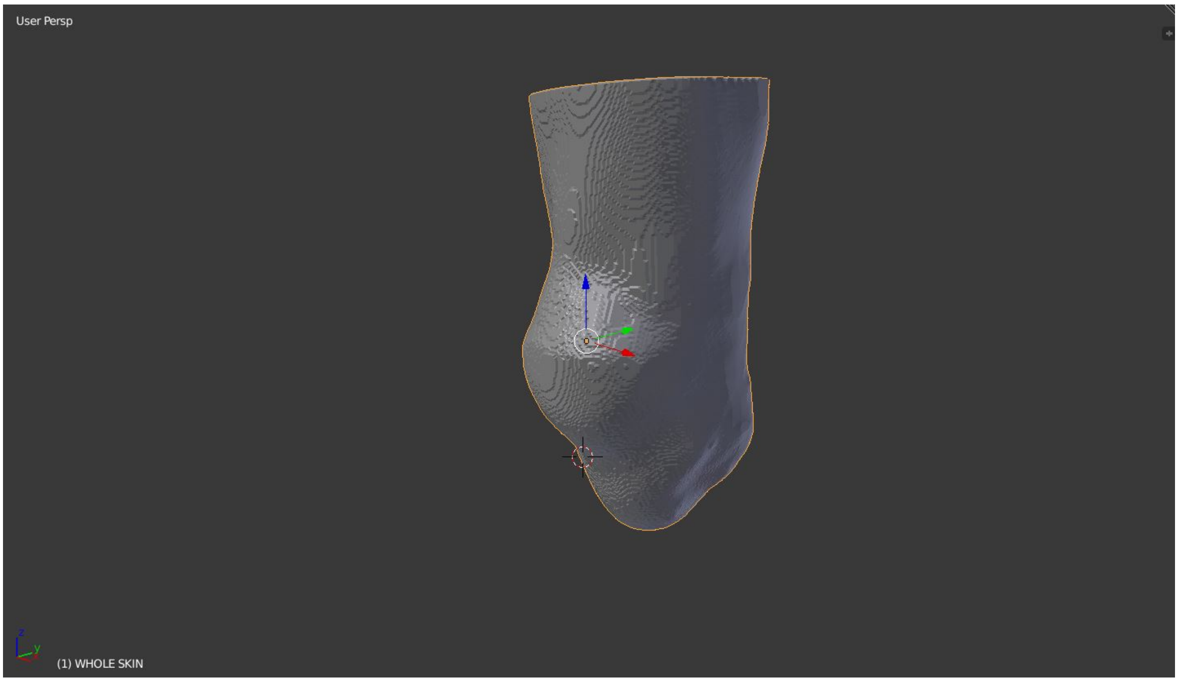

Figure 2-21 Imported laser scan in Blender

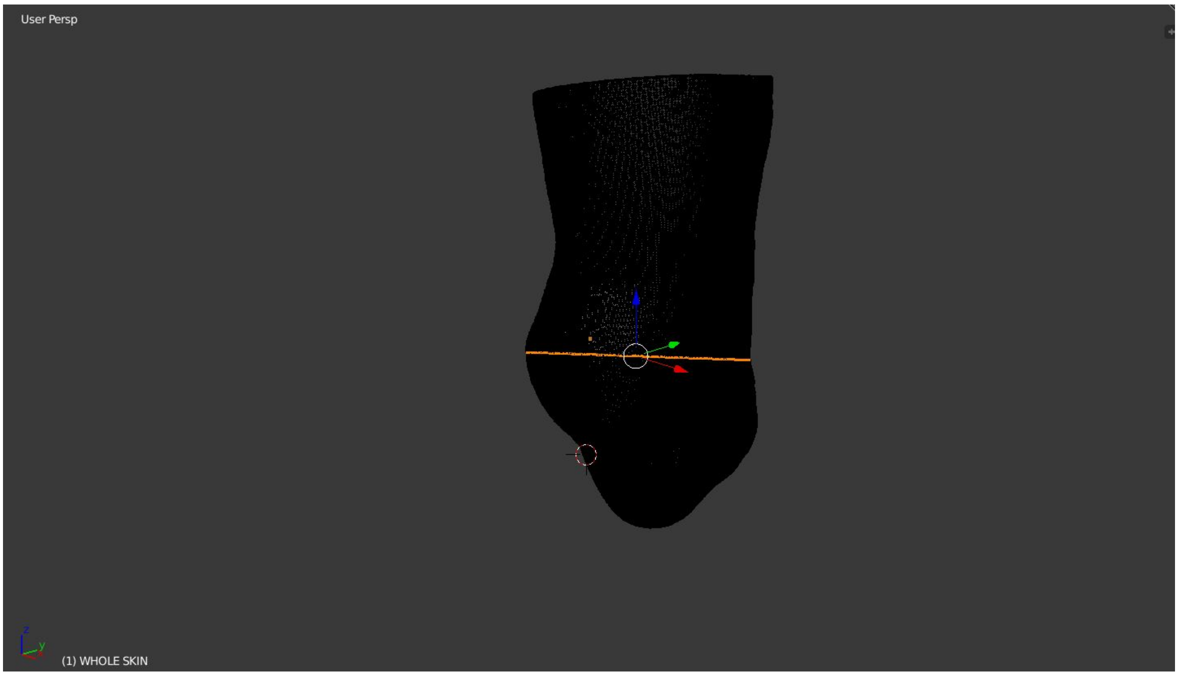

Figure 2-22 Definition of a plane with the Bisect Tool in Blender

Entering the *Edit Mode*, in the *Tool Panel* the *Bisect* command is selected. A plane is therefore qualitatively defined, to cut the model right above the patellar region. (Fig. 2-22)

In the *Bisect* menu, *Clear Outer* option is checked, thus removing the desired region. (Fig. 2-23) The model can be saved and exported again as *STL* file.

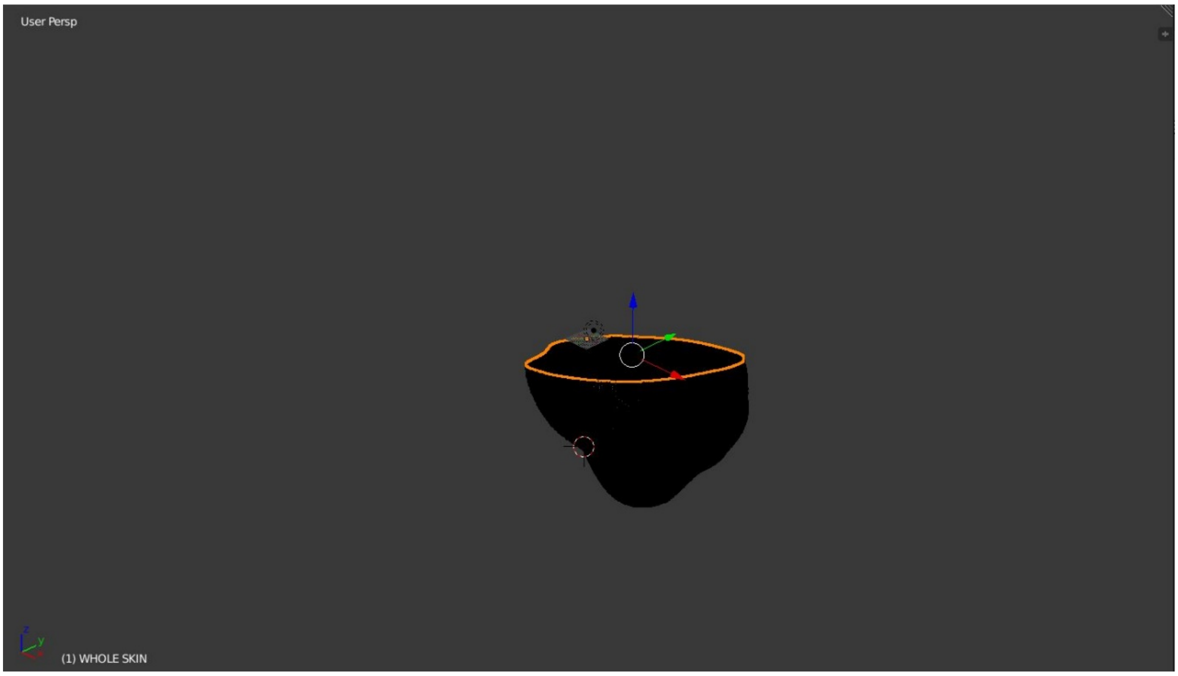

Figure 2-23 Cleared model after outliers' removal in Blender

The files regarding both MRI-base stump and laser scan are imported and displayed in *MATLAB*, using the *stlread* [69] library to convert them in a set of vertices and faces.

What is first noticed is that the two bodies, as they come from different imaging technique and of course different reference systems, are not aligned between each other, thus requiring a further pre-processing step. (Fig. 2-24)

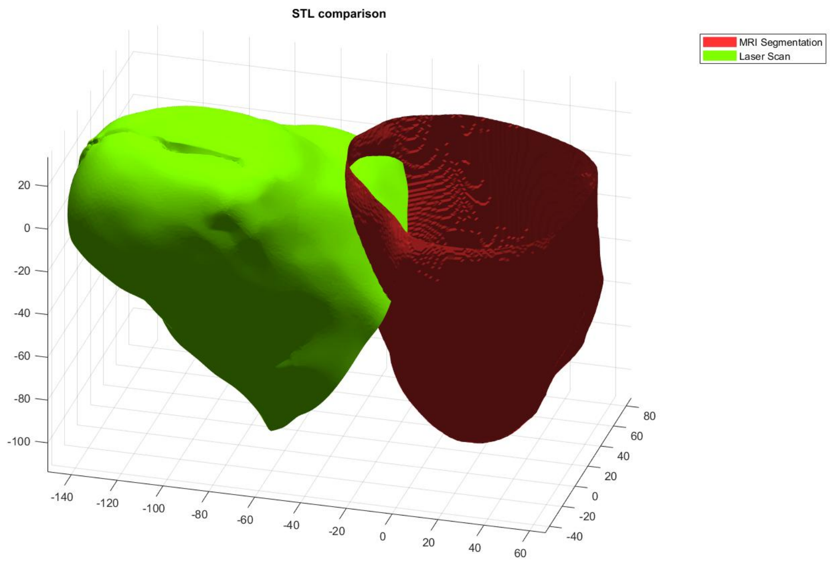

Figure 2-24 Initial configuration

2.3.2 ICP Algorithm

As a matter of flexibility and velocity, we chose to obtain the best alignment of the 3D models using the Iterative Closest Point (*ICP*) algorithm.

ICP provides a change in pose of one body with respect to the other at each iteration, trying to minimize the point-to-plane error metric using standard non-linear least-squares methods [70].

It converges in a monotonic way toward the nearest local minimum, meaning that if the starting pose is not precise enough it may miss the global one [71].

To avoid this issue, an initial estimate of the pose should be known, and models must be rotated in a qualitative way to further reduce uncertainty and provide the best starting point, allowing to have a good convergence that is especially fast during the first few iterations [71], [72].

The algorithm at each step will provide to calculate the error metric between them, then generating a transformation matrix that should minimize it [73].

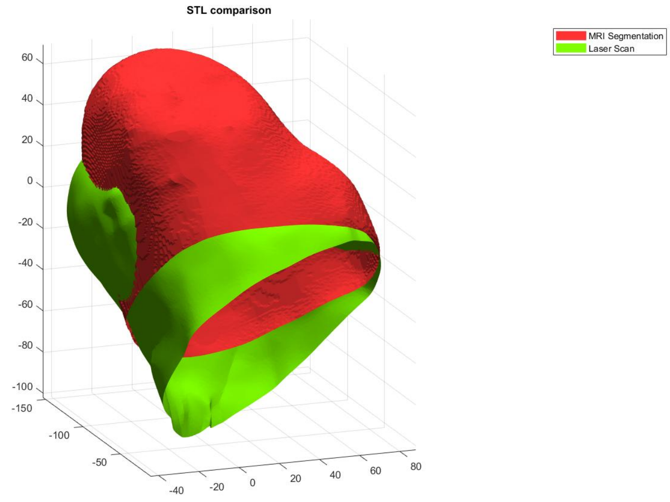

Figure 2-25 Models after qualitative rotation, to allow for a better convergence of the ICP algorithm

The icp library was downloaded, as already provided in *MATLAB FileExchange* website and implemented in a *MATLAB* Code [74].

Prior starting the simulation, the models were qualitatively aligned through sequential transformation, to ensure an easier convergence toward the global minimum. This is easily performed by defining a rotation matrix and a translation vector in *MATLAB*, then applied to the nodes. (Fig. 2-25)

Due to the high number of nodes for each model (194028 for the MRI model and 673902 for the laser scan) the *ICP* simulation took time to be performed, for an approximate time of more or less 40 minutes per iteration.

A total of 20 iterations were done, until reaching a rotation matrix similar to the identity one, meaning that no further rotation was needed, and a translation vector approximatively zero. (Fig. 2-26)

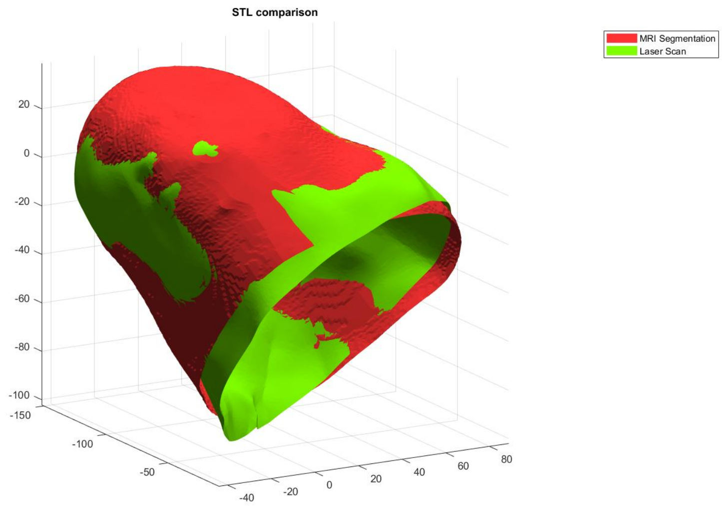

Figure 2-26 Final alignment after 20 iterations of ICP algorithm

2.3.3 Results

An algorithm was implemented in *MATLAB* to compute the distance of closest points between the two rotated models.

The code iterates for each point of one reference model (the laser scan in our case) searching for the correspondent point in the other one with minimum distance, returning the mean and standard deviation.

Hence, the average distance among nodes in the reference model is computed to understand the relative error between MRI skin acquisition and laser scan one, thus normalizing our results.

The mean error is m = 0.19 cm, while the standard deviation is std = 0.13 cm.

Normalizing them with the average dimension of the reference model, equal to 7.9 cm, we finally have an error of ε_m 2.45 % and ε_{std} = 1.72%.

Considering several factors, as the highly deformable soft tissue of the skin that contributes to large deformation according to the position (the fact that the patient for laser scan was in vertical position while during laser scan and prone position during MRI) and the mainly manual procedure to perform the images' segmentation, those results are considered more than acceptable. Thus, meaning that anatomical features obtained from 3D segmentation can be considered as reliable.

CHAPTER 3 : MATERIALS AND METHODS

In this chapter we will describe how, taking advantage of the *Abaqus CAE/6.14* [75], the results were obtained. In particular, the process was tailored on the 4th patient we scanned.

It is divided in different subsections, each focusing on one specific module of the program, to exploit a step-by-step approach in the description of the problem.

3.1 Part Module

After the pre-processing step with *Geomagic*, we were able to import the different parts of the model as *.step* files in *File* → *Import* → *Part* as solid models. (Fig 3-6)

As a matter of simplicity, some simplifications needed to be performed: skin, muscles and fat had to be considered altogether, as a merged body, because considering them separated would have meant introducing interactions and constraint between them, exponentially increasing the complexity and needed computational power of the simulation.

The parts we got at the end were:

- Femur (Fig. 3-1)
- Fibula (Fig. 3-2)
- Patella (Fig. 3-3)
- Tibia (Fig. 3-4)
- Soft tissue (Fig. 3-5)

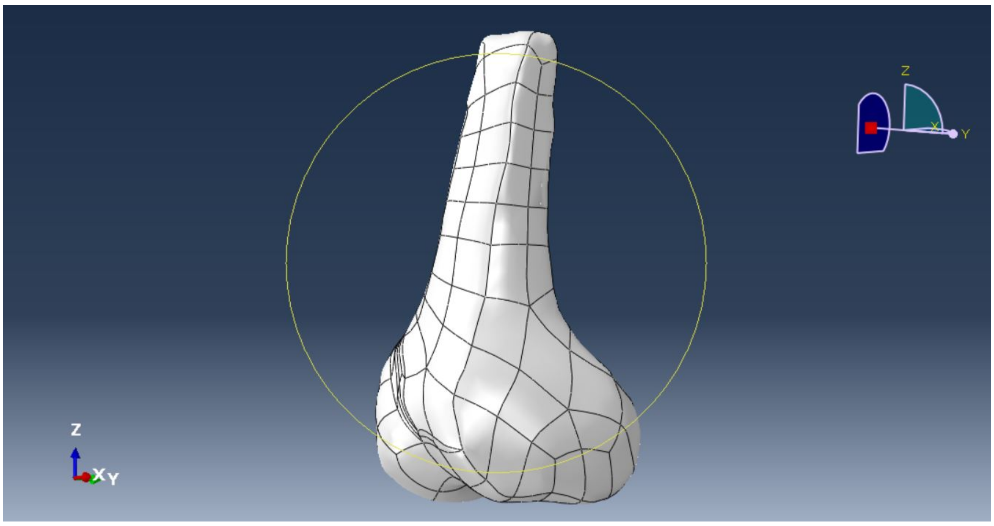

Figure 3-1 Femur part

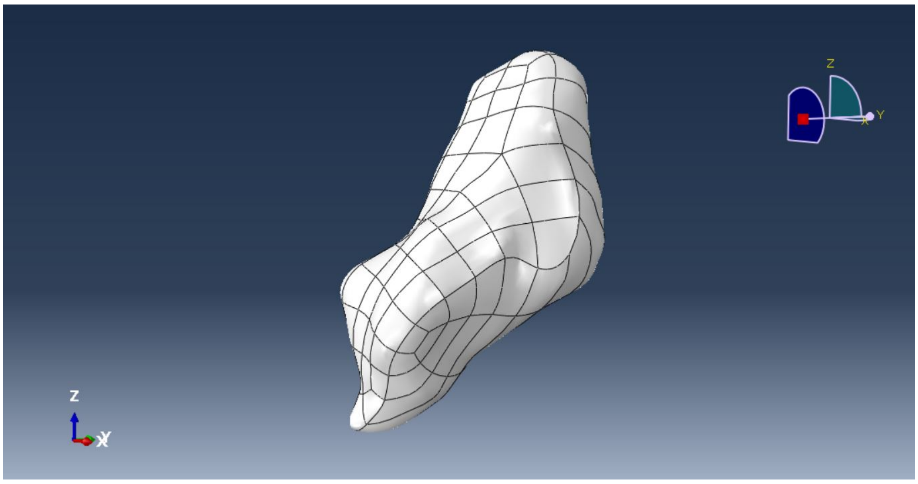

Figure 3-2 Fibula part

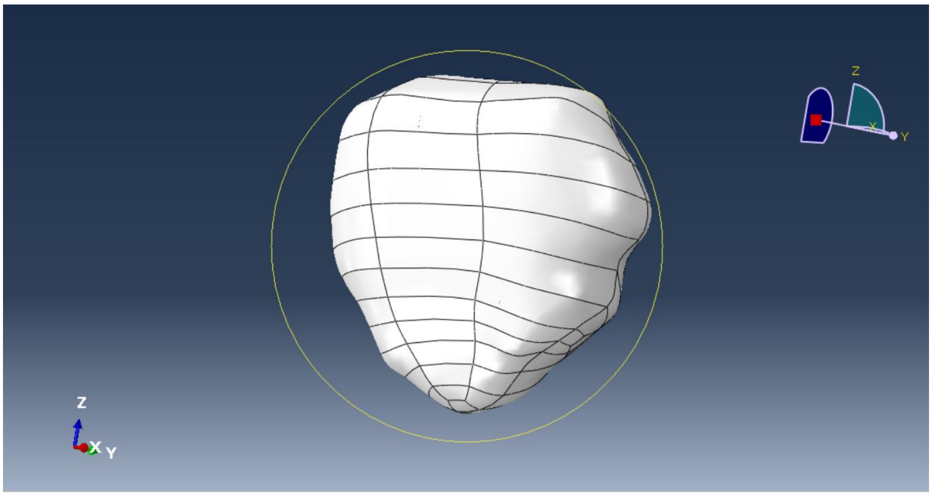

Figure 3-3 Patella part

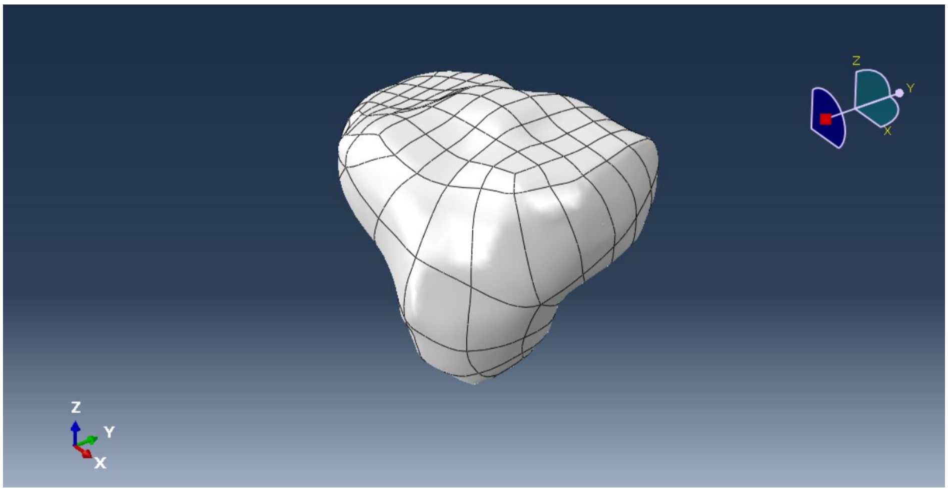

Figure 3-4 Tibia part

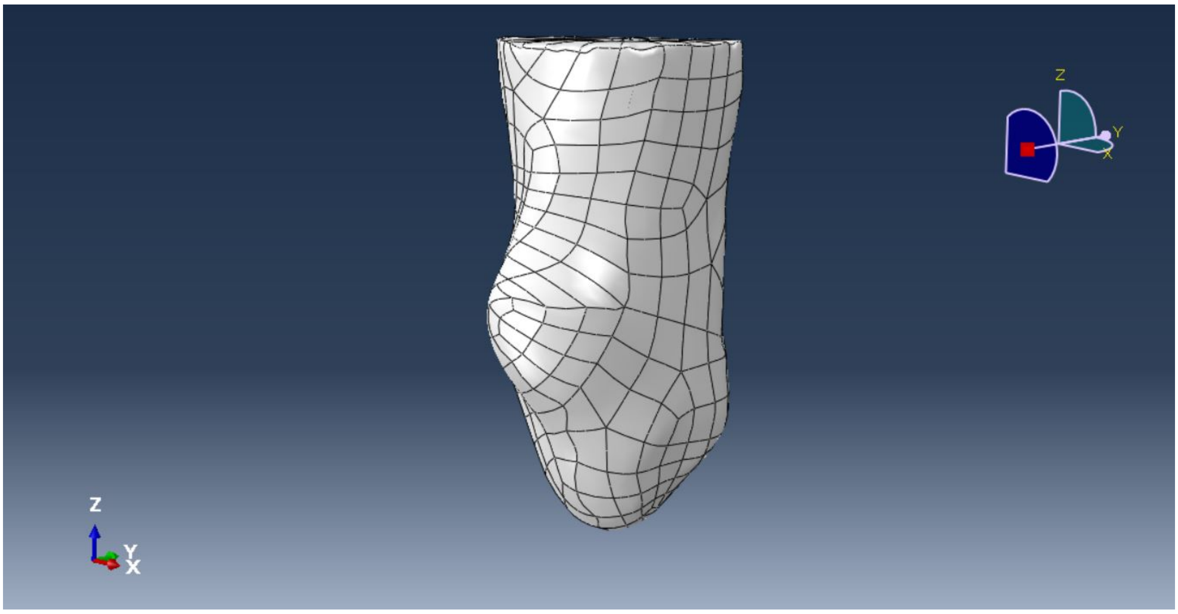

Figure 3-5 Skin part

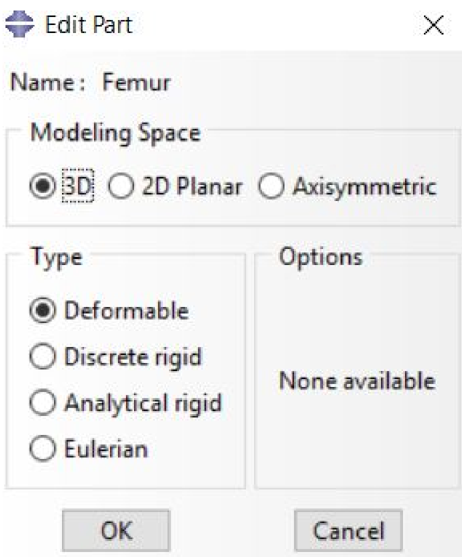

Figure 3-6 Part options in Abaqus

3.2 Property Module

Materials needed to be defined. In the *Property* module we used *Create Material*: *Abaqus/CAE* allows you to choose among several material properties, going from general to electric ones. For our purpose, only the *Mechanical* ones are required. in the *Elasticity* part, we can set the parameters which indicate the description of the desired model.

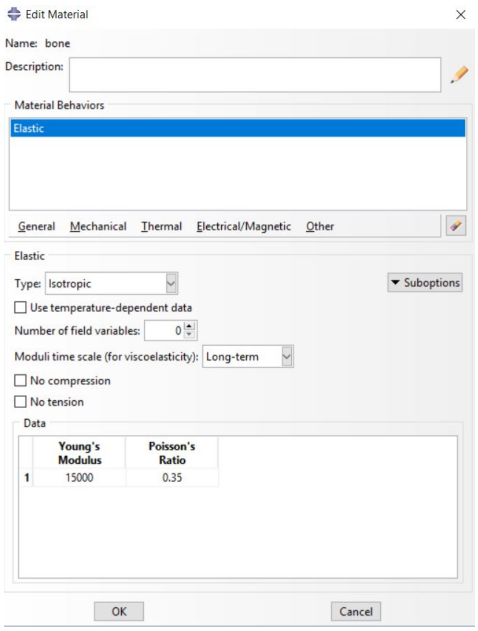

Figure 3-7 Material parameters for bone

Bone was set to be a linear elastic isotropic material with a very high stiffness, although its real material properties would be quite different. the considered caseloads are so small that it will not be affected by almost any strain. Therefore, it can be considered somehow rigid (Fig. 3-7).

For our purpose, we decided to compare 3 different kind of materials regarding soft tissue:

- Linear isotropic elastic
- Hyperelastic – Mooney Rivlin formulation
- Hyperelastic – Neo Hookean formulation

In all cases, parameters were imposed by choosing coefficients according to literature[48].

All used coefficients are depicted in Table 3-1.

	E [MPa]		ν		C10[MPa]	C01[MPa]	D1[MPa^{-1}]
Homogenous, isotropic, Linear elastic	Bones	Soft tissue	Bones	Soft tissue	NA	NA	NA
	15000	0.2	0.35	0.49			
Mooney Rivlin (Soft tissue)	NA		NA		0.0081	0	4.4
Neo Hookean (Soft tissue)	NA		NA		0.005034	NA	4

Table 3-1 Material parameters for soft tissue

Two homogeneous solid sections were then created, assigning to the first one material properties for bone and to the other one, those for soft tissue. Sections were then assigned to respective parts in the model, thus relating to them.

3.3 Assembly module

Five instances were created, related to the different parts we had. All of them were set to be independent on mesh: this means that mesh will have to be created in the assembly and it is not strictly related to the part.

As a matter of refinement, we took advantage of the *Merge/Cut* tool, to cut away bones from the soft tissue in order to avoid any kind of overclosure that might have been created during the processing phase of the images.

Instances are composed by many surfaces patched together, due to the *Geomagic* step that converted the model from a cloud of point to a solid one. in order to retrieve the best mesh quality and considered the geometry complexity, *Virtual Topology* in the *Mesh* module was utilized to incorporate the whole surfaces together. (Fig. 3-8, 3-9)

With this 'native' geometry it is then possible to perform clever partitions that would result in an easier and better-quality mesh.

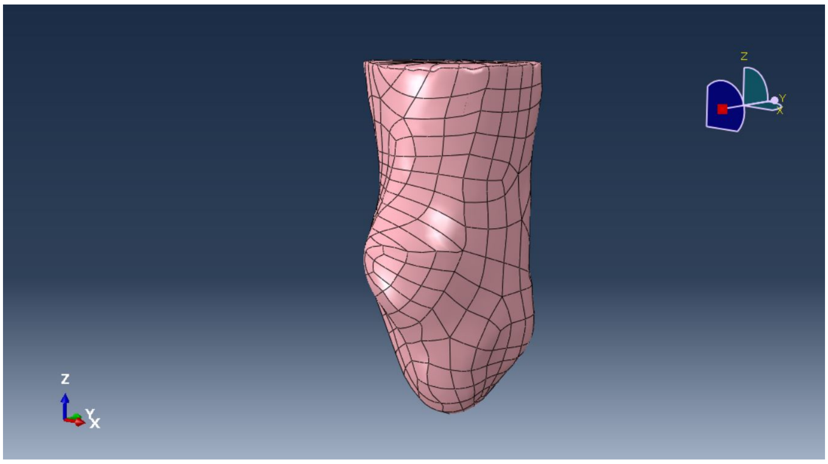

Figure 3-8 Skin before virtual topology

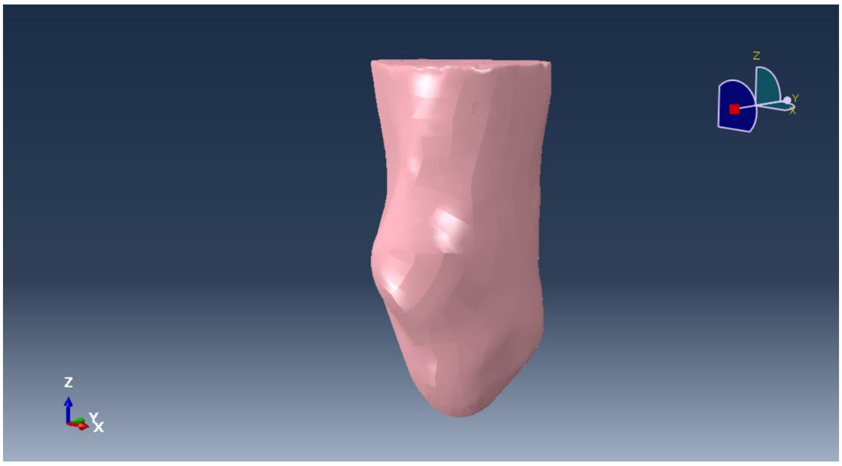

Figure 3-9 Skin after virtual topology

3.4 Mesh Module

The ideal case for our FEM analysis would be managing to have a total hexahedral mesh, both for bones and soft tissue. Unfortunately, as geometry is very complex, such this feature cannot be obtained even by carefully partitioning the models.

To optimize seeds distribution, datum planes were defined with the focus of obtaining the best partition pattern. Cell partition was performed in different directions, thus resulting in a shape subdivided in many cells. (Fig. 3-10)

Moreover, some surface partitions were essential to define the principal loading areas of the stump: they were set to be approximatively on the patellar tendon region, frontal distal part of leg and posterior proximal region of leg, to resemble the distribution we have in [chapter1]. (Figs 3-11, 3-12)

In this way, Surface could be defined in all those regions and in the remaining lower leg part. In total, we obtained four loaded areas:

- Patellar tendon region
- Frontal distal leg
- Frontal proximal leg
- General lower stump: remaining part of the stump, except for the lower muscle pad that must not be subject to any load

Elements type was imposed to be tetrahedral for the whole model: they were set to be linear and, in the case of soft tissue, as the Poisson ratio is very high resembling an incompressible material, hybrid formulation was chosen, represented by *C3D4H* element type, whereas for bones *C3D4* element was chosen.

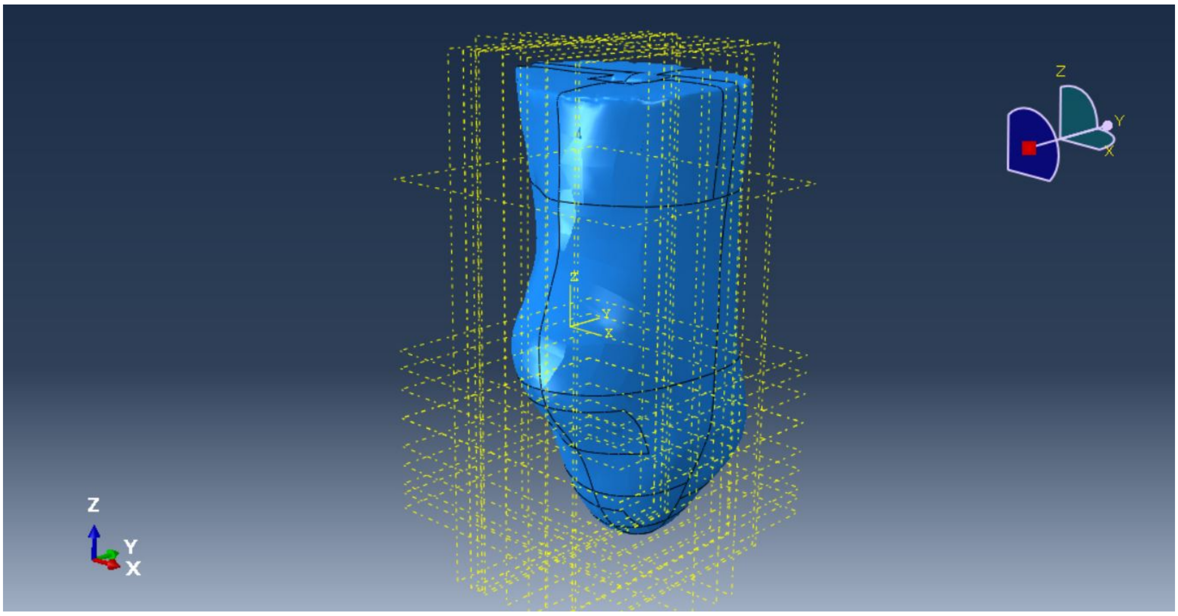

Figure 3-10 Partition planes defined in the assembly module

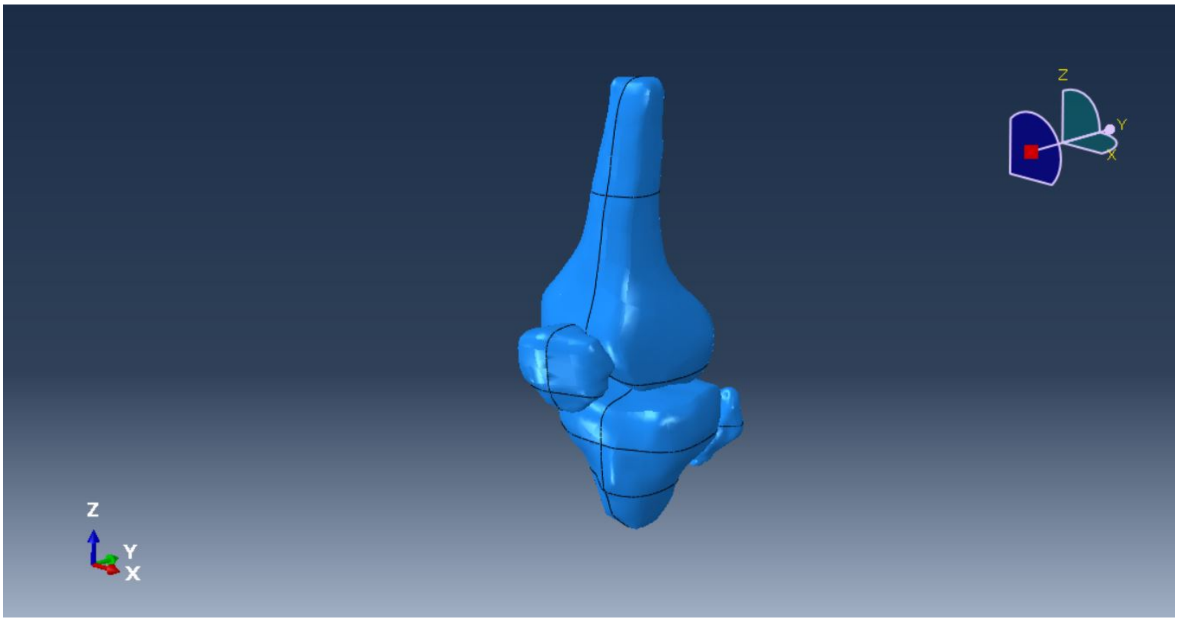

Figure 3-11 Partitioned bones

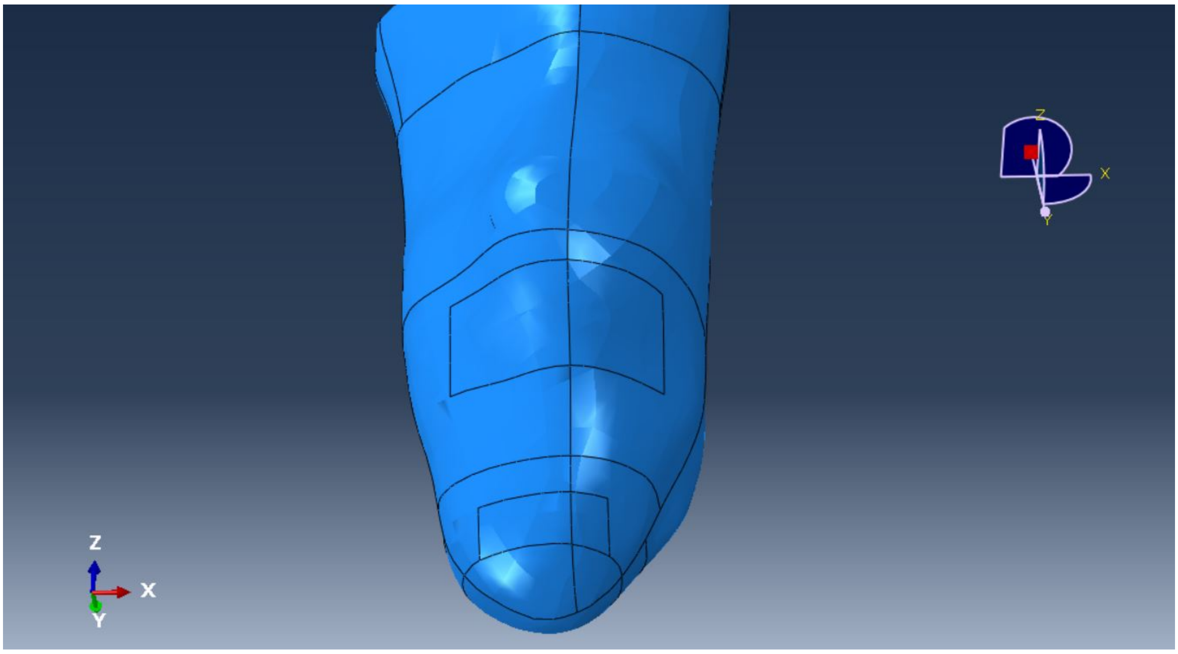

Figure 3-12 Frontal skin partitions for load areas

A general mesh size of 5.5 was set for soft tissue, while for bones general element dimension was imposed to 5.

The system could then be meshed, resulting in a total of 19495 elements for femur, 3140 for patella, 17517 for tibia, 3751 for fibula and 94748 for soft tissue, for a total of 138651 elements (Fig 3-13, 3-14).

As a matter of simplicity, encastred node sets for bones were defined on mesh nodes: four nodes were considered for each bone. This will be useful even later, for checking the reaction forces acting on the system.

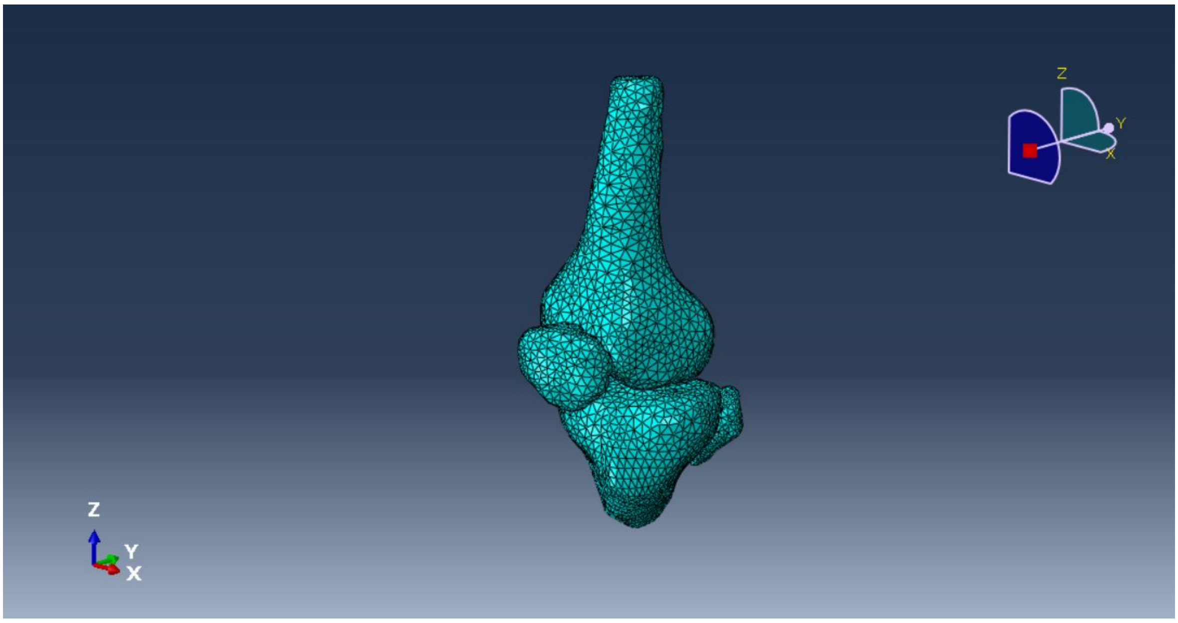

Figure 3-13 Mesh on bones. Tetrahedral elements were applied

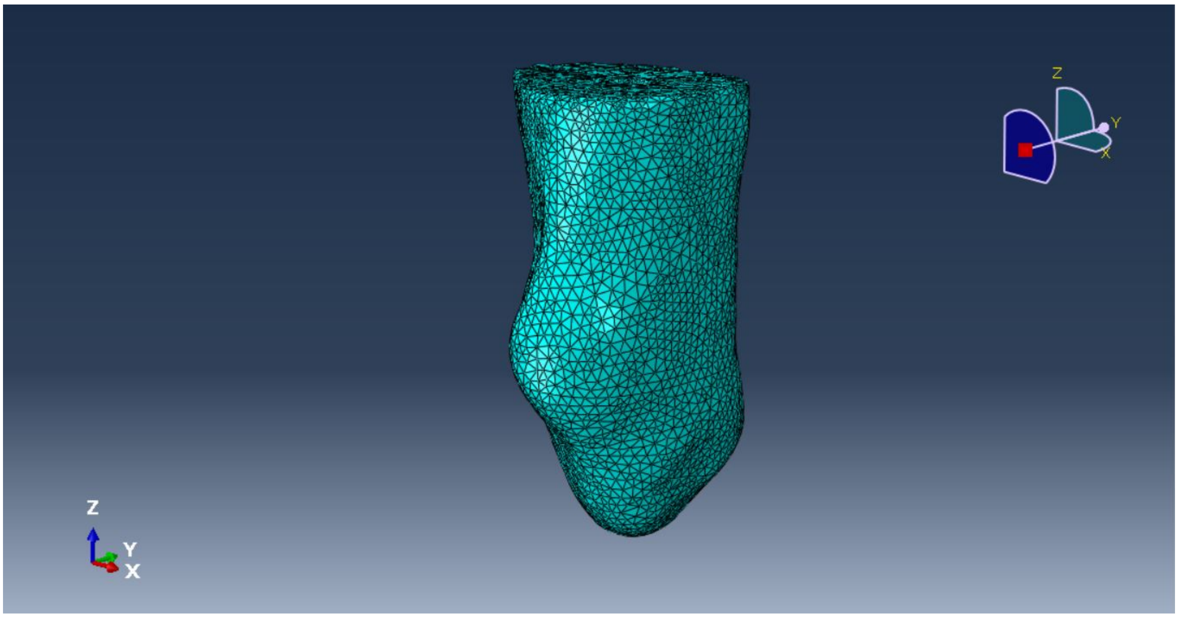

Figure 3-14 Mesh on skin. Even here the choice of tetrahedral elements was compulsory

3.5 Interaction Module

As bones and soft tissues are separated parts, unless we define a specific kind of interaction between them *Abaqus/CAE* will not be able to relate them.

For our purpose and in order not to increase the already high complexity of the problem, a *Tie Constraint* was utilized: in this way, bones surfaces are thoroughly attached to internal surfaces of the soft tissue which cover the bones. Thus, it does not allow any relative displacement. Master and slave surfaces needed to be defined: master surface is usually chosen as the stiffer one, in our case bone, while slave surfaces tend to be the softest one, and choice couldn't help on falling on soft tissue. In this way, slave surfaces are constrained to follow the movement of the master one.

The *Tie Constraint* allows to choose an option called '*Adjust slave surface initial positio*n'. This possibility should be useful to reduce any possible gap between the interacting surfaces. In our case, as the model was designed to reduce as much as we could any void making them as fit as possible, we unchecked this option as it may lead to some excessive distortion of elements, thus resulting in failure of the simulation. (Fig. 3-15)

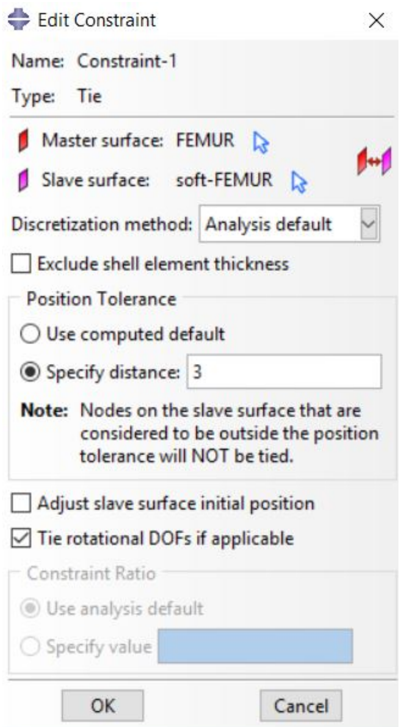

Figure 3-15 Tie Constraint options between bones and skin

3.6 Step Module

A *Static General* step was created. Due to the large deformation that will take place in the system, the *Nlgeom* option was ticked, to ensure a better convergence of the simulation.

As the problem is complex, an adaptive incremental value was used and the value of minimum, maximum and initial time was decreased, to avoid failed attempts, while the maximum number of increments was increased (Figs. 3-16, 3-17).

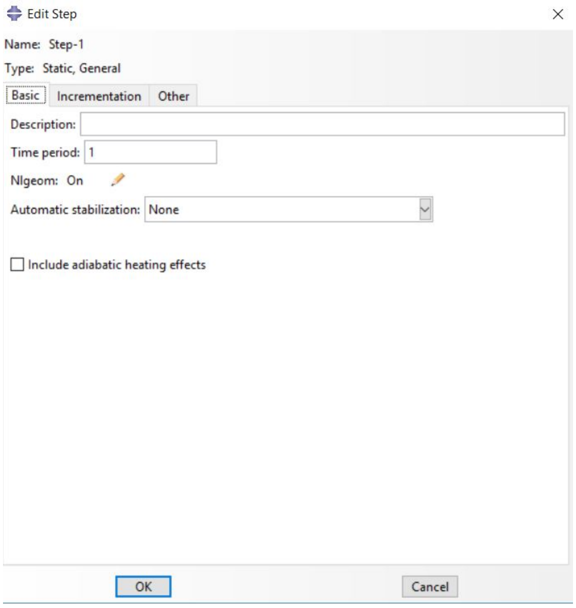

Figure 3-16 Step option. Notice that Non-linear Geometry feature is selected. The simulation lasted 1 second in total

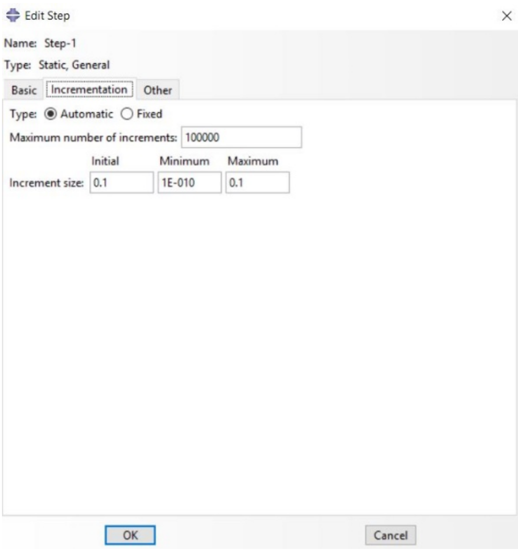

Figure 3-17 Step options. The number of increments had to be increased to ensure the simulation to reach the solution

3.7 Load module

At this point, only boundary and loading conditions need to be set up.
Concerning the first ones, a *Mechanical Encastre* was created on the 4-points set we defined for each bone, in order to prevent any movement. This was done assuming bones not to move with respect to each other, considering the leg as still and blocking any joint movement. (Figs 3-18, 3-19, 3-20)

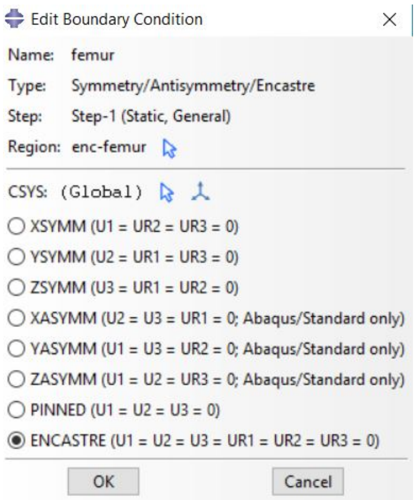

Figure 3-18 Encastre boundary condition on bones

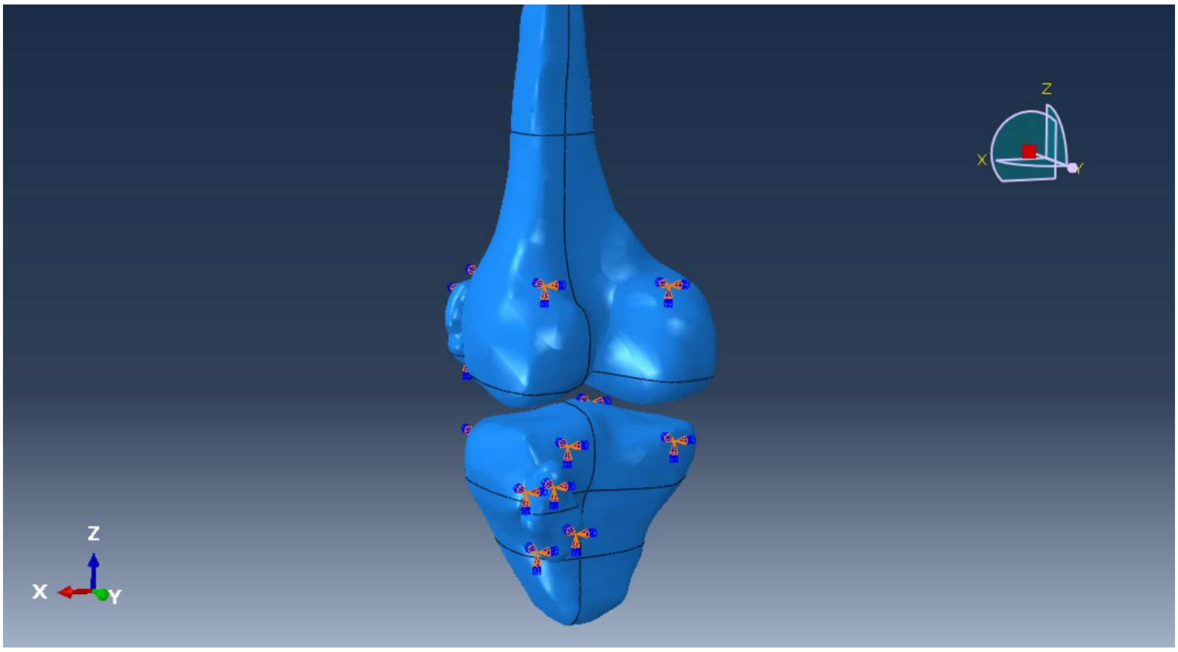

Figure 3-19 Encastres from the posterior point of view

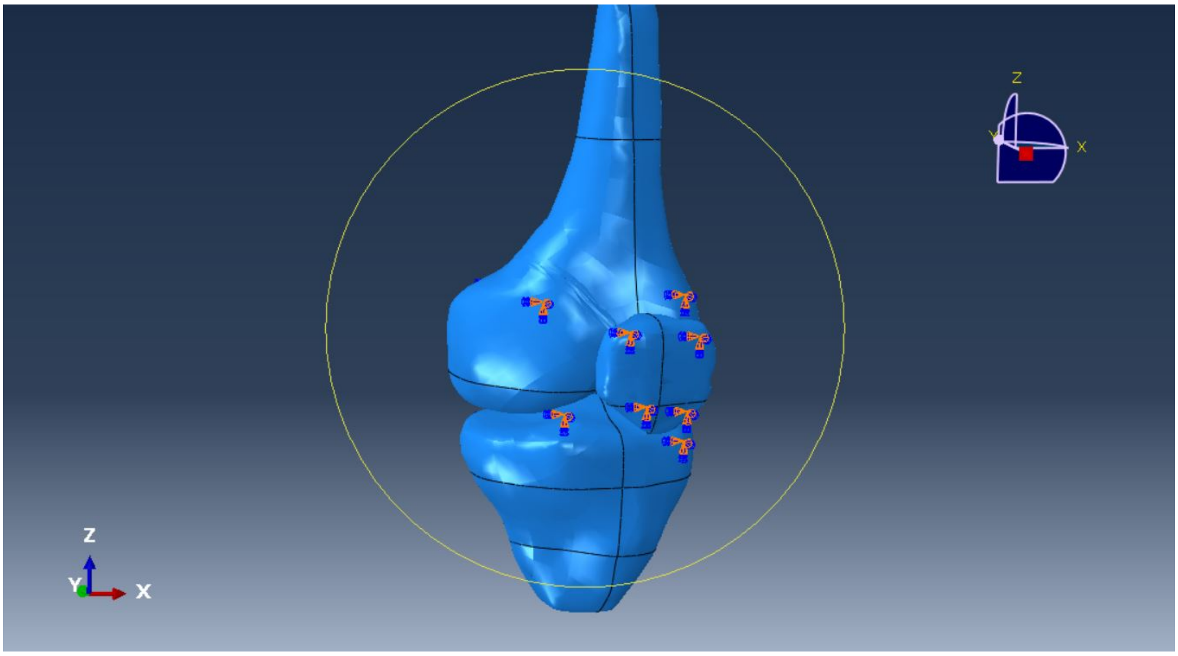

Figure 3-20 Encastres from the frontal point of view

As the goal of the simulation is considering single and two-legs stance, such assumption was thought as reasonable.
For what concerns loading conditions, many attempts needed to be performed before obtaining the optimal pressure values in all regions satisfying our goals. Uniform pressure was applied in the *Load* module, considering its amplitude as Ramp: this means that at the beginning of the simulation pressure will start from zero, thus increasing and reaching the maximum imposed value at the end. Starting values were set taking reference from literature experimental data[76], [77]. (Fig. 3-21) At each simulation, resulting values of reaction forces on the encastres was evaluated, until reaching the goal of single stance for the elastic material and two-legs stance for the hyper elastic ones, by progressively increasing or decreasing pressures in the loading regions.
Final obtained pressure values are depicted in Tables (3-2, 3-3, 3-4).

LINEAR ELASTIC	APPLIED PRESSURE [kPa]
Patellar tendon region	150
Frontal distal leg	80
Posterior proximal leg	110
General pressure	90

Table 3-2 Applied pressure values in the linear elastic case

MOONEY RIVLIN	APPLIED PRESSURE [kPa]
Patellar tendon region	150
Frontal distal leg	80
Posterior proximal leg	110
General pressure	60

Table 3-3 Applied pressure values in the Mooney-Rivlin case

NEO HOOKEAN	APPLIED PRESSURE [kPa]
Patellar tendon region	50
Frontal distal leg	50
Posterior proximal leg	50
General pressure	50

Table 3-4 Applied pressure parameters in the Neo-Hookean case

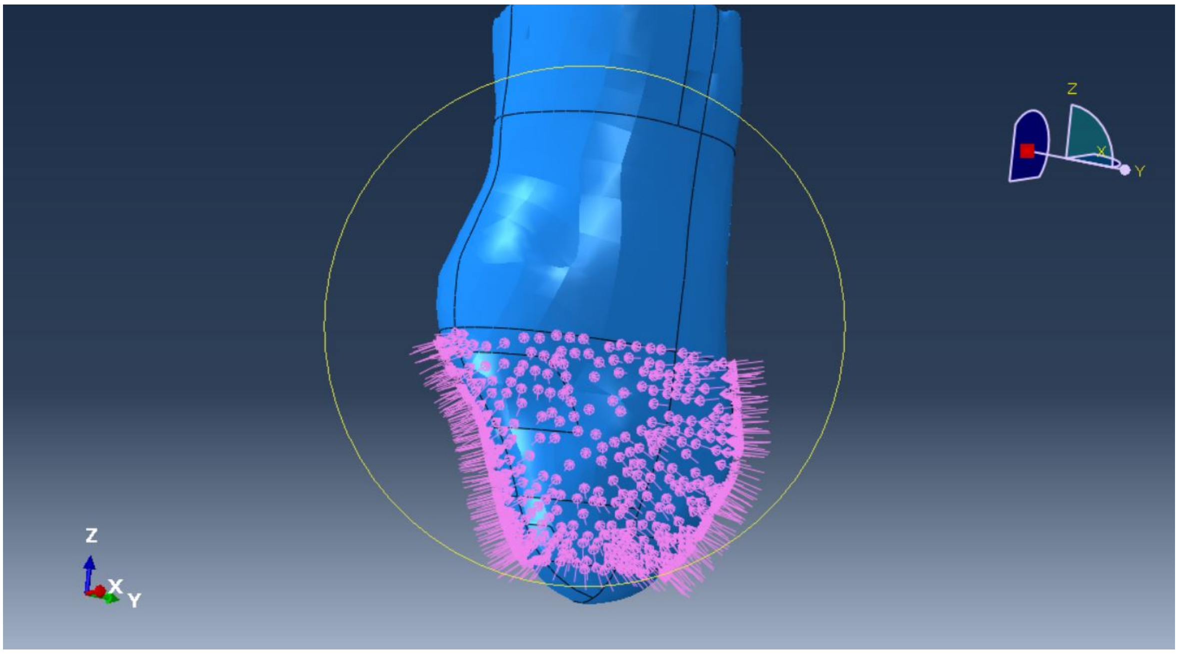

Figure 3-21 Pressure applied on the stump

CHAPTER 4 : RESULTS

When the model is set up, the input file was generated by creating the job. Simulation time is contingent upon the total number of elements applied to the mesh and the complexity of the deformation since element distortion may lead to a smaller time increment throughout the simulation.

The result is an *.odb* file containing the field output results. They can be thoroughly monitored in the *Visualization* Module in *Abaqus/CAE 6.14* software, that allows to analyze and postprocess the outcome.

4.1 Reaction forces and Moments computation

According to the data mentioned in *Materials and Methods* section, the required simulation is performed several times, applying different values of pressure distributions to accomplish appropriate reaction forces (RF) on the encastred nodes of the bones.

Reaction Forces (RF) were evaluated in accordance with the Field Output result via checking the last frame of the simulation corresponding to the highest imposed pressure. Maximum reaction which would resemble full body weight and half of it, are stated by single leg stance and two leg stances respectively. For this reason, Display Groups of the encastred node sets (one for each bone) were created in the Visualization module.

Tools → Display Group → Create

The node sets of bones can be investigated through:

Tools → Query → Probe Values

This valuable tool helps the user retrieve values of the desired variables in a specific frame for certain sets of elements or nodes.

An *.rpt* file can be exported, containing the RFs in all directions and coordinates for each node. Since one node may belong to different elements, the exported file will contain each node as many times as the elements to which it belongs. By implementing a MATLAB code, we managed to classify each node once for the calculation of the real RF, removing repetitions.

Therefore, moments were computed by applying cross product between force components and node's coordinates, by assuming the system in static equilibrium. Hence, the moment must be the same computed with respect to any point.

Case 1 – Elastic material, single stance

In accordance with imposed pressures on the prone areas of the stump estimated through experimental data [76], [77], the RFs and moments are evaluated in femur, patella, tibia and fibula which are illustrated in Table 4-1. It is worthwhile to mention that the regions in which pressures are exerted are classified into loadable and unloadable areas. The measurements of pressures were performed in [76], [77] through TACTILUS pressure sensor in different steps of gait analysis. Since the aim is to set up a virtual prototyping of socket shape derived from deformations on the external surface of the stump, the values of pressures are comparable to data obtained in literature and exerted on patellar tendon, popliteal fossa, frontal distal part of the stump in our model.

	REACTION FORCES			REACTION MOMENTS		
	Rx (N)	Ry (N)	Rz (N)	Mx (Nm)	My (Nm)	Mz (Nm)
TIBIA	-13.5787	-73.8153	-22.446	2.8033	-1.7722	1.5097
FEMUR	-9.401	-68.1016	-557.342	-0.4751	-0.2534	2.3162
FIBULA	15.9282	35.7529	-23.3981	5.2198	-1.5219	2.6355
PATELLA	-11.0197	54.9056	-152.667	-0.931	0.803782	0.872484
TOTAL	-18.0712	-51.2584	-755.853	6.617132	-2.74372	7.333884
NORMALIZED (with mass [U]/kg))	-0.2337	-0.66288	-9.77476	0.085573	-0.03548	0.094843

Table 4-1 Reaction forces and moments in the linear elastic case

These data are obtained by considering as goal the full load on single leg stance and the material of the soft tissue as linear elastic. Generally, we posited that the weight of the patient is roughly 750 N assuming the body mass of 75 kg. Some attempts are followed by

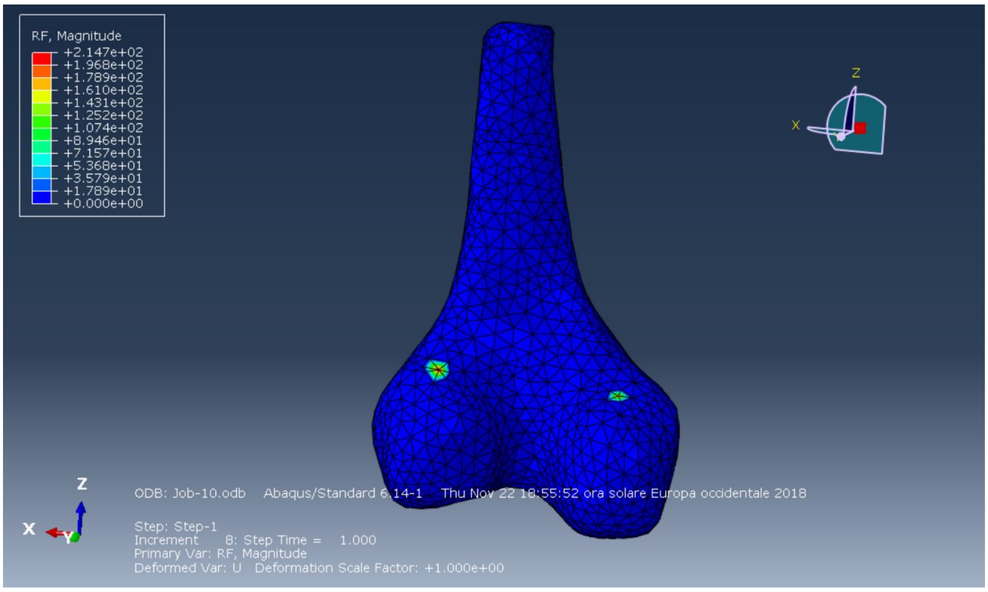

Figure 4-1 RFs on the back part of the femur

incrementing pressure progressively in order to reach the ideal data. Figs. (4-1, 4-2, 4-3, 4-4, 4-5) depict the influence and position of RFs on nodes which are placed in the aforementioned bones.

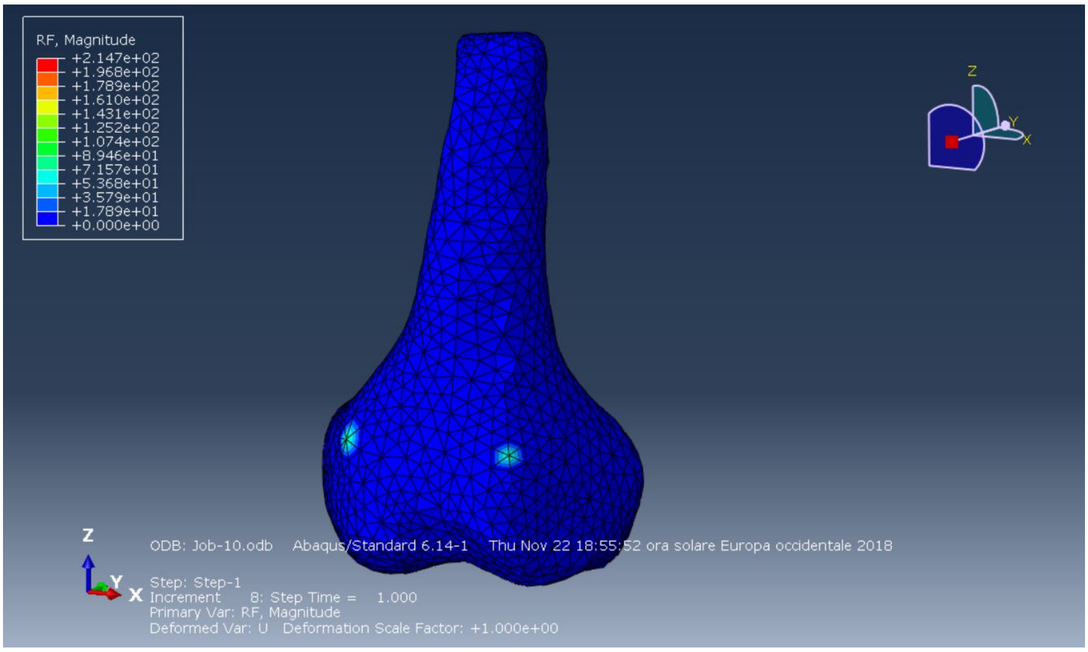

Figure 4-2 RFs on the frontal part of femur

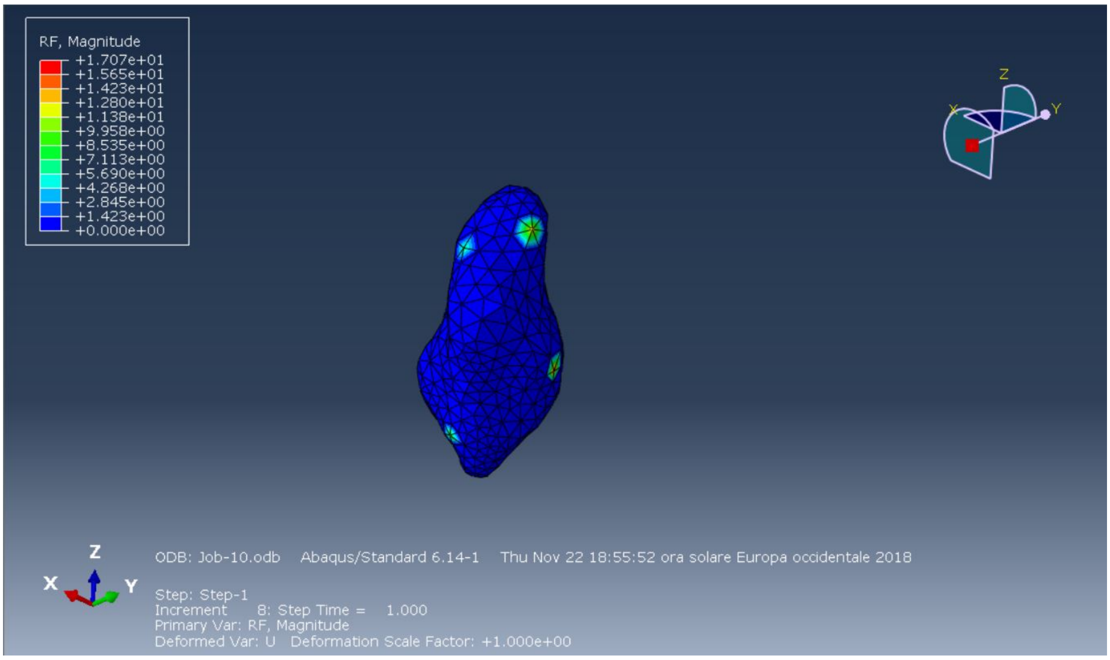

Figure 4-3 RF on fibula

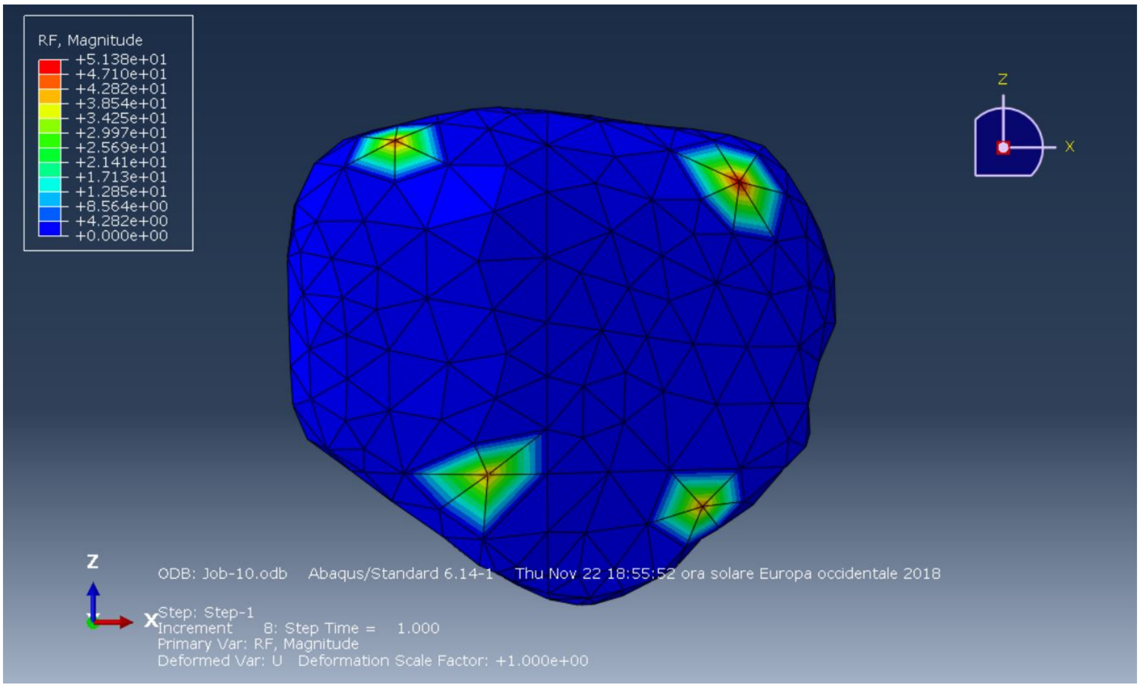

Figure 4-4 RF on patella

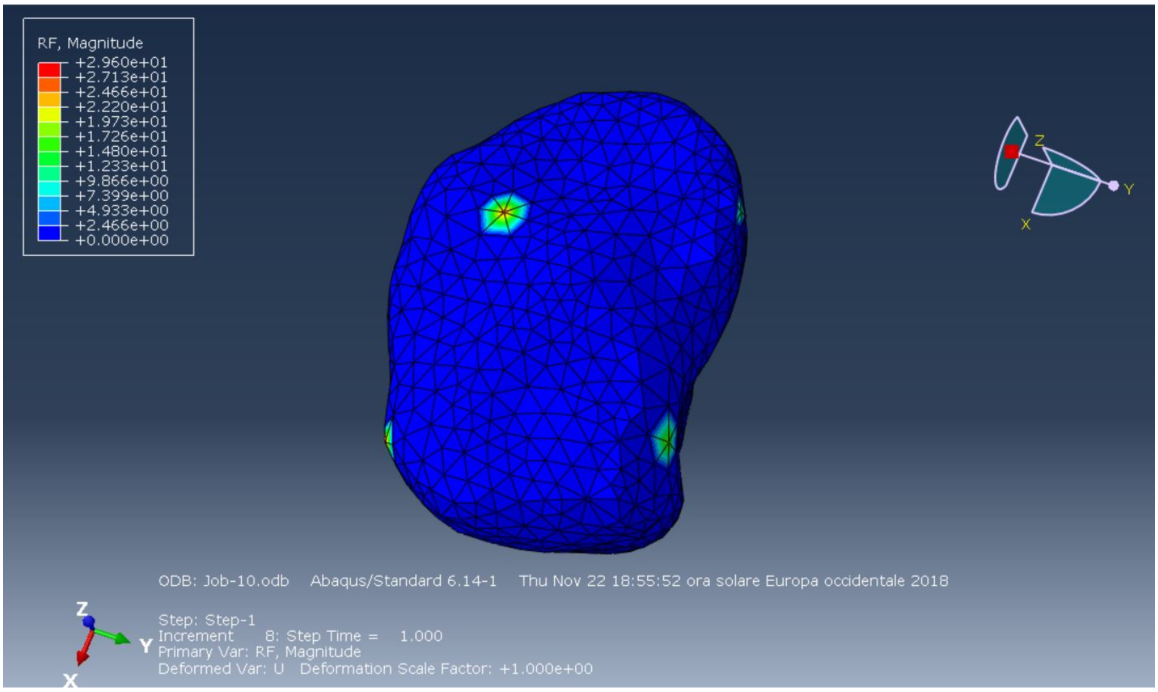

Figure 4-5 RF on tibia

Case 2 – Hyperelastic material (Neo-Hookean), two-leg stance

Hyper elastic material properly embodies biological soft tissue properties. Thus, the same simulation was carried out in this case considering as goal the half load corresponding to a two-leg stance. In this case a Neo-Hookean material was investigated.

Table 4-2 depicts the results obtained in this specific case.

	REACTION FORCES			REACTION MOMENTS		
	Rx (N)	Ry (N)	Rz (N)	Mx (Nm)	My (Nm)	Mz (Nm)
TIBIA	-15	19.055	-43	-0.9955	-2.193	-0.4745
FEMUR	-7.742	18.18	-275	5.7206	-4.1682	-0.3222
FIBULA	-4	19	-58	-1.796	-1.524	-0.359
PATELLA	4.814	20	-11	-0.377	-0.251184	-0.588532
TOTAL	-21.928	76.235	-387	2.5521	-8.13638	-1.74423
NORMALIZED (with mass [U]/kg))	-0.29237	1.0164667	-5.16	0.034028	-0.10849	-0.02326

Table 4-2 Reaction forces and moments in Neo-Hookean case

Case 3 – Hyperelastic material (Mooney-Rivlin), two-leg stance

Hyper elastic material properly embodies biological soft tissue properties. Thus, the same simulation was carried out in this case considering as goal the half load corresponding to a two-leg stance. In this case a Mooney-Rivlin material was investigated.

Table 4-3 depicts the results obtained in this specific case.

	REACTION FORCES			REACTION MOMENTS		
	Rx (N)	Ry (N)	Rz (N)	Mx (Nm)	My (Nm)	Mz (Nm)
TIBIA	-3.6339	-103.149	-313.568	4.1232	-4.8858	1.4945
FEMUR	5.5264	-163.993	-29.3766	2.6923	-3.3469	-1.1386
FIBULA	8.6759	25.2704	-15.5768	24.49	-15.317	4.627
PATELLA	-9.7815	40.0552	-135.991	-4.2739	-3.614	-0.7047
TOTAL	0.7869	-201.816	-494.512	27.0316	-27.164	4.2782
NORMALIZED (with mass [U]/kg))	0.010492	-2.69088	-6.5935	0.360421	-0.3622	0.057043

Table 4-3 Reaction forces and moments for Mooney-Rivlin case

4.2 Analysis of the results

In accordance with applied pressures, deformation process, displacements and stresses are investigated.

Case 1 – Elastic material, single stance

In Fig. 4-6 the deformation process is depicted in different frames, to show the progression of applied pressures on the stump, increasing as a ramp.

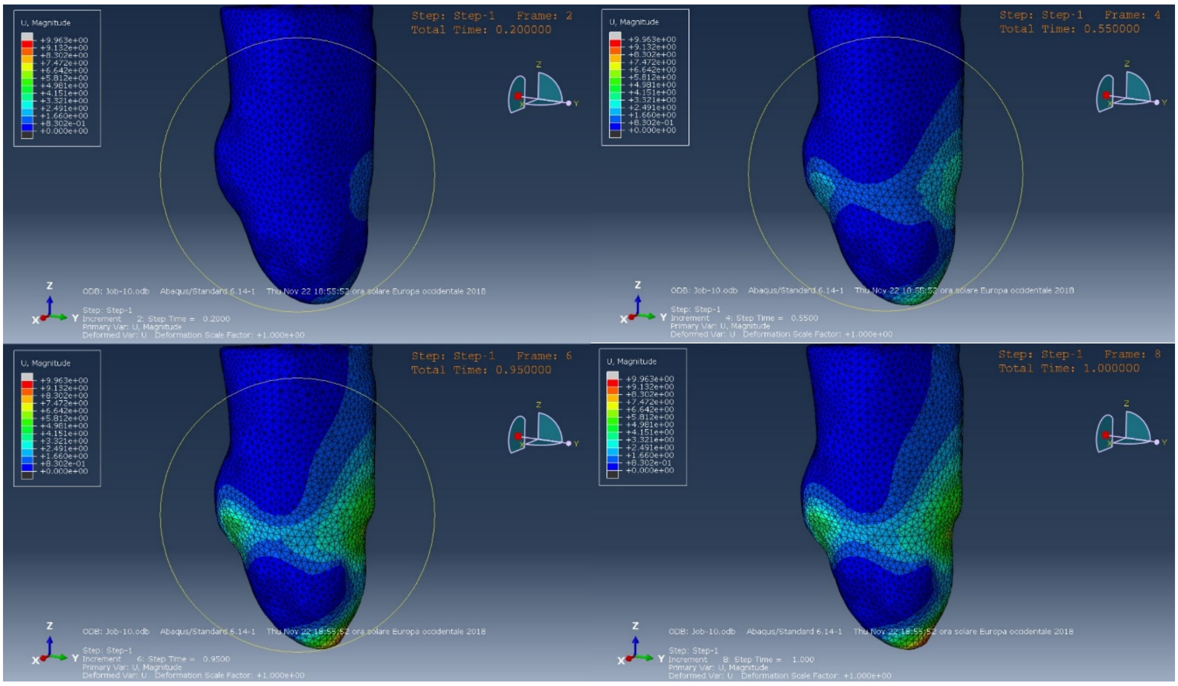

Figure 4-6 Displacement distribution over time

We now focus on the displacement regarding the last frame.

Here we can notice different views in Fig. 4-7 that represents the initial condition. In Figs. (4-8, 4-9) the effects of deformations are depicted.

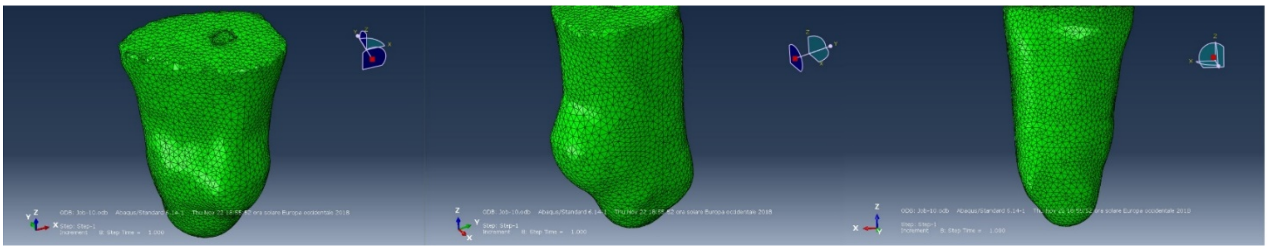

Figure 4-7 Initial configuration of the stump

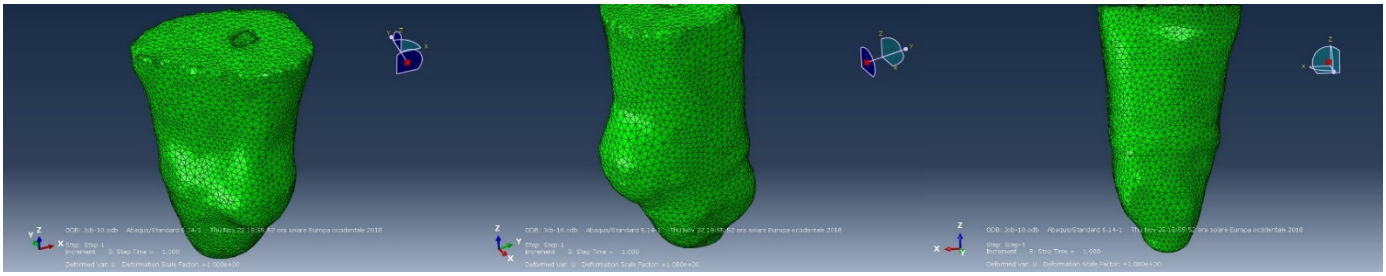

Figure 4-8 Deformed configuration for the linear material

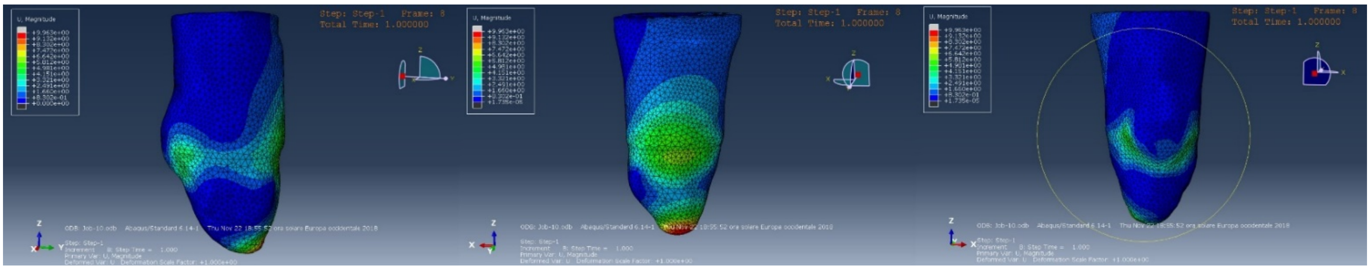

Figure 4-9 Displacement field for linear elastic material

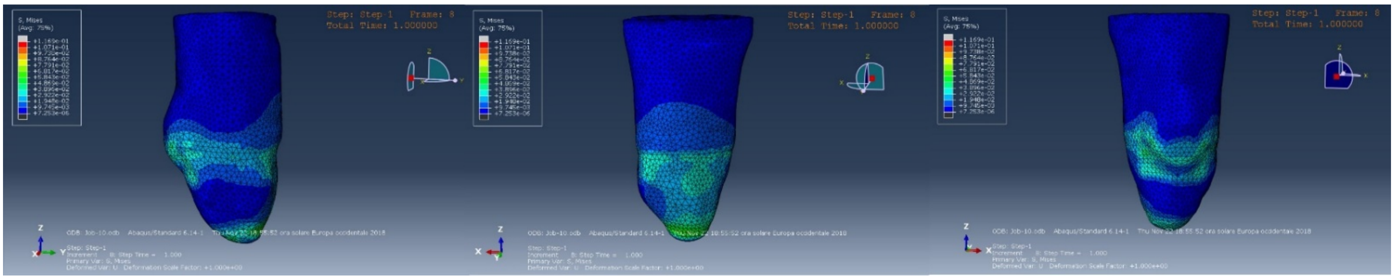

Figure 4-10 Von Mises stress distribution for linear elastic material

As we can notice, most of displacement took place in the highly loaded regions and in the non-loaded one, corresponding to the bottom-edge of the stump. In the latter, there is the pad of muscles, comprised of resection of soleus and gastrocnemius, below the tibia and fibula which are very short. Hence, this region is quite susceptible to deformations.

The maximum displacement that was obtained for nodes was 9.963 mm.

The stress assessment is conducted as a result from the applied pressures on the external surface of the stump. Von Mises stress are here shown in Fig. 4-10. The maximum stress was 116.9 kPa.

This approach was followed in order to compare the results with threshold values taken from literature, to guarantee safety and avoid pressure ulcer and deep tissue injuries such as ischemia in the patient.

Taking advantage of the *ViewCut* tool, we managed to inspect the consequence of such pressure in the deeper tissues, as shown in Figs. (4-11, 4-12).

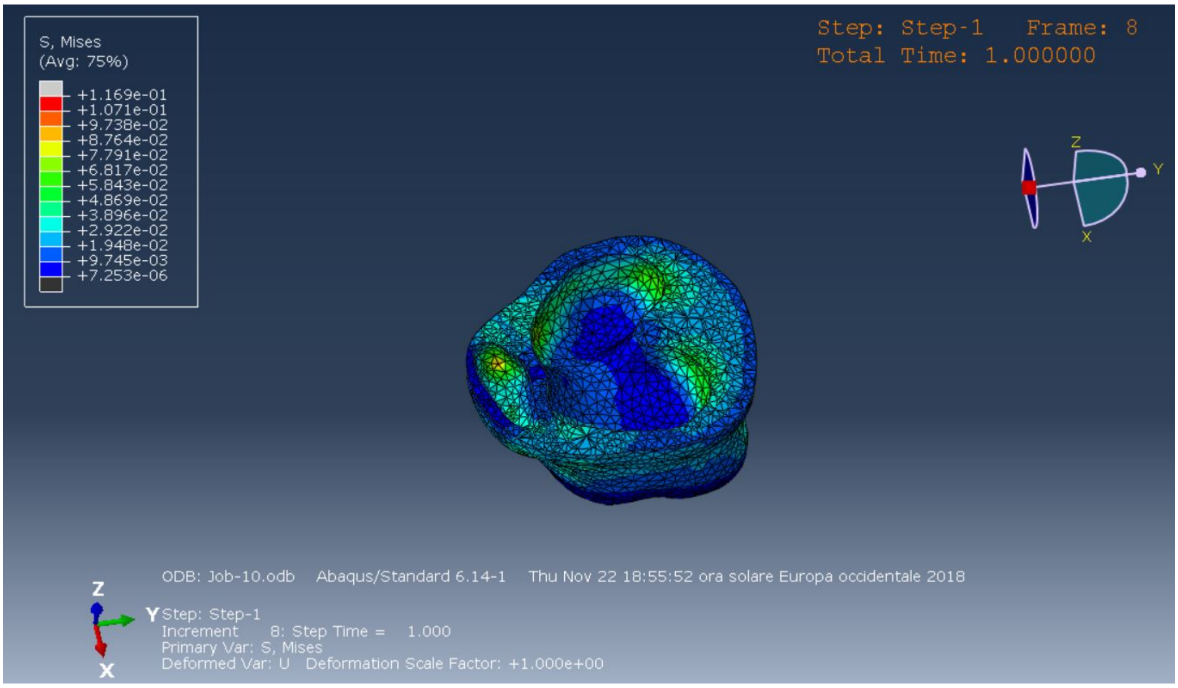

Figure 4-11 *Viewcut* showing the internal situation of Von Mises stress at the level of tibia in the linear elastic case

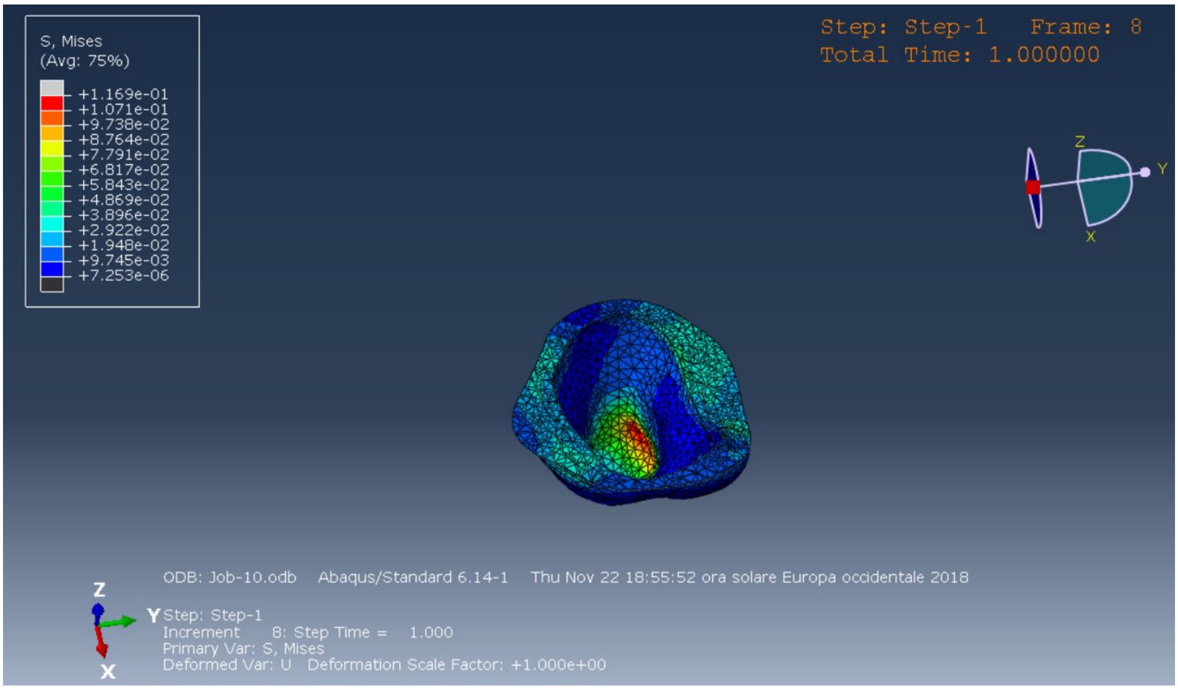

Figure 4-12 *Viewcut* showing internal situation of Von Mises stress at the level of Femur and Patella in the linear elastic case

Case 2 – Hyperelastic material (Neo-Hookean), two leg stance

The deformed configuration is shown in Fig. 4-13 and Fig. 4-14 the deformation process is depicted in different frames, to show the progression of applied pressures on the stump, increasing as a ramp.

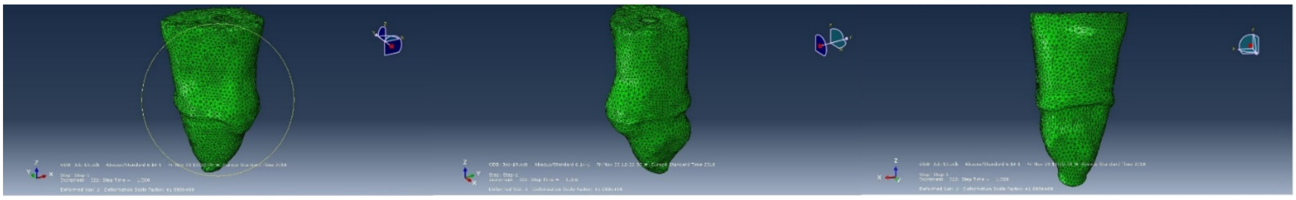

Figure 4-13 Deformed configuration for Neo-Hookean material

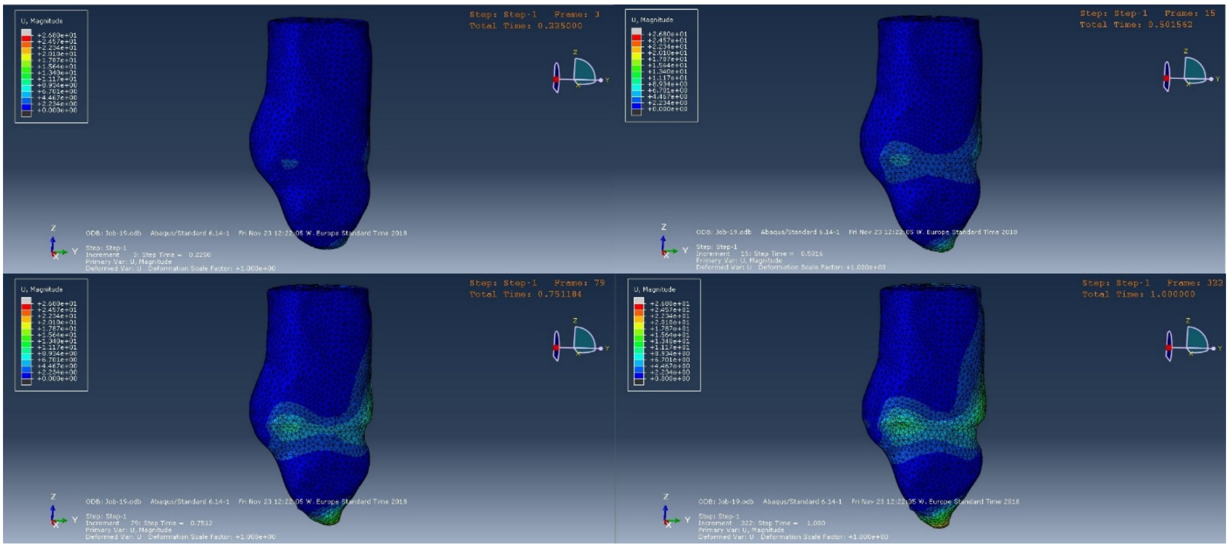

Figure 4-14 Displacement time evolution for Neo-Hookean material

We now focus on the displacement regarding the last frame.

In Fig. 4-15 we can notice different views, to better understand the deformation.

In this case, although the applied pressures are significantly lower with respect to the linear case, the overall obtained displacements are higher, resulting in a more compliant material.

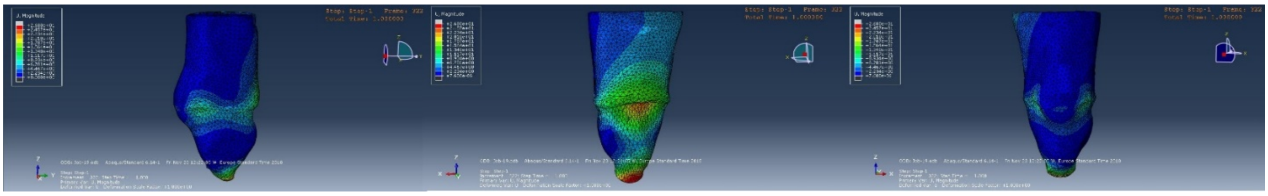

Figure 4-15 Displacement field at the last frame for Neo-Hookean material

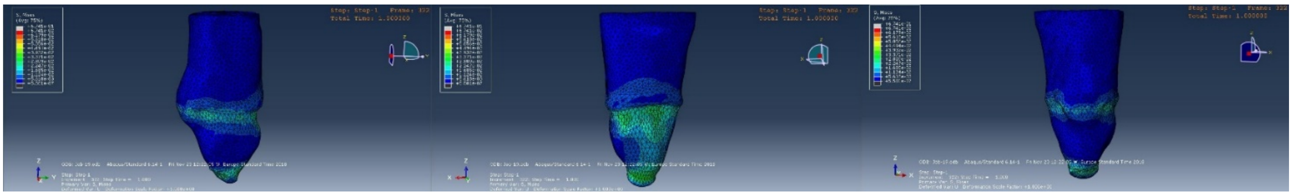

Figure 4-16 Von Mises stress distribution for Neo-Hookean material

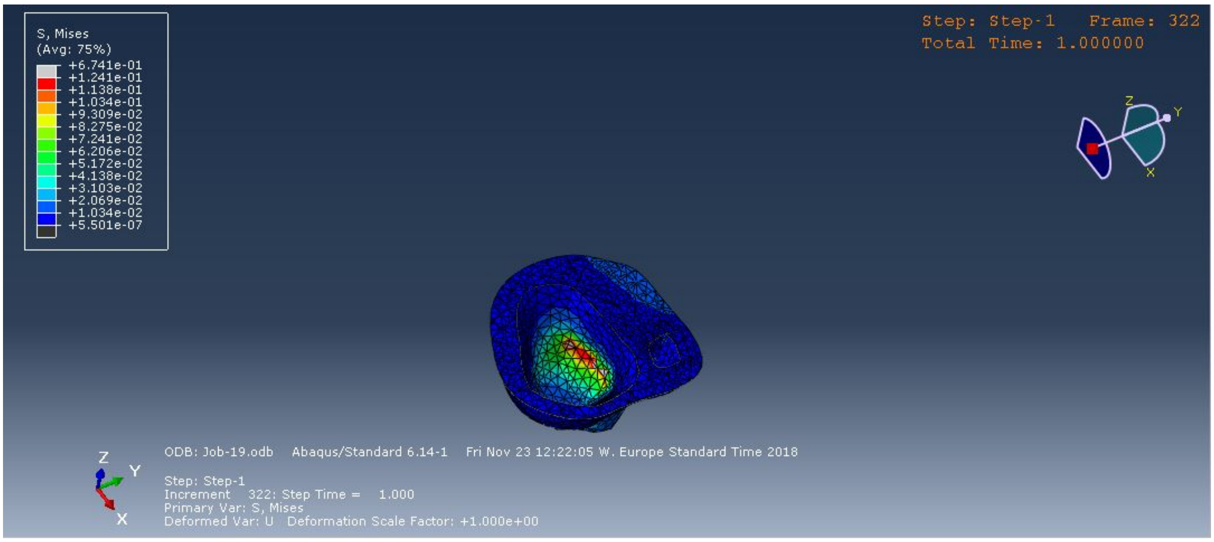

Figure 4-17 *Viewcut* showing the internal situation of Von Mises stress at the level of tibia in Neo-Hookean case

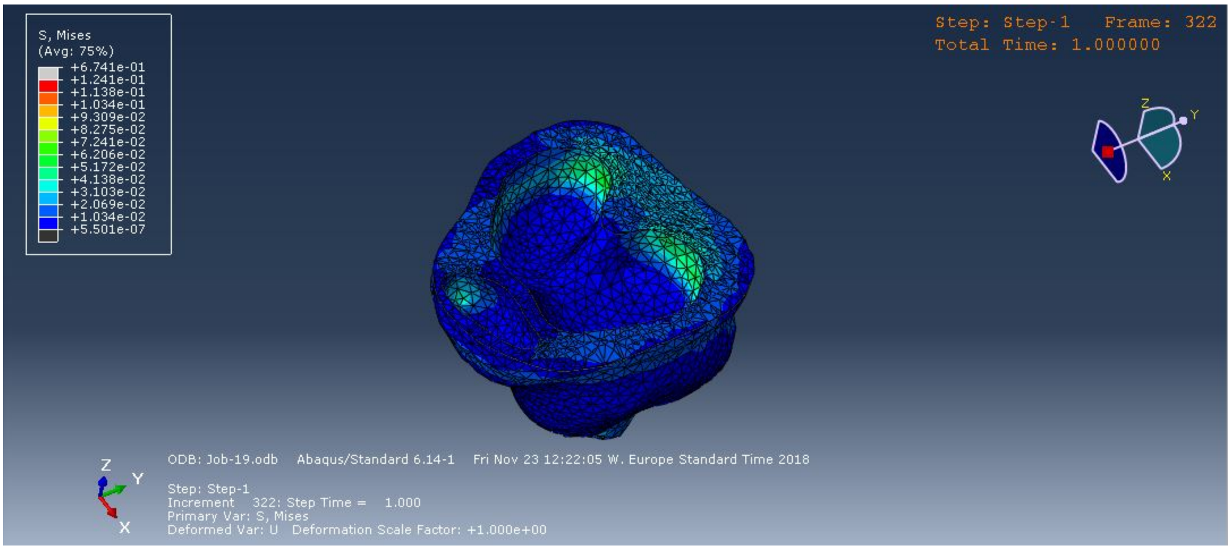

Figure 4-18 *Viewcut* showing internal situation of Von Mises stress at the level of Femur and Patella in Neo-Hookean case

Furthermore, there is a no-brainer to assume that this result can be much more reliable compared to elastic material because it indicates better description of soft tissues.

The maximum displacement that was obtained for nodes was 26.8 mm.

The stress assessment is conducted as a result from the applied pressures on the external surface of the stump. Von Mises stress are here shown in Fig. 4-16. The maximum stress was 674.1 kPa.

This approach was followed in order to compare the results with threshold values taken from literature, to guarantee safety and avoid pressure ulcer and deep tissue injuries such as ischemia in the patient.

Taking advantage of the *ViewCut* tool, we managed to inspect the consequence of such pressure in the deeper tissues, as shown in Figs. 4-17, 4-18.

Case 3 – Hyperelastic material (Mooney-Rivlin), two-leg stance

The deformed configuration is shown in Fig. 4-19 and Fig. 4-20 the deformation process is depicted in different frames, to show the progression of applied pressures on the stump, increasing as a ramp.

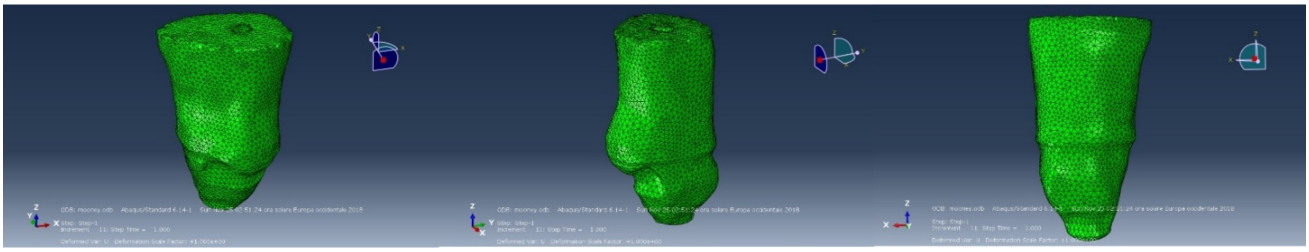

Figure 4-19 Deformed configuration for Mooney-Rivlin material

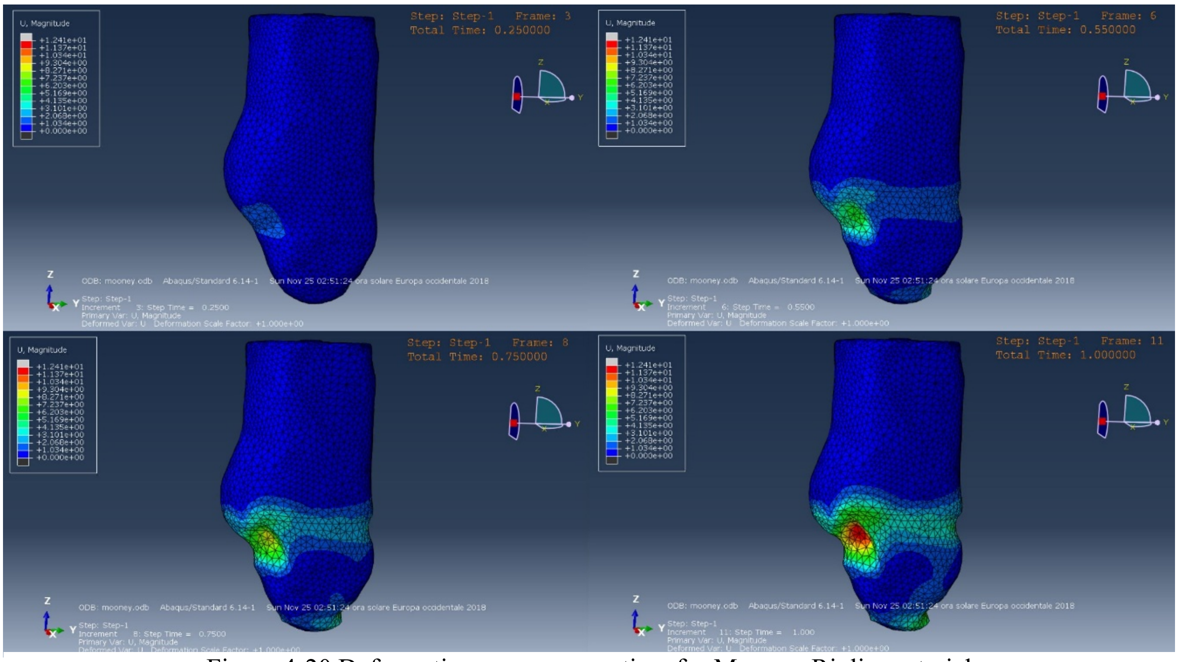

Figure 4-20 Deformation process over time for Mooney-Rivlin material

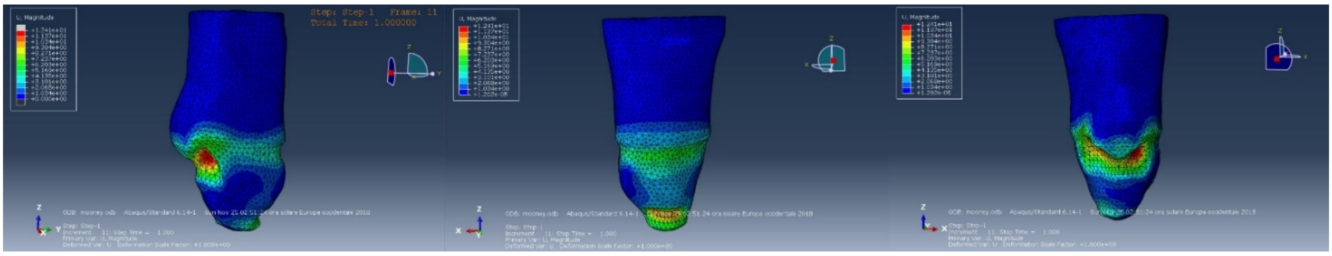

Figure 4-21 Displacement field for Mooney-Rivlin material

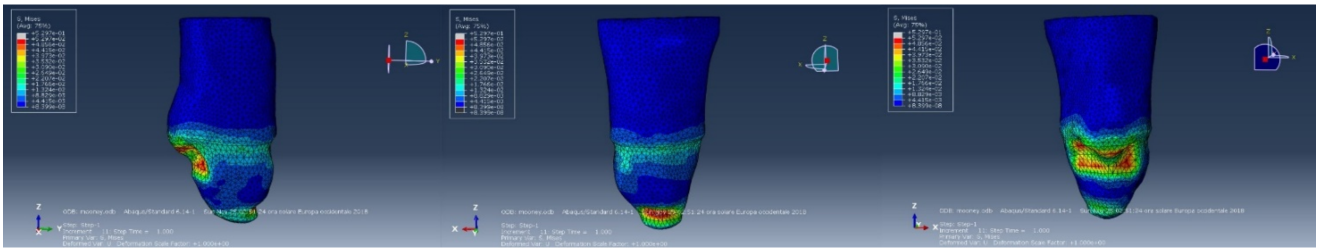

Figure 4-22 Von Mises distribution for Mooney-Rivlin material

We now focus on the displacement regarding the last frame.

In Fig. 4-21 we can notice different views, to better understand the deformation.

In this case, although the applied pressures are significantly lower with respect to the linear case, the overall obtained displacements are higher, resulting in a more compliant material.

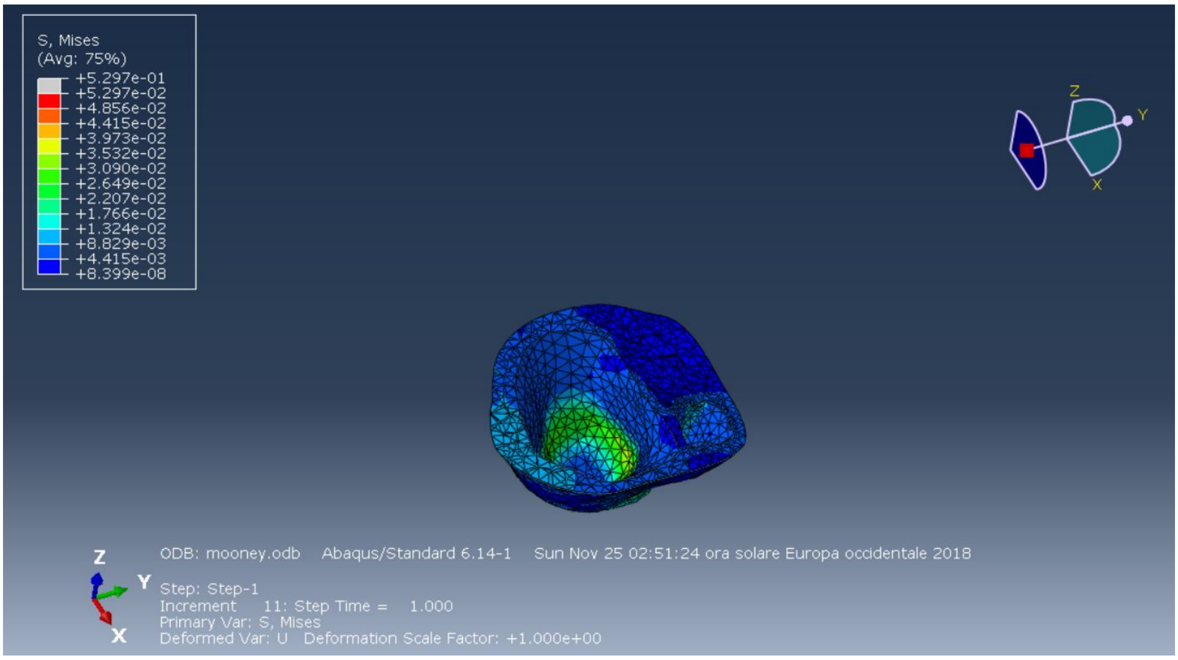

Figure 4-23 *Viewcut* showing the internal situation of Von Mises stress at the level of tibia in Mooney-Rivlin case

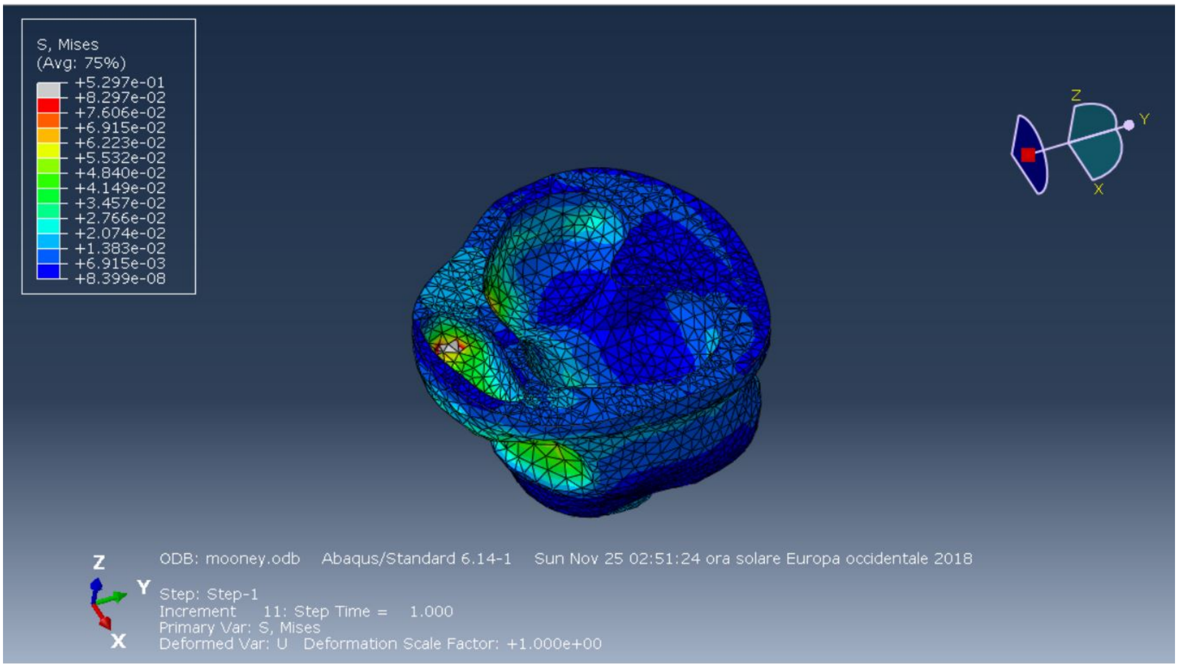

Figure 4-24 *Viewcut* showing internal situation of Von Mises stress at the level of Femur and Patella in Mooney-Rivlin case

Furthermore, there is a no-brainer to assume that this result can be much more reliable compared to elastic material because it indicates better description of soft tissues.

The maximum displacement that was obtained for nodes was 26.8 mm.

The stress assessment is conducted as a result from the applied pressures on the external surface of the stump. Von Mises stress are here shown in Fig. 4-22. The maximum stress was 674.1 kPa.

This approach was followed in order to compare the results with threshold values taken from literature, to guarantee safety and avoid pressure ulcer and deep tissue injuries such as ischemia in the patient.

Taking advantage of the *ViewCut* tool, we managed to inspect the consequence of such pressure in the deeper tissues, as shown in Fig. 4-23, 4-24.

CHAPTER 5 : DISCUSSION AND CONCLUSION

At first, there were some concerns about reaction moments happening on the knee joint, as if they were too high, they would have caused some problems in internal soft tissues and patient would feel pain. The safety of procedure can be ensured through assessment of physiological values checking whether they are meant to fall inside a safety interval or not.

Fig. 5-1 illustrates the biomechanics of human movement elucidating knee extension, rotation and abduction moments[78].

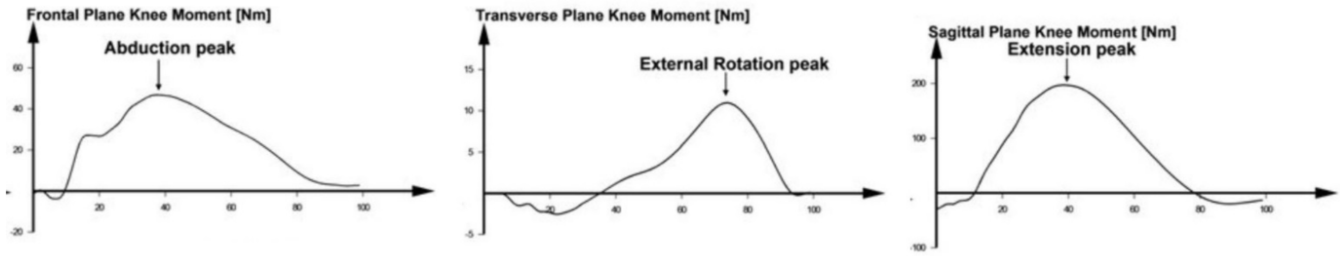

Figure 5-1 External moments acting on the knee. From left to right: abduction, rotation and extension

Since the image acquisition of our model was thorough magnetic resonance imaging, the position of the patient was supine. Thus, some flexion may intervene into the result and it is not quite extension. The peak value of moment around Z direction which depicts the external rotation of the knee by imposing pressure on the external surface of the stump, is 7.33 Nm. This value is related to the simulation by supposing homogeneous, linear isotropic material property for soft tissue in the load scenario of full static load (body weight) on the patient. In accordance with literature(ref), the physiological range for transverse plane knee moment is [-5,15] Nm. Hence, there would not be any severe problem for knee rotation by the values of pressure applied to the model. According to the position of the simulated body with respect to the reference frame, M_x portrays the knee flexion moment resulted from applied pressure. The peak value is 27.0316 Nm in this case which belongs to a simulation by accounting 3-parameter hyperelastic Mooney-Rivlin material property for soft tissue. the values are 2.55 Nm ,6.61Nm In Neo-Hookean hyperelastic and linear elastic assumption the model respectively. The physiological range for knee extension moment is roughly between [-20,200] Nm. Therefore, the safety of finite element process can also be posited for the knee flexion. Moreover, the normal condition of knee adduction moment approximately falls within a range of [-5,50] Nm. The worst scenario in our simulation again is related to Mooney-Rivlin model by exerting the half load (two leg stance) on the patient. The magnitude of M_y is 27.1636 Nm. In linear elastic case, the magnitude of moment around Y direction is 2.74 while in Neo-Hookean hyperelastic presumption is 8.14. the adduction moment obtained in this simulation is near to physiological conditions although is not inside a range. Although in latter cases i.e. both linear elastic and Neo-Hookean are inside a range. Thus, this fluctuation cannot influence on modelling of the new socket. Furthermore, in hyperelastic version of our simulation, the model is highly deformed which is quite difficult to handle with this and rely on the data. Thus, setting up further tests and practical analysis can also overcome these artifacts.

The peak value of von Mises stress in homogenous linear isotropic elastic material is 116.9 KPa. The peak values of von Mises stresses in Moony-Rivlin and Neo-Hookean hyperelastic are 529.7KPa and 674.1 KPa respectively. These discrepancies between values are reasonable due to the fact that the utilized hyperelastic materials are more compliant than linear isotropic one because hyperelastic materials are highly elastic and they can also recover the original shape even after large deformations. Therefore, the results based on displacement also buttress this hypothesis that hyperelastic material is more compliance. Accordingly,The displacement values evaluated for linear elastic, Mooney-Rivlin and Neo-Hookean hyperelastic are 9.963 mm, 12.41 mm and 26.8 mm respectively.

The most important criterion which needs to be taken into account is that imposed pressure must be less than threshold value. Otherwise, if the pressure exceeds the threshold and pain-pressure tolerance, the patient encounters severe problems. Consequently, the strain and stress are going to be elevated. Thus, the rupture of skin or pressure ulcer with different degrees of severity may occur. Moreover, the increase of stress especially in the region of proximity to sharp edge or curved site cause Deep tissue injury such as ischemia. Table 5-1 indicates[50] the threshold values of pain pressure and pain pressure tolerance.

	Fibular head	Medial condyle	Popliteal fossa	End of stump	Patellar tendon
Pain pressure threshold (KPa)	599.6 ± 82.6	555.2 ± 132.2	503.2 ± 134.2	396.3 ± 154.5	919.6 ± 161.7
Pain pressure tolerance (KPa)	789.8 ± 143.0	651.0 ± 111.1	866.6 ± 77.3	547.6 ± 109.1	1158.3 ± 203.2

Table 5-1 Pain pressure threshold and tolerance

In linear elastic and Mooney-Rivlin hyperelastic, the pressure imposed on the patellar tendon is 150 KPa, lower than the pain pressure threshold and pain pressure tolerance. Moreover, this region can tolerate higher pressure compared to the other regions. In popliteal fossa region, the exreted pressure was 110 KPa while the threshold and tolerance values are 503.2 KPa and 866.6 KPa respectively. The applied pressure on the frontal distal residuum was 80 KPa. Thus, the safety also guaranteed in the end of stump in accordance with the threshold values mentioned in table 1. It is also worthwhile to mention that this region is highly sensitive to pressure response. On the other hand, Due to the excessive distortion occurred in simulation of the model by considering Neo-Hookean hyperelastic material properties of the soft tissue, we could not manage to increase the values of pressures more than 50 KPa in all regions although the static load scenario of half load of body weight was satisfied with this pressure. Thus, the linear elastic and Mooney-Rivlin hyperelastic data are much more reliable. As a result, the safety of procedure can be verified where all values are in normal condition. Hence, virtual prototyping of socket shape can be followed. The socket design derived from the deformation of the external surface of the stump which is exposed to loading condition. The expectation would be the patient feel more comfortable after donning the prosthesis and rehabilitation can be expedited.

Many comments regarding issues and future improvements need to be done based on the finite element analysis of the model:

- At first, geometry validated through the ICP algorithm with the laser scan albeit, is not perfect. Some criteria can be followed in order to justify this result: the validation was uniquely performed on the external surface of the skin. Thus, there is no guarantee that the internal shapes of the different features including bones, muscles and fats are quite reliable. Then, the laser scan might be totally performed in a different position i.e. the standing one with respect to the supine one in which patients were constrained to achieve the MRI scan, possibly leads to different joint angle concerning the knee. Thus, it influences the whole validation process.
- Moreover, geometry underwent a strong simplification. As a matter of fact, all internal and external soft tissues, including skin, muscles, fat, tendons and cartilages were incorporated altogether. This assumption was required to impede the complexity of the problem, since maintaining all of them separated, would have meant to introduce interactions between all bodies. This action would have exponentially increased computational power. Then the simulation is not rational to be conducted on a conventional laptop and it is essential to take the advantage of auxiliary system or super-computers from specialized centers. Further works may investigate the effect of step-by-step increasing the complexity of the problem, by considering just the whole muscles together and trying to simulate their interaction with fat and skin. since this choice would allow the user to define distinct material properties for each part. Consequently, the quality of the result would be much more reliable and potentially can be a good way to assess mechanical properties of soft tissue residuum.
- For what concerns materials, some simplifications needed to be taken into consideration. Material parameters were taken from literature, by investigating what was used in previous studies to achieve results related to our main subject. Linear isotropic elastic materials are strong simplifications of what happens in the reality of the mechanics of soft tissue, and although hyper-elastic materials better approach this goal, they are still an approximation for their common behavior. On the other hand, the choice of a linear isotropic elastic material for bone is acceptable, since the range of loads imposed on bone, leads to small deformations that can be easily considered.
- Although bone was described with a highly stiff material (that is almost 10000 times stiffer than the value chosen for the linear elastic soft tissue), it is not actually rigid. This means that, it may undergo some small deformations although the amount is meager. Hence, it affects the computation of the reaction forces on the encastred

nodes following the rigid body hypothesis. The choice of such this material instead of a rigid one, was needed because in *Abaqus/CAE,* all boundary conditions and loads must be applied to the reference points of rigid bodies, which is the geometrical feature to which all nodes of the body refers to translate or rotate. As a matter of better approximation, we evaluated the reaction forces and the moments in 4 points, following the same approach which is usually performed with some dynamometric platforms.

- The loads applied to the stump and their location were initially taken from experimental values mentioned in literature and then progressively increased step-by-step until it reached the desired reaction force on the encastred nodes. This may be a source of errors, as pressure regions and their values should be strongly patient-specific and tailored corresponding to the single case. Exact pressure and bearing areas should be first experimentally determined on the patient, to better describe the real case in the model.
- One important thing that has to be mentioned is that, the patient was in supine position while performing the MRI scanner procedure, the knee is not perfectly extended but a bit flexed. This may have led to some imprecisions on the computation of the reaction forces, as we assumed the patient to be perfectly in standing position. Thus, it probably results in force components in other directions than the z one (the vertical direction in our case) and in the overall moment components due to not ideal joint angles.
- It was already mentioned that the geometry was extremely complex, as many curvatures were present in the external parts while the internal one for soft tissue had irregular voids being the negative of bones shape. Mesh was definitely affected by this feature: although cell partitions were subtly distributed, it was intricate to define hexahedral elements, which would have given a better approximation to the high deformation process occurred in soft tissue and for the interaction constraint between bones and soft tissue itself. Subsequently, tetrahedral elements were defined for the whole system. It facilitates to obtain a good quality mesh with them albeit, they are a source of huge number of problems in contact and large deformation problems. For what concerns contact problems, it was explained that in the *Tie Constraint* the choice regarding the surface adjustment was removed. Such choice was needed as many simulations were failed and couldn't manage to reach convergence because the adjustment of the slave surface (the softer one) on the master surface was introducing some displacements to nodes of the mesh, resulting in sets of bad tetrahedral elements with negative volume. When it comes to large deformations, this problem was more evident when trials were performed on utilized hyper-elastic materials which are more compliant compared to the linear elastic one. During the simulation, many failed attempts were reported due to excessive distortion of the elements, resulting in a slower and sometimes impossible convergence as the time increment plummeted to an infinitesimal power, potentially leading to abortion of the *Abaqus job*.
- In the hyper-elastic case, only half load scenario was accomplished with a reasonable deformation of the stump. Values found in literature turned into a too compliant

model that, even with less than half of the pressures that were imposed in the linear elastic case, was deformed up to 50% more. For this reason, more reliable parameters should be found, if possible pertaining to the real patient by performing some indentation tests, as the percentage of atrophied muscles may change from case to case, according to their activities, shape of the stump and kind of surgery intervention, ending up in a model that may be almost compliant according to the ratio of fatty tissue with respect to the healthy ones.

Starting from the deformations that occurred to the stump, it would be possible to retrieve a negative shape that may be a good starting point for the fabrication of a new kind of prosthetic device. The socket would then need some rectification procedure to happen in order to obtain the final shape that could be used from the patient.

In a future study, the designed socket could be analyzed by virtue of the finite element modelling of the interaction between the stump and socket, in order to deeply assess the donning procedure of such a prosthesis. This would be the first step for the validation of this model. Therefore, once the system is validated in the ‘theoretical model world’, a real prosthesis could be manufactured to perform tests on the patient and retrieving useful data such as contact pressures and real deformations utilizing pressure sensors inserted in the prosthetic device and deformable strain gauges on the stump.

Appendix A – Continuum Mechanics of soft tissues

Biological materials like bones and soft tissues are complex composites whose mechanical properties are outstanding.

An elastic material is a material for which the current stress in the body is determined by the current configuration of the body. In this case, the stress does not rely on the rate in which the deformation occurs or the other aspects of the deformation history[79].

In linear elasticity and tension notation, Hook's law is followed by[48]:

$$\sigma = \lambda tr\,(\varepsilon)\, I + 2\, G\, \varepsilon \qquad (1)$$

Where the σ is the infinitesimal stress tensor:

$$\sigma = \begin{pmatrix} \sigma 11 & \sigma 12 & \sigma 13 \\ \sigma 21 & \sigma 22 & \sigma 23 \\ \sigma 31 & \sigma 32 & \sigma 33 \end{pmatrix} \qquad (2)$$

And ϵ is the infinitesimal strain tensor:

$$\epsilon = \begin{bmatrix} \epsilon 11 & \epsilon 12 & \epsilon 13 \\ \epsilon 21 & \epsilon 22 & \epsilon 23 \\ \epsilon 31 & \epsilon 32 & \epsilon 33 \end{bmatrix} \qquad (3)$$

And where *(I)* is the second order identity tensor. λ and G are the two Lamé coefficients, which are given in terms of two material constants, the Young's modulus *E* and the Poisson's ratio ν:

$$\lambda = \frac{E\nu}{(1+\nu)(1-2\nu)} \qquad (4)$$

$$G = \frac{E}{2(1+\nu)} \qquad (5)$$

G is the shear modulus, the elasticity modulus for shear or torsion. If the linear elastic material model is extended simply, the strain energy density (W), a scalar, is given by the St. Venant–Kirchhoff model:

$$W = \frac{1}{2}\, \lambda [tr(\epsilon)]^2 + \mathrm{Gtr}(\epsilon)^2 \qquad (6)$$

Hyperelastic constitutive laws are utilized to analyze materials which are subjected to large strains[80]. In other words, hyperplastic materials are those which behave elastically recovering original shape even after large deformations. It does this by storing the energy utilized to deform it as strain energy, which is released upon release of the applied load. This is in contradiction to plasticity at large or small deformations, in which the original shape is not recovered [79].

Hyper elasticity relates a strain energy density to stretch as a function of one or more invariants of a deformation tensor. The left and right Cauchy-Green deformation tensors (**b** and **C**) are commonly used[81]:

$$b = F.F^{T}$$
$$C = F^{T}.F \tag{7}$$

Where ***F*** is the deformation gradient $\partial \boldsymbol{x} / \partial \boldsymbol{X}$, and can be defined in terms of the principal stretch ratios λi:

$$F = \begin{bmatrix} \lambda 1 & 0 & 0 \\ 0 & \lambda 2 & 0 \\ 0 & 0 & \lambda 3 \end{bmatrix} \tag{8}$$

From Rivlin[81], for an isotropic incompressible material where the total volume ratio is:

$$J = det\,(F) = \lambda_1 \lambda_2 \lambda_3 = 1 \tag{9}$$

The deformation tensor invariants are:

$$I_1 = \lambda_1^2 + \lambda_2^2 + \lambda_3^2 \tag{10}$$
$$I_2 = \lambda_2^2\lambda_3^2 + \lambda_3^2\lambda_1^2 + \lambda_1^2\lambda_2^2 = \lambda_1^{-2} + \lambda_2^{-2} + \lambda_3^{-2} \tag{11}$$

A Neo-Hookean model was developed for rubber materials by Treloar[82]with the assumption of incompressibility. This allows initially linear stress–strain behavior, and non-linear behavior after a defined threshold level. Its strain energy density function considers the first deformation tensor invariant $\boldsymbol{I_1}$ and the shear modulus only:

$$W_{NH} = \frac{G}{2}(I_1 - 3) \tag{12}$$

Treloar demonstrated its validity for compression but showed shortcomings in tension and shear[83]. This was followed by what is commonly referred to as the Mooney-Rivlin model[84], which was reported to agree with experimental data for soft rubber at strains between 50% compression and 400% extension:

$$W_{MR} = C_{10}(I_1 - 3) + C_{01}(I_2 - 3) \tag{13}$$
$$G = 2(C_{10} + C_{01}) \tag{14}$$

Compressibility can be included by removing the restriction that the volume ratio $J = 1$ and constructing the SED from separate deviatoric W_d and volumetric W_v terms. Deviatoric strain invariants are used, which are functions of the deviatoric stretches ($\overline{\lambda_i}$):

$$\overline{I_1} = \overline{\lambda_1}^2 + \overline{\lambda_2}^2 + \overline{\lambda_3}^2$$
$$\overline{I_2} = \overline{\lambda_1}^{-2} + \overline{\lambda_2}^{-2} + \overline{\lambda_3}^{-2} \tag{15}$$

The deviatoric stretches are related to the principal stretches as a function of the total volume ratio:

$$\bar{\lambda}_i = J^{-1/3}\lambda i \tag{16}$$

In the case of incompressible materials (J = 1), these are equivalent. For example, compressibility can be added as an extension to the Neo-Hookean model:

$$W = W_d + W_v = C_{10}(\bar{I}_1 - 3) + \frac{1}{D_1}(J-1)^2 \tag{17}$$

C_{10} and D_1 are constitutive model parameters, with C_{10} still equal to half the shear modulus, and D_1 related to the bulk modulus K, where:

$$D_1 = \frac{2}{K} \tag{18}$$

$$K = \frac{E}{3(1-2v)} = \frac{2G(1+v)}{3(1-2v)} \tag{19}$$

The strain energy density function was proposed to be an infinite expansion of the two deformation tensor invariants I_1 and I_2 by Mooney[84] and Rivlin[81], given in general form by Ogden[85] :

$$W = \sum_{i,j=0}^{\infty} C_{ij}(I_1 - 3)^i (I_2 - 3)^j \quad C_{00} = 0 \tag{20}$$

And is alternatively given in generalized polynomial form, with polynomial order m:

$$W = \sum_{i+j=1}^{m} C_{ij}(I_1 - 3)^i (I_2 - 3)^j \tag{21}$$

Finally, the generalized polynomial form can be modified to include compressibility effects:

$$W = \sum_{i+j=1}^{m} C_{ij}(\bar{I}_1 - 3)^i (\bar{I}_2 - 3)^j + \sum_{i=1}^{m} \frac{1}{D_1}(J-1)^{2i} \tag{22}$$

With general constitutive model parameters C_{ij} and D_1.

The Neo-Hookean and Mooney Rivlin models are 1st order formulations, utilized to model scar, fat muscle, and combined soft tissues in literature. The extended Mooney model is a 2nd order formulation, used to represent the skin:

$$w = C_{10}(I_1 - 3) + C_{11}(I_1 - 3)(I_2 - 3) \tag{23}$$

Finally, the James-Green–Simpson model is a 3rd order formulation, which has been employed to represent the combined structure of soft tissue layers together[86], [87]:

$$W = C_{10}(I_1 - 3) + C_{01}(I_2 - 3) + C_{11}(I_1 - 3)(I_2 - 3) + C_{20}(I_1 - 3)^2 + C_{30}(I_1 - 3)^3 \quad (24)$$

The derivative of the strain energy function with respect to a particular strain component ε_{ij} gives the corresponding stress component σ_{ij}:

$$\sigma_{ij} = \frac{\delta W}{\delta \varepsilon_{ij}} \quad (25)$$

And these SED functions are employed by performing an empirical fit of a proposed material model to experimental stress–strain experimental data, by selecting appropriate terms and constitutive model parameter values for C_{ij} and D_1 .

A typical modeling formulation[52] employing FE package ABAQUS is to calculate the finite strain 'Green-Lagrange strain tensor'.

$$E = \frac{1}{2}(C - I) \quad (26)$$

Using applied bone displacement boundary conditions, from which the 'second Piola-Kirchhoff stress tensor' (S) is calculated:

$$S = \frac{\partial W}{\partial E} \quad (27)$$

And finally, the Cauchy (true) stress tensor (σ) can be derived:

$$\sigma = J^{-1} F . S . F^T \quad (28)$$

These stresses are then plotted as in conventional linear elastic FEA utilized to delineate tissue damage risk predictions in comparison to threshold damage levels, and equivalent stress magnitude (often referred to in FEA packages as 'von Mises' stress).

Appendix B – Finite Element Method

General considerations

Considering a mathematical model describing a physical system, some fundamental equations are necessary to describe it.

We refer to:

Compatibility equations, relating strains and displacements

$$\varepsilon_{ij} = \frac{1}{2}\left(\frac{\partial u_i}{\partial x_j} + \frac{\partial u_j}{\partial x_i}\right) \tag{1}$$

Equilibrium equations between body forces and stresses:

$$\sigma_{i,j} + b_j = 0 \tag{2}$$

Constitutive equations, representing the relation between stresses and strains 4th order tensor:

$$\sigma_{ij} = D_{ijhk}\varepsilon_{hk} \tag{3}$$

Boundary conditions, on boundary surfaces and in equilibrium with applied loads

$$\begin{cases} u_i = \overline{u_i} \\ \sigma_{ij} n_j = \overline{f_i} \end{cases} \tag{4}$$

A Finite Element model is described as a system formed by many elements, each with a specific thickness and represented by a ‘inner’ stiffness matrix.

$$[K_e] * \{u_e\} = \{F_e\} \tag{5}$$

with K_e being the stiffness matrix, u_e the collection of all the degrees of freedom and F_e the applied external loads.

The overall system can be described by the following linear system, accounting for the contribution of all the elements:

$$[K] * \{u\} = \{F\} \tag{6}$$

Such relation can be obtained by applying the Principal of Virtual Work (PVW). Considering Π as the difference between the internal energy in a system U and the external work of the body (b), surface (fs) and external forces (F) W, we have:

$$\Pi = U - W = \frac{1}{2}\int_{\Omega} \underline{\varepsilon}^T \underline{\sigma}\, dV - \int_{\Omega} \underline{u}^T \underline{b} dV - \int_{\Gamma} \underline{u}^T \underline{f_s} dS - \sum_i \underline{u_i^T}\, \underline{F_i} \tag{7}$$

A system is in equilibrium if, according to PVW, the perturbation of Π is zero. Therefore, $\delta\Pi = 0$, by applying some virtual displacements. This means that:

$$\frac{1}{2}\int_{\Omega} \underline{\delta\varepsilon^T}\, \underline{\sigma}\, dV = \int_{\Omega} \underline{\delta u^T}\, \underline{b} dV + \int_{\Gamma} \underline{\delta u^T}\, \underline{f_s} dS + \sum_i \underline{\delta u_i^T}\, \underline{F_i} \tag{8}$$

The concept of element is introduced. Due to integral's linear property, each integral over a domain can be seen as the sum of the integrals of smaller subdomains whose sum corresponds to the initial one. Moreover, displacements, strains and stresses over the element can be related through matrixes to nodes' degrees of freedom.

$$\begin{cases} \underline{u^e(x)} = \underline{\underline{\Phi}}\, \underline{U} \\ \underline{\varepsilon^e(x)} = \underline{\underline{B}}\, \underline{U} \\ \underline{\sigma^e(x)} = \underline{\underline{D}}\, \underline{\varepsilon(x)} + \underline{\sigma_0} \end{cases} \tag{9}$$

With $\underline{U}$ being the vector containing the whole degrees of freedom of the element, Φ the interpolation matrix containing shape functions (later further described), B a matrix containing combinations of derivatives of Φ to allow the relation between strains and displacements, D the constitutive matrix relating strains and stresses and σ_0 the pre-stress that may be applied to the element.

So, subdividing the Ω domain in N elements, the PVW considering all the elements can be rewritten as:

$$\begin{aligned} &\sum_{i=1}^{N} \int_{\Omega i} \underline{u^T}\, \underline{\underline{B^e D B^e}}\underline{u}\, dV \\ &\quad = \sum_{i=1}^{N} \left\{ \int_{\Omega i} \underline{u^T}\, \underline{\underline{\Phi^e}}\underline{b}\, dV + \int_{\Gamma i} \underline{u^T}\, \underline{\underline{\Phi^{es\,T}}}\underline{f_s}\, dV \right\} + \sum_j \underline{u^T}\, \underline{\underline{\Phi^T}}\, \underline{F_j} \\ &\quad - \sum_{i=1}^{N} \int_{\Omega i} u^T B^{eT} \sigma_0 dV \end{aligned} \tag{10}$$

Obtaining:

$$\sum_{i=1}^{N} \underline{\underline{K_j^e}}\, \underline{U} = \underline{F_B} + \underline{F_s} + \underline{F_c} + \underline{F_0} \tag{11}$$

This can be simplified in the previously shown:

$$[K] * \{u\} = \{F\} \tag{6}$$

3D Elements and shape functions

In a 3D domain different kind of elements can be chosen, according to the possibility to use them and the need. The most common ones are tetrahedral and hexahedral ones. (Fig. B1-B2)[88], [89]

FE Analysis is usually performed using isoparametric functions, considering a local reference system with an ideal element shape. Shape functions for every node can therefore be defined in this new frame, thus making the whole analysis easier to be performed. A shape function must fulfill the following property:

$$N_i(x_j) = \begin{cases} 1 \; if \; i = j \\ 0 \; if \; i \neq j \end{cases} \tag{12}$$

Considering for example the simplest 4-node tetrahedral element in an isoparametric domain, its shape functions related to the different nodes will be[90], [91]:

$$\begin{cases} N_1 = r \\ N_2 = s \\ N_3 = t \\ N_4 = 1 - r - s - t \end{cases} \tag{13}$$

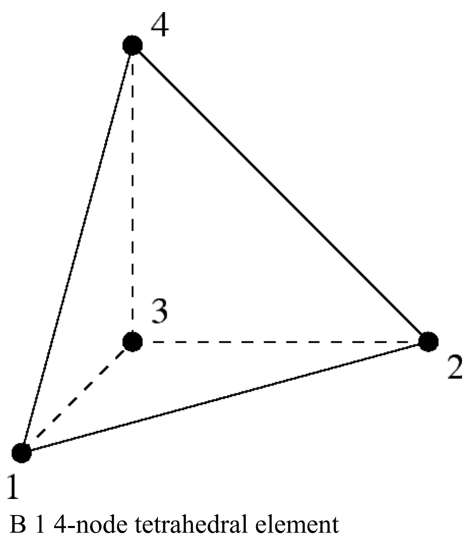

B 1 4-node tetrahedral element

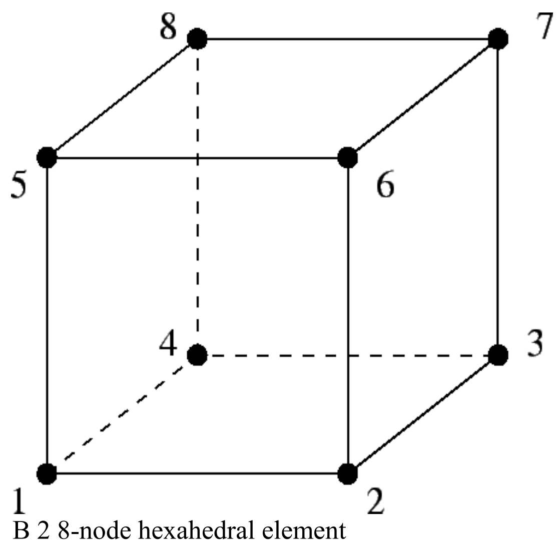

B 2 8-node hexahedral element

Role of mesh distortion

As mentioned before, isoparametric functions are used to simplify the analysis: shape functions are therefore defined in a (r, s) reference system, needing a transformation to go back to the local one.

Considering the derivative of displacement along direction r (as to define strains we need to use them), for the chain rule we would have:

$$\frac{\partial u}{\partial r} = \frac{\partial u}{\partial x} * \frac{\partial x}{\partial r} + \frac{\partial u}{\partial y} * \frac{\partial y}{\partial r} + \frac{\partial u}{\partial z} * \frac{\partial z}{\partial r} \tag{14}$$

Meaning that in 3D we will have:

$$\begin{bmatrix} \frac{\partial u}{\partial r} \\ \frac{\partial u}{\partial s} \\ \frac{\partial u}{\partial t} \end{bmatrix} = \begin{bmatrix} \frac{\partial x}{\partial r} & \frac{\partial y}{\partial r} & \frac{\partial z}{\partial r} \\ \frac{\partial x}{\partial s} & \frac{\partial y}{\partial s} & \frac{\partial z}{\partial s} \\ \frac{\partial x}{\partial t} & \frac{\partial y}{\partial t} & \frac{\partial z}{\partial t} \end{bmatrix} \begin{bmatrix} \frac{\partial u}{\partial x} \\ \frac{\partial u}{\partial y} \\ \frac{\partial u}{\partial z} \end{bmatrix} \tag{15}$$

Where the matrix J is the Jacobian, whose entries may not be constant.

It can be proven that element's stiffness matrix is related to the determinant of the Jacobian, meaning that mesh distortion may lead to errors in the evaluation of the stiffness of the system[90], [91].

Non linearities

Non linearities are important to be treated. Dealing with soft materials, undergoing large strains and displacements, and contacts, it's fundamental to understand the possible consequences and effects on the system.

Large strains mean totally different configurations at different time frames.

Therefore, the PVW can be rewritten, in the unknown configuration i+1 as:

$$\begin{aligned} \int_{V^{i+1}} \delta\varepsilon^{(i+1)\,T}\, \sigma^{(i+1)} dV^{(i+1)} \\ = \int_{V^{i+1}} \delta u^{(i+1)\,T}\, b^{(i+1)} dV^{(i+1)} \\ + \int_{S^{i+1}} \delta u^{(i+1)\,T}\, f^{(i+1)} dS^{(i+1)} \end{aligned} \tag{16}$$

According to the reference configuration that is taken into account, there are two possible approaches:

- Total lagrangian formulation; reference is the initial one
- Updated lagrangian formulation: reference is the last known one.

Considering the first case and rewriting the system according to the chosen reference, we obtain the following equations:

$$\begin{cases} K^{(t)}\Delta U = \{R^{(t+1)} - F^{(t)}\} \\ U_k^{(t+1)} = U_{k-1}^{(t+1)} + \Delta U_k \end{cases} \tag{17}$$

With k being the number of iterations to reach the solution and ΔU the incremental displacement.

The solution reaches convergence after k iterations are done, when the ΔU = 0, therefore meaning that $R^{(t+1)} - F^{(t)} = 0$, which represents a sort of balance between external and internal nodal forces[90], [91].

Bibliography

[1] W. Lovegreen, D. P. Murphy, W. K. Smith, and P. Stevens, *Lower Limb Amputation and Gait*. Elsevier Inc., 2016.

[2] “Healthline.”Available:https://www.healthline.com/health/diabetes/diabetes-amputation (for diabetes).

[3] P. F. Pasquina, M. Miller, A. J. C. Michael, J. Vandersea, and E. Johnson, “Special Considerations for Multiple Limb Amputation,” pp. 273–289, 2014.

[4] H. P. Ledermann, W. B. Morrison, and M. E. Schweitzer, “MR Image Analysis of Pedal Osteomyelitis : Distribution , Patterns of Spread , and Frequency of Associated,” no. 7, pp. 747–755, 2002.

[5] C. Thomas-ramoutar, E. Tierney, and R. Frykberg, “Osteomyelitis and Lower Extremity Amputations in the Diabetic Population,” pp. 18–27, 2010.

[6] “Osteomyelitis.” Available: https://rarediseases.org/rare-diseases/osteomyelitis/.

[7] “Frostbite.” Available: https://orthoinfo.aaos.org/en/diseases--conditions/frostbite/.

[8] L. B. Rozeman and P. C. W. Hogendoorn, “Pathology of primary malignant bone and cartilage tumours,” pp. 437–444, 2006.

[9] P. Varma, M. G. Stineman, and T. R. Dillingham, “Epidemiology of Limb Loss Amputation Limb loss Dysvascular Transfemoral Transtibial,” vol. 25, pp. 1–8, 2014.

[10] M. Roeder, “Review of secondary physical conditions associated with lower-limb amputation and long-term prosthesis use,” vol. 45, no. 1, pp. 15–29, 2008.

[11] R. Sakkers and I. Van Wijk, “Amputation and rotationplasty in children with limb deficiencies : current concepts,” *J. Child. Orthop.*, vol. 10, no. 6, pp. 619–626, 2016.

[12] A. Courvoisier, F. Sailhan, R. Vialle, and J. Damsin, “Congenital tibial deficiencies : Treatment using the Ilizarov ’ s external fixator,” 2009.

[13] “Atlas of Limb Prosthetics.” [Online]. Available: http://www.oandplibrary.org/alp/.

[14] R. L. Waters, J. Perry, D. Antonelli, and H. Hislop, “Energy cost of walking of amputees : the influence of level of amputation The Influence of Walking of Level of Amputees : of Amputation,” pp. 42–46, 2010.

[15] Frank A. Gottschalk, “Rehabilitation: Gait, Amputations, Prostheses, Orthoses, and Neurologic Injury.” [Online]. Available: https://clinicalgate.com/rehabilitation-gait-amputations-prostheses-orthoses-and-neurologic-injury/.

[16] M. M. D. Burgess, “Amputations Below the Knee,” pp. 1–12.

[17] “Lower-ExtremityAmputations.”Available: https://emedicine.medscape.com/article/1232102-overview.

[18] Available: https://www.hopkinsmedicine.org/healthlibrary/test_procedures/cardiovascular/amp

utation_92,P08292.

[19] B. C. Taylor and A. Poka, “Osteomyoplastic transtibial amputation : technique and tips,” pp. 6–9, 2011.

[20] C. Huston and T. R. Dillingham, “Chapter 4 REHABILITATION OF THE LOWER LIMB AMPUTEE,” pp. 79–159.

[21] C. Amputations, C. R. R. Granville, L. Colonel, D. A. Gajewski, W. Reed, A. Medical, B. Army, and F. S. Houston, “Heterotopic Ossification Following Traumatic and Combat-Related Amputations,” pp. 476–486, 2007.

[22] K. M. Norton, “A Brief History of Prosthetics.”

[23] R Chinathurai, "*Short-Textbook-of-Prosthetics-and-Orthotics"* © 2010, Jaypee Brothers Medical Publishers (P) Ltd.

[24] H. Gholizadeh, N. A. A. Osman, A. Eshraghi, S. Ali, and N. A. Razak, “Clinical Biomechanics Transtibial prosthesis suspension systems : Systematic review of literature,” *JCLB*, vol. 29, no. 1, pp. 87–97, 2014.

[25] S. Ali, N. Azuan, A. Osman, and M. M. Naqshbandi, “Qualitative Study of Prosthetic Suspension Systems on Transtibial Amputees ’ Satisfaction and Perceived Problems,” *YAPMR*, vol. 93, no. 11, pp. 1919–1923, 2012.

[26] G. Pirouzi, N. Azuan, A. Osman, A. A. Oshkour, S. Ali, H. Gholizadeh, and W. A. B. W. Abas, “Development of an Air Pneumatic Suspension System for Transtibial Prostheses,” vol. c, pp. 16754–16765, 2014.

[27] H. Hashimoto, T. Kobayashi, F. Gao, M. Kataoka, and M. S. Orendur, “Gait & Posture The e ff ect of transverse prosthetic alignment changes on socket reaction moments during gait in individuals with transtibial amputation,” vol. 65, no. June, pp. 8–14, 2018.

[28] K. Devinuwara, A. Dworak-Kula, and R. J. O’Connor, “Rehabilitation and prosthetics post-amputation,” *Orthop. Trauma*, vol. 32, no. 4, pp. 234–240, 2018.

[29] K. Ida, “Ida - 2015 - Rehabilitation of lower limb amputees,” vol. 117, no. 1, pp. 147–159, 2015.

[30] A. Hershkovitz, I. Dudkiewicz, and S. Brill, “Rehabilitation outcome of post-acute lower limb geriatric amputees,” *Disabil. Rehabil.*, vol. 35, no. 5, pp. 221–227, 2013.

[31] C. K. G. Chu and M. S. Wong, “Comparison of prosthetic outcomes between adolescent transtibial and transfemoral amputees after Sichuan earthquake using Step Activity Monitor and Prosthesis Evaluation Questionnaire,” *Prosthet. Orthot. Int.*, vol. 40, no. 1, pp. 58–64, 2016.

[32] W. E. Evans, “Clinical pharmacodynamics of anticancer drugs: a basis for extending the concept of dose-intensity,” *Blut*, vol. 56, no. 6, pp. 241–248, 1988.

[33] Available: http://www.apta.org/.

[34] I. Churilov, L. Churilov, and D. Murphy, “Do rigid dressings reduce the time from amputation to prosthetic fitting? A systematic review and meta-analysis,” *Ann. Vasc.*

Surg., vol. 28, no. 7, pp. 1801–1808, 2014.

[35] B. Sign, "Therapy advice following your above knee amputation," no. October, pp. 1–12, 2018.

[36] F. T. NHS, "Rehabilitation after your lower limb amputation," *Guy's St Thomas*, p. 19, 2016.

[37] B. Hordacre, L. V. Bradnam, and M. Crotty, "Reorganization of the primary motor cortex following lower-limb amputation for vascular disease: a pre-post-amputation comparison," *Disabil. Rehabil.*, vol. 39, no. 17, pp. 1722–1728, 2017.

[38] Available: https://www.physio-pedia.com/Prosthetic_rehabilitation.

[39] B. J. Darter, A. J. Bastian, E. J. Wolf, E. M. Husson, B. A. Labrecque, and B. D. Hendershot, "Locomotor adaptability in persons with unilateral transtibial amputation," *PLoS One*, vol. 12, no. 7, pp. 1–18, 2017.

[40] C. T. Barnett, R. C. J. Polman, and N. Vanicek, "Longitudinal kinematic and kinetic adaptations to obstacle crossing in recent lower limb amputees," *Prosthet. Orthot. Int.*, vol. 38, no. 6, pp. 437–446, 2014.

[41] A. Kharb, V. Saini, Y. Jain, and S. Dhiman, "A review of gait cycle and its parameters," *IJCEM Int J Comput Eng Manag*, vol. 13, no. July, pp. 78–83, 2011.

[42] "PROTESI PER."

[43] "MR1.pdf." .

[44] H. Asao, Y. Nishizawa, S. Arai, T. Sato, M. Hirai, K. Yoshida, A. Shinmyo, and T. Hibi, *Enhanced resistance against a fungal pathogen sphaerotheca humuli in transgenic strawberry expressing a rice chitinase gene*, vol. 14, no. 3. 1997.

[45] F. Cards, *M A ST E R anatomy your way*. .

[46] T. Y. Eng and P. Luff, "Competing and developing competitive advantage in the digital world," *Technol. Anal. Strateg. Manag.*, vol. 23, no. 9, pp. 947–950, 2011.

[47] F. . K. G.E. Wadsworth, H.O. Kendall, *Muscles – Testing and Function*, 2th ed. .

[48] A. S. Dickinson, J. W. Steer, and P. R. Worsley, "Finite element analysis of the amputated lower limb: A systematic review and recommendations," *Med. Eng. Phys.*, vol. 43, pp. 1–18, 2017.

[49] M. Zhang and C. Roberts, "Comparison of computational analysis with clinical measurement of stresses on below-knee residual limb in a prosthetic socket," *Med. Eng. Phys.*, vol. 22, no. 9, pp. 607–612, 2001.

[50] M. Hengstberger and M. Stark, "Fibre and particle release from cigarette filters," *Beitrage zur Tab. Int. Contrib. to Tob. Res.*, vol. 23, no. 6, pp. 338–350, 2009.

[51] D. Lacroix and J. F. Ramírez Patiño, "Finite element analysis of donning procedure of a prosthetic transfemoral socket," *Ann. Biomed. Eng.*, vol. 39, no. 12, pp. 2972–2983, 2011.

[52] S. Portnoy, Z. Yizhar, N. Shabshin, Y. Itzchak, A. Kristal, Y. Dotan-Marom, I. Siev-

Ner, and A. Gefen, “Internal mechanical conditions in the soft tissues of a residual limb of a trans-tibial amputee,” *J. Biomech.*, vol. 41, no. 9, pp. 1897–1909, 2008.

[53] J. F. Ramírez and J. A. Vélez, “Incidence of the boundary condition between bone and soft tissue in a finite element model of a transfemoral amputee,” *Prosthet. Orthot. Int.*, vol. 36, no. 4, pp. 405–414, 2012.

[54] J. Sullivan, M. Uden, K. P. Robinson, and S. Sooriakumaran, “Rehabilitation of the trans-femoral amputee with an osseointegrated prosthesis: The United Kingdom experience,” *Prosthet. Orthot. Int.*, vol. 27, no. 2, pp. 114–120, 2003.

[55] H. H. Aschoff, R. E. Kennon, J. M. Keggi, and L. E. Rubin, “Transcutaneous, distal femoral, intramedullary attachment for above-the-knee prostheses: An endo-exo device,” *J. Bone Jt. Surg. - Ser. A*, vol. 92, no. SUPPL. 2, pp. 180–186, 2010.

[56] K. Hagberg, R. Brånemark, B. Gunterberg, and B. Rydevik, “Osseointegrated trans-femoral amputation prostheses: Prospective results of general and condition-specific quality of life in 18 patients at 2-year follow-up,” *Prosthet. Orthot. Int.*, vol. 32, no. 1, pp. 29–41, 2008.

[57] E. E. Haggstrom, E. Hansson, and K. Hagberg, “Comparison of prosthetic costs and service between osseointegrated and conventional suspended transfemoral prostheses,” *Prosthet. Orthot. Int.*, vol. 37, no. 2, pp. 152–160, 2013.

[58] P. Stenlund, M. Trobos, J. Lausmaa, R. Brånemark, P. Thomsen, and A. Palmquist, “Effect of load on the bone around bone-anchored amputation prostheses,” *J. Orthop. Res.*, vol. 35, no. 5, pp. 1113–1122, 2017.

[59] G. N. Srinivasan, “Segmentation Techniques for Target Recognition,” vol. 1, no. 3, pp. 75–81, 2007.

[60] S. Egmentation, D. L. Pham, C. Xu, and J. L. Prince, “C m m i s,” 2000.

[61] S. Dietler, “Lower Limb Segmentation,” 2009.

[62] M. Ct and O. Microscopy, “CHAPTER 3 FINITE ELEMENT MODELING OF TIBIA BONE AND IMPLANT,” pp. 59–82.

[63] Available: http://pi.math.cornell.edu/~web6140/TopTenAlgorithms/JPEG.html.

[64] Available: http://www.xrayhead.com/theatlas.php?id=lower_leg.

[65] “STL(fileformat).”Available: https://en.wikipedia.org/wiki/STL_%28file_format%29.

[66] G. Design, “Geomagic Design X User Guide,” no. November, 2013.

[67] “STEP file.” [Online]. Available: http://www.pcb-3d.com/tutorials/step-file-faq/.

[68] “IGES.” [Online]. Available: https://en.wikipedia.org/wiki/IGES.

[69] Available: https://it.mathworks.com/matlabcentral/fileexchange/6678-stlread.

[70] T. Joliveau and Y. Michelin, “Approche paysagère et Système d’Information Géographique pour la prospective concertée d’un territoire rural,” no. February, pp. 2–4, 2000.

[71] “Besl1992.” .

[72] M. Naim, “Latin America: Post-Adjustment Blues,” *Foreign Policy*, vol. 92, pp. 133–50, 1993.

[73] F. Pomerleau, F. Colas, R. Siegwart, and S. Magnenat, “Comparing ICP variants on real-world data sets,” *Auton. Robots*, vol. 34, no. 3, pp. 133–148, 2013.

[74] “https://www.mathworks.com/matlabcentral/fileexchange/”

[75] D. Systèmes, “Getting Started With Abaqus/Cae 2016,” 2016.

[76] V. Rajtukova, R. Hudak, J. Zivcak, P. Halfarova, and R. Kudrikova, “Pressure distribution in transtibial prostheses socket and the stump interface,” *Procedia Eng.*, vol. 96, pp. 374–381, 2014.

[77] H. Gholizadeh, N. A. Abu Osman, A. Eshraghi, N. Arifin, and T. Y. Chung, “A comparison of pressure distributions between two types of sockets in a bulbous stump,” *Prosthet. Orthot. Int.*, vol. 40, no. 4, pp. 509–516, 2016.

[78] J. W. Wannop, J. T. Worobets, and D. J. Stefanyshyn, “Normalization of ground reaction forces, joint moments, and free moments in human locomotion,” *J. Appl. Biomech.*, vol. 28, no. 6, pp. 665–676, 2012.

[79] “Elasticity 4.1,” pp. 67–80.

[80] A. F. Bower, “Constitutive Models Relations between Stress and Strain,” 2008.

[81] “Large elastic deformations of isotropic materials,” no. October, 1948.

[82] R. M. Barrer and B. L. R G Treloar, “THE ELASTICITY OF A NETWORK OF LONG- CHAIN MOLECULES-11. Derivation of Strain-energy Function,” pp. 241–246, 1943.

[83] W. Dickinson, “STRESS - STRAIN Data for Vulcanised,” 1943.

[84] M. Mooney, “A theory of large elastic deformation,” *J. Appl. Phys.*, vol. 11, no. 9, pp. 582–592, 1940.

[85] R. W. Ogden, “Large Deformation Isotropic Elasticity: On the Correlation of Theory and Experiment for Compressible Rubberlike Solids,” *Proc. R. Soc. A Math. Phys. Eng. Sci.*, vol. 328, no. 1575, pp. 567–583, 1972.

[86] E. Tönük and M. B. Silver-Thorn, “Nonlinear elastic material property estimation of lower extremity residual limb tissues,” *IEEE Trans. Neural Syst. Rehabil. Eng.*, vol. 11, no. 1, pp. 43–53, 2003.

[87] E. Tönük and M. B. Silver-Thorn, “Nonlinear elastic material property estimation of lower extremity residual limb tissues,” *IEEE Trans. Neural Syst. Rehabil. Eng.*, vol. 11, no. 1, pp. 43–53, 2003.

[88] “FEM.”Available: http://web.mit.edu/calculix_v2.7/CalculiX/ccx_2.7/doc/ccx/node26.html.

[89] “FEM.”Available: http://web.mit.edu/calculix_v2.7/CalculiX/ccx_2.7/doc/ccx/node32.html.

[90] P. di M. E. Votta, Slide from ‘Computational Biomechanics’ Course, “FEM.”

[91] “FEM.” Available: https://ocw.mit.edu/courses/mathematics/18-085-computational-science-and-engineering-i-fall-2008/video-lectures/.